

Nansen Environmental and Remote Sensing Center



*A non-profit
environmental research center
affiliated with the
University of Bergen*

*Edv. Griegsv. 3a
N-5059 Bergen, Norway
Tel: + 47 55 29 72 88
Fax: + 47 55 20 00 50*

Technical Report No. 166

prepared for

Faroës G. E. M., Met Ocean Group
under Project No. 23-16-3.

Tides and tidal simulation in the area around the Faroe Islands

by

Knud Simonsen*

**c/o Fiskirannóknarstovan,
(Fisheries Laboratory of the Faroes),
Noatun, FO-100 Torshavn
Faroe Islands
Tel: + 298 31 50 92
Fax: + 298 31 82 64*

May, 1999

This is contribution no. 31 from G. C. Rieber Institute at NERSC

Contents

1	Introduction	3
2	The tidal model	4
2.1	Formulation	4
2.2	Harmonic analysis of model results	5
2.3	External forcing data	6
2.4	Bathymetry	6
2.5	Tidal simulations	6
3	Validation towards observed data	9
3.1	Harmonic constants from measured elevation data	13
3.2	Validation of the elevation	16
3.3	Harmonic constants from measured current data	23
3.4	Validation of the current simulation	29
3.5	Conclusion	41
4	Model results	42
4.1	Tidal Charts	42
4.2	Tidal Currents	47
4.2.1	Tidal current ellipses	47
4.2.2	Extreme tidal current speed	52
4.2.3	Residual tidal currents	57
4.2.4	Tidal current maps	61
5	Database	98
6	Interactive tidal presentation	100
6.1	The CD-ROM	100
7	Conclusion	103

Disclaimer:

The data area thoroughly checked and quality controlled within the constraints given by the project definition. The originators of the data or their representatives shall not be held responsible for any conclusion based upon the data.

1 Introduction

On the Faroe Plateau and on the surrounding ridges and banks the tides and then especially the tidal current, are of major practical importance for all marine based activities in the area. Although the descriptive knowledge of the tides is known from centuries of experience by local fishermen, and from observations and tidal model simulations over the last decades, the tides and tidal currents are in general poorly quantified.

The tide on the Faroe Plateau is in general semidiurnal, except in the region in the vicinity of Tórshavn, where the tide has a diurnal character. The diurnal tide in this region seems to be rather normal, whereas the semidiurnal tide is suppressed [Hansen, 1978]. However, the current in Nólsoyarfjørð, just off Tórshavn, is strongly semidiurnal, but the features of this flow are anomalous. In all sounds on the Faroe Islands the tidal currents run for about 6 hours in each direction, except in Nólsoyarfjørð, where the NE-current lasts for only about 4 hours while the reverse current (SW) runs for about 8 hours [Hansen, 1978, Heinesen, 1985, Simonsen, 1992]. Previous experience with tidal models (with 2 nautical miles and 0.5 nautical miles resolution) strongly indicate that accurate simulation of the tide and in particular the tidal currents in the vicinity of Tórshavn, requires accurate simulation of the flow through the channels to the north and to the south of Tórshavn. In addition, the channels between the north eastern islands are important path-ways for the fish larvae from the spawning area north of the Faroes to the banks on the eastern shelf [Hansen et al., 1994]. On the Faroe Plateau [Hansen, 1979, 1992] and on the Faroe Bank [Hansen et al., 1986, 1991b] there is an anti-cyclonic residual flow, which is preserving passive tracers like fish larvae's and pollution on the shallow water. The self water is slightly cooler and fresher than the surrounding waters, and the transition between these waters appears as a distinct temperature front in satellite images. Hansen [1992] suggested that tidal rectification is one of the mechanisms for maintaining the stability of the anti-cyclonic circulation.

In this report simulations with a 0.5 nautical miles- resolution model for the entire Faroe Plateau and the surrounding to the south and west are described. The model is described in Section 2. The model needs data to be specified along the artificial boundaries of the model domain, which is obtained from tidal work on larger areas (Section 2.3). For accurate simulation a fairly representative model depth matrix is required. For this project a new depth matrix is created from various data sources (Section 2.4). The model simulations are validated towards tidal harmonics derived from measured data in Section 3 and the model results are presented as tidal charts in Section 4.1 and maps of tidal current ellipse axis and tidal current maps are provided in Section 4.2. Residual flows is shown in Section 4.2.3. The model results are stored into a database (Section 5), which may serve as forcing fields in very high resolution local area simulation of the tides as well for other purposes. A proto-type interactive system is developed, which makes it easy to extract tidal information from the data base (Section 6) an the report is

concluded in Section 7.

2 The tidal model

2.1 Formulation

The applied tidal model is an improved version of the model by Simonsen [1992], which again is based on the models by Gjevik and Straume [1989] and Flather [1981, 1976]. The model is based on the depth integrated hydrodynamic equations, which in a Cartesian system with the axis x, y , and the corresponding volume transports (U, V) may be written:

$$\frac{\partial U}{\partial t} + \frac{U}{h} \frac{\partial U}{\partial x} + \frac{V}{h} \frac{\partial U}{\partial y} - fV = -gh \frac{\partial \eta}{\partial x} + A_x + B_x \quad (1)$$

$$\frac{\partial V}{\partial t} + \frac{U}{h} \frac{\partial V}{\partial x} + \frac{V}{h} \frac{\partial V}{\partial y} + fU = -gh \frac{\partial \eta}{\partial y} + A_y + B_y \quad (2)$$

where g is acceleration due to gravity, h is the mean depth, f is the Coriolis parameter and η is the vertical displacement of the sea surface from its undisturbed position. A_x, A_y are the components of the bottom friction, and B_x, B_y are the components of the lateral friction, which will be defined subsequently.

The continuity equation reads

$$\frac{\partial \eta}{\partial t} + \frac{\partial U}{\partial x} + \frac{\partial V}{\partial y} = 0 \quad (3)$$

The bottom stress is parameterized by

$$A_x = -kU/h; A_y = -kV/h \quad (4)$$

where k is the bottom friction coefficient, which optionally is expressed in linear form,

$$k = c_D u_s \quad (5)$$

or on quadratic form

$$k = c_D [U^2 + V^2]^{1/2}/h \quad (6)$$

where u_s is a typical scale for the tidal current. In shallow water the bottom friction significantly influence the tidal propagation, while it is little influenced in water deeper than about 50 m [Prandle, 1997].

The lateral friction is modeled by

$$B_x = \nu \nabla^2 U, B_y = \nu \nabla^2 V \quad (7)$$

where ν is the horizontal eddy viscosity. In some applications it is related to the water depth as proposed by Schwiderski [1980];

$$\nu = qh \quad (8)$$

where q is a constant. Glorioso and Flather [1995, 1997] used $q=5 \text{ m s}^{-1}$ in their model with $1/6^\circ$ and $1/8^\circ$ resolution in longitude and latitude, respectively (i.e. 10 km and coarser), while Gjevik et al. [1994] used a value of 25 m s^{-1} in a 25 km resolution model. In some applications ν is considered as a constant partly determined by the grid resolution. Kowalik and Proshutinsky [1996] used ν equal to 50, 500, and $1000 \text{ m}^2 \text{s}^{-1}$ in models with 1.389, 4.63 and 13.89 km resolution, respectively. Here the $q=5 \text{ m s}^{-1}$ is adopted.

The equation of motion have been discretized on a space–staggered C-grid [Mesinger and Arakawa, 1976] using a forward–backward scheme usually credited to Sielecki [1968]. The dispersion and stability conditions for this scheme is discussed by Sielecki [1968], Martinsen et al. [1979] and, Simonsen [1992]. The advective terms are implemented by a forward centered scheme, which is known for its high diffusivity. The model is implemented using a Mercator projection relative to the 7°W meridian.

2.2 Harmonic analysis of model results

The harmonic analysis of the model results is based on a least square fit [Foreman, 1977] of the amplitudes, A_j and phases, ϕ_j in the function

$$y_i = C_0 + \sum_{j=1}^M A_j \cos[2\pi\sigma_j t_i + \phi_j] \quad (9)$$

where C_0 is the residual, M is number of constituents, and σ_j is the frequency. This approach is used on the sea surface elevation and on the current components.

The tidal current may also be described as two rotating vectors expressed in complex notation as:

$$\begin{aligned} \vec{R}(t)_+ &= \frac{1}{2}[(U \cos \phi_u + V \sin \phi_v) + i(V \cos \phi_v - U \sin \phi_u)]e^{i\sigma t} \\ \vec{R}(t)_- &= \frac{1}{2}[(U \cos \phi_u - V \sin \phi_v) + i(V \cos \phi_v + U \sin \phi_u)]e^{-i\sigma t} \end{aligned} \quad (10)$$

where the constituent subscript j is dropped, U, V and ϕ_u, ϕ_v is the amplitude and phase of the current components, respectively, and the subscript signs refer to the direction of the rotation. Combining these two rotating motions results into an ellipse, where the length of the major- and minor semi axis become

$$\begin{aligned} V_{max} &= |\vec{R}_+| + |\vec{R}_-| \\ V_{min} &= |\vec{R}_+| - |\vec{R}_-| \end{aligned} \quad (11)$$

The phases of the rotary motions are expressed by

$$\tan \phi_{\pm} = Im(R_{\pm})/Re(R_{\pm}) \quad (12)$$

and the phase of the net motion by

$$\phi = (\phi_- - \phi_+)/2 \quad (13)$$

and the inclination of the maximum current relative to east is expressed by

$$\theta = (\phi_- + \phi_+)/2 \quad (14)$$

2.3 External forcing data

Data used to force the model are in form of amplitude and phase for sea surface elevation constituents derived from a global element tidal model and corrected towards altimeter measured elevation data through application of data assimilation methods [Andersen, 1995]. The data are kindly provided by O. B. Andersen, Kort- and Matrikelstyrelsen, Denmark.

2.4 Bathymetry

The depth matrix is constructed from several different bathymetries. For the outer regions the bathymetry generated by Westerberg [1990] is adopted, except along the southern border, where it is merged with the ETOPO5 bathymetry. The ETOPO5 bathymetry was found to show shallow depths in areas nearby steep bathymetries, in particular in the Faroe Bank Channel area. Westerberg [1990] used the IOS bathymetric map for the North East Atlantic [Roberts et al., 1979] as basis, and redrew on the Iceland Faroe Ridge from Fleischer et al. [1974], on the Faroe shelf and slope out to approximately 600 m from Føroya Jarðfrøðissavn [1981] and in Wyville-Thomson Ridge area from the survey by Ellet [1988]. The resolution in the Westerberg [1990] data is 5 and 2.5 minutes in meridional and zonal directions respectively, which is too coarse to resolve the Faroe Islands properly. For the inner regions a new bathymetry is generated with the model resolution on the basis of various available data sources in addition to depths adopted from navigation maps. The model depth matrix is shown in Figure 1.

Land occupies 1518.6 km² in the generated depth matrix (Table 1), which is higher than the usually referred area of 1399 km² [Rasmussen, 1981]. This difference is mainly because narrow channels and fjords are closed in the depth matrix. The obtained area within 200 m depth and 500 m is 21380.9 km² and 44378.6 km², respectively, which is in agreement with the areas obtained by Rasmussen [1981].

2.5 Tidal simulations

The model is in general spun up from rest in 10 days run, and data are stored in the subsequent days for harmonic analysis. Simulations are performed for individual constituents, where data are collected from two days of simulation. Simulations including the non-linear terms (C) or changed friction coefficient (D) are however started from 10 days spin up with the default (A) model and run for two days before data are collected for analysis. A separate simulation (B) including six constituents is run for 30 days, which is just above the 27.6 days required to resolve the involved

Table 1: Area (km^2) in the generated depth matrix within given depth intervals, and total area shallower than the lower limit of the interval for Bill Baily Bank, Faroe Bank, and the Faroe Plateau.

Depth	Bill Baily Bank		Faroe Bank		Faroe Plateau	
	Area	Acc.	Area	Acc.	Area	Acc.
	Area	Area	Area	Area	Area	Area
Land	0.0	0.0	0.0	0.0	1518.6	1518.6
0 – 100	0.0	0.0	247.8	247.8	5164.5	6683.1
100 – 200	790.0	790.0	2670.4	2918.2	14697.9	21380.9
200 – 300	717.9	1507.9	1444.5	4362.7	12006.3	33387.3
300 – 400	856.7	2364.6	1566.2	5928.9	5313.6	38700.8
400 – 500	826.7	3191.3	1323.6	7252.4	5677.8	44378.6

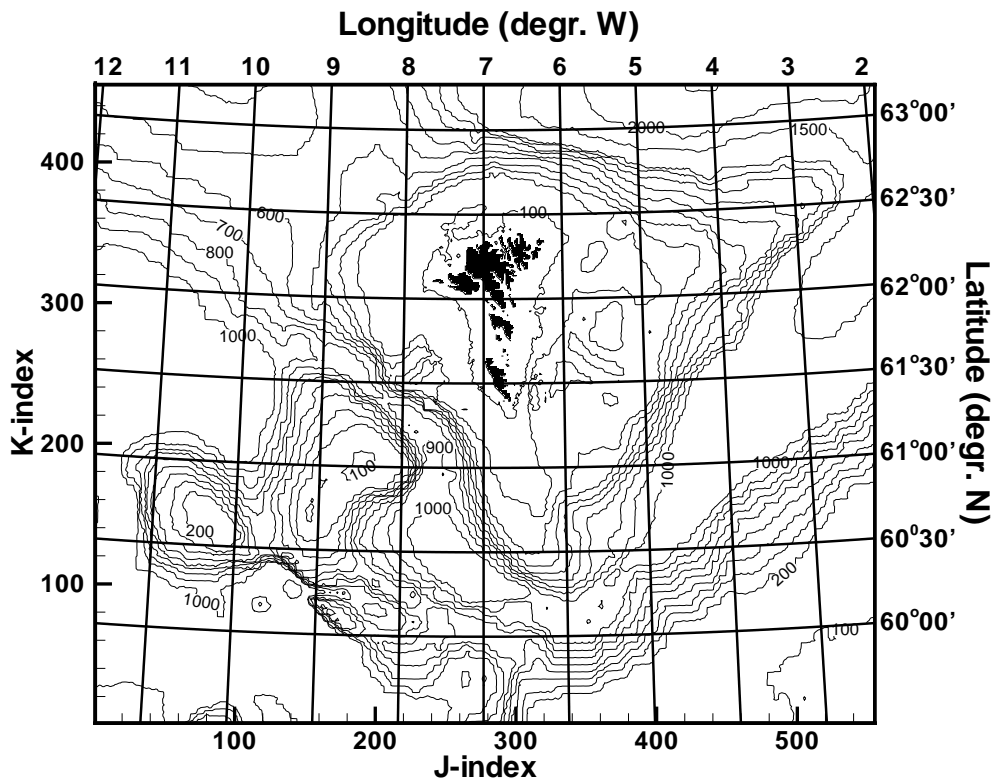


Figure 1: The model representation of the bathymetry. The map is in Mercator projection relative to 7°W .

frequencies in a harmonic analysis. The results from run B was quite close to the results obtained in the A-runs, and are not included in the further discussion. Details of each run is provided in Table 2.

The simulations are performed on the Cray Origin 2000 at the University in Bergen through the partial ownership by NERSC. Using four processes the model runs with a speed of approximately four times faster than in nature.

Table 2: Details of the model runs. Period of the included constituents is included in Table 3.

Run	Constituent(s) included	Advection terms incl.	q m s^{-1}	Friction Type	c_f
A-Q ₁	Q ₁	No	0	Quad.	0.0026
A-O ₁	O ₁	No	0	Quad.	0.0026
A-K ₁	K ₁	No	0	Quad.	0.0026
A-P ₁	P ₁	No	0	Quad.	0.0026
A-N ₂	N ₂	No	0	Quad.	0.0026
A-M ₂	M ₂	No	0	Quad.	0.0026
A-S ₂	S ₂	No	0	Quad.	0.0026
A-K ₂	K ₂	No	0	Quad.	0.0026
B6	Q ₁ +O ₁ +K ₁ +N ₂ +M ₂ +S ₂	No	0	Quad.	0.0026
C-O ₁	O ₁	Yes	5	Quad.	0.0026
C-K ₁	K ₁	Yes	5	Quad.	0.0026
C-M ₂	M ₂	Yes	5	Quad.	0.0026
C-S ₂	S ₂	Yes	5	Quad.	0.0026
D-Q ₁	Q ₁	Yes	5	Quad.	0.0033
D-O ₁	O ₁	Yes	5	Quad.	0.0033
D-K ₁	K ₁	Yes	5	Quad.	0.0033

Table 3: Symbol, name, and period of the constituents included in the simulations.

Symbol	Name	Period Hours
<i>Diurnal constituents</i>		
Q ₁	Larger lunar elliptic	26.8682
O ₁	Principal lunar diurnal	25.8192
P ₁	Principal solar diurnal	24.0659
K ₁	Luni-solar diurnal	23.9345
<i>Semi diurnal constituents</i>		
N ₂	Large lunar ellipses	12.6583
M ₂	Principal lunar	12.4206
S ₂	Principal solar	12.0000
K ₂	Luni solar semi diurnal	11.9673

3 Validation towards observed data

Harmonic constituents derived from measured time series are adopted from various available sources as listed in Tables 4 and 5. The location of each measurement site is shown in Figure 2, and the coastal areas are blow up in Figure 3.

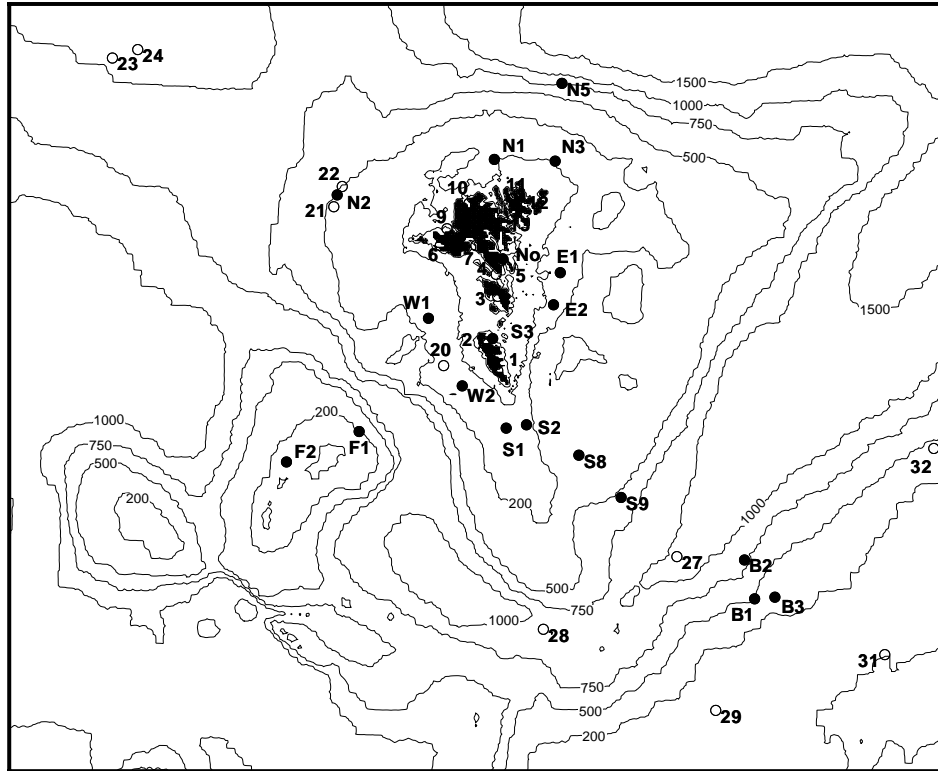


Figure 2: Station positions where harmonic constituents are available from measured data. Elevation stations are indicated by open circles, while current measurements sites are shown by filled dots. Details are provided in Tables 4 and 5.

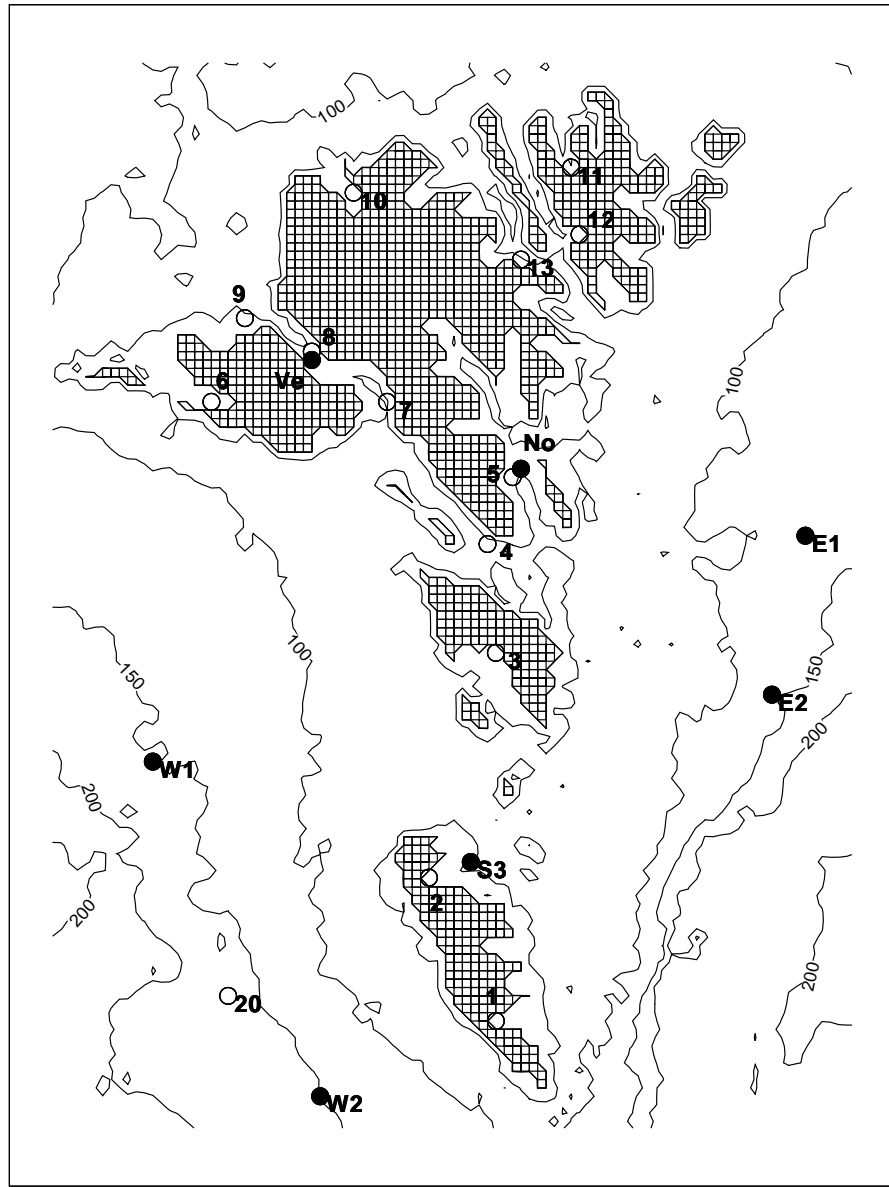


Figure 3: Blow up of Figure 2 for the coastal areas of the Faroe Islands. The mesh on land shows the model grid resolution.

Table 4: Tidal gauge stations where tidal harmonics are available for validation of the model. Empty space indicate that the actual information is not available.

St. No	Latitude ° min	Longitude ° min	Depth (m) Inst	Dur. Bot.	Location Days	Source
<i>Coastal gauge stations</i>						
1	61 27.74	6 46.42			Vágur	Farvandsvæsenet [1998]
2	61 35.75	6 54.77	10	10	Hvalba	Hansen [1978]
3	61 49.74	6 46.26			Sandur	Farvandsvæsenet [1998]
4	61 57.24	6 48.34			Kirkjuður	Farvandsvæsenet [1998]
5a	62 00.23	6 44.06		174	Tórshavn	Cartwright et al. [1980a]
b				292	Tórshavn	Hansen [1978]
c					Tórshavn	Farvandsvæsenet [1998]
6a	62 04.72	7 22.45		60	Sørvag	Cartwright et al. [1980a]
b				85	Sørvag	Hansen [1978]
c					Sørvag	Farvandsvæsenet [1998]
7	62 04.60	6 59.80	72	73	S Vestmannas.	Simonsen [1989]
8	62 07.50	7 09.60		330	Oyrargjógv	Hansen et al. [1991a]
9	62 09.90	7 18.10	62	63	N Vestmannas.	Simonsen [1989]
10	62 17.25	7 04.34			Eiði	Farvandsvæsenet [1998]
11	62 18.90	6 34.21	27		Haraldssund	Simonsen [1989]
12	62 14.72	6 35.34			Klaksvík	Farvandsvæsenet [1998]
13	62 12.73	6 40.73			Leivík	Farvandsvæsenet [1998]
<i>Of coastal gauge stations</i>						
20	61 29.00	7 20.00	170		21 W of Suðuroy	Cartwright et al. [1980a]
21	62 16.00	8 30.00	168		NW Faroe Shelf	Cartwright et al. [1980a]
22	62 22.00	8 25.00			NW Faroe Shelf	Kowalik and Proshutinsky [1998]
23	62 57.00	10 57.00	444		23 IFR	Cartwright et al. [1980a]
24	63 00.00	10 40.00			IFR	Kowalik and Proshutinsky [1998]
27	60 32.00	4 59.00	1027		165 FSC	IAPSO
28	60 11.00	6 20.00	1198		28 FSC	Cartwright et al. [1980a]
29	59 46.00	4 39.00	104		10 Scottish Shelf	Cartwright et al. [1980a]
31	60 00.00	2 58.00	90		30	Cartwright et al. [1980a]
32	61 00.00	2 20.00			N of Shetland	Kowalik and Proshutinsky [1998]

Table 5: Current measurements stations where tidal harmonics are available for validation of the model. Stations names are mainly adopted from Hansen and Larsen [1999].

St. No	Latitude ° min	Longitude ° min	Depth (m) Inst	Dur. Bot.	Location Days	Source
<i>Coastal current meter stations</i>						
S3	61 37.16	6 49.36	20	55	32	Suðuroyarfjørð Hansen and Larsen [1999]
Ve	62 07.00	7 09.13	a	48	27	Vestmannasund Hansen et al. [1991a]
No	62 00.80	6 43.00	15	30	25	Nólsøyarfjørð Hansen [1978]
<i>Of coastal current meter stations</i>						
F1	61 09.38	8 11.38	40	119	60	Faroe Bank Hansen and Larsen [1999]
F2	60 59.80	8 55.46	40	119	100	Faroe Bank Hansen and Larsen [1999]
W1	61 43.40	7 29.60	40	148	(b)	W Faroe Shelf Hansen and Larsen [1999]
W2	61 23.30	7 08.00	40	150	30	W of Suduroy Hansen and Larsen [1999]
N1	62 30.30	6 47.80	40	85	(d)	N Faroe Shelf Hansen and Larsen [1999]
N2	62 19.50	8 28.40	40	95	(c)	NW Faroe Shelf Hansen and Larsen [1999]
N3	62 29.41	6 09.51	20	96	49	NE Faroe Shelf Hansen and Larsen [1999]
N5	62 52.70	6 04.30	150	702	47	N of Faroe Shelf Hansen and Larsen [1999]
E1	61 56.40	6 06.50	40	127	30	E Faroe Shelf Hansen and Larsen [1999]
E2	61 47.32	6 11.80	40	120	(e)	E Faroe Shelf Hansen and Larsen [1999]
S1	61 10.80	6 41.00	40	106	75	Munkagrunnurin Hansen and Larsen [1999]
S2	61 11.70	6 29.30	40	139	(f)	Munkagrunnurin Hansen and Larsen [1999]
S8	61 02.30	5 57.00	258	276	24	SE of Munkagr. Simonsen [1992]
S9	60 49.80	5 31.50	305	595	83	SE of Munkagr. Simonsen [1992]
<i>Of coastal current profile stations</i>						
B1	60 18.70	4 13.10	40	412	28	Foinaven Sherwin et al. [1999]
B2	60 29.90	4 18.80	57	830	31	Ocean Alliance Sherwin et al. [1999]
B3	60 18.60	4 01.20	300	300	41	Scot. Shelf, NWOCE Sherwin et al. [1999]

a: Average of 4 m intervals from 9 to 41 m measured by a bottom mounted ADCP

b: Avearge of 8 timeseries of length 30–60 days.

c: Avearge of 2 timeseries of length 30 and 60 days.

d: Avearge of 4 timeseries of length 30 days.

e: Avearge of 14 timeseries of length 30 – 60 days at bottom depths from 108 m to 135 m.

f: Avearge of 6 timeseries of length 30 – 60 days at bottom depths from 128 m to 144 m.

3.1 Harmonic constants from measured elevation data

The harmonic constants derived from measurements of the sea surface elevation is adopted from various sources (Table 4) and listed in Table 6. The analysis are performed at different institutes, which have not used identical analysis method. The constituents found in Cartwright et al. [1980a], and probably also the stations found in the IAPSO are derived using the 'response' method [Munk and Cartwright, 1969] with reference station on the Hebrides (Sites 20, 21, 23, 28 and 29), Shetland (Lerwick) (Site 31) and Iceland (Reykjavik) (Site 23). The harmonics found in Hansen [1978], Hansen et al. [1991a], Simonsen [1989, 1992] are derived by a least square based method [Godin, 1972, Hansen, 1978], and a similar method is used by Farvandsvæsenet [1998]. No information on used methods is found in the remaining sources.

In the 'response' method the measured data are related to an artificial created 'reference tide'. However, when timeseries of shorter duration is analyzed, the measured data may be related to a wellposed reference station nearby. Unfortunately, no 'reference' station is worked out for the Faroese area, and thus are stations at the neighboring islands applied. The frequency resolution in least square methods is determined by the length of the time series according to the so-called Rayleigh criteria. This criteria implies that the time series should have a duration of at least 14.77 days to separate the M_2 and the S_2 and at least 27.6 days to separate the M_2 , S_2 , N_2 , O_1 , Q_1 , and K_1 from each other. If K_2 and P_1 are added then 182.6 days of measurements are required. When the duration of a timeseries is to short to resolve frequency pairs, the assumption of linear relations ship between the frequency pairs is applied. This implies that the analysis is done with only the main frequency included, and the contribution from the minor frequency is found by using the relations ship in the astronomical tide or at a reference station nearby.

Harmonic constants for Sørvag (Site 6) and Tórshavn (Site 5) are found in three different sources [Hansen, 1978, Cartwright et al., 1980a, Farvandsvæsenet, 1998], but not with completely identical results (Table 6). All three sources cites the same origin of the data, but the length of the analyzed time series varies. The use of different methods may also be part of the explanation for the non-identical results.

Table 6: Amplitudes and Greenwich phase lags derived from measurements of sea surface elevation. Details on each station is shown in Table 4. Empty space is due to lack of information.

St no		Constituents						
		Q_1	O_1	P_1	K_1	N_2	M_2	S_2
1	Amp		5.7		5.8		27.2	11.3
	Pha		25		140		192	222
2	Amp	1.4	4.5	2.3	5.9	8.3	44.7	17.5
	Pha	350	55	139	127	172	199	232
3	Amp		5.4		7.0		49.5	20.4
	Pha		33		137		192	228
4	Amp		6.2		6.8		31.1	12.6
	Pha		45		137		191	222
5a	Amp	2.4	7.2	1.6	5.1	1.9	10.3	5.4
	Pha	9	50	141	143	171	198	217
5b	Amp	2.6	10.0	1.4	4.8	1.8	9.9	5.8
	Pha	22	57	116	130	175	196	226
5c	Amp		7.3		4.3		10.4	5.6
	Pha		53		142		201	218
6a	Amp	2.2	5.3	2.4	8.5	14.0	66.5	24.8
	Pha	306	14	137	145	190	211	245
6b	Amp	2.5	7.0	3.1	9.0	14.2	65.1	26.7
	Pha	328	28	149	134	180	207	245
6c	Amp		5.7		9.5		69.7	26.1
	Pha		15		143		211	245
7	Amp	1.7	5.9		9.5	11.6	59.3	18.5
	Pha	337	40		131	184	195	241
8	Amp	1.9	5.7	2.4	8.9	11.6	55.2	22.5
	Pha	337	35	126	136	191	212	247
9	Amp	3.9	8.5		12.4	12.1	60.5	17.3
	Pha	311	13		156	224	234	280
10	Amp		7.7		9.5		61.3	21.2
	Pha		15		163		253	286
11	Amp	2.1	9.7		9.1	11.9	47.8	11.2
	Pha	281	20		164	249	275	303
12	Amp		8.6		7.3		35.4	11.2
	Pha		30		171		274	309
13	Amp		8.3		8.2		43.8	15.4
	Pha		21		169		275	307

continues on the next page

Table 6: *continued from previous page*

St no		Constituents							
		Q_1	O_1	P_1	K_1	N_2	M_2	S_2	K_2
20	Amp	2.0	4.9	2.0	7.1	10.9	55.9	22.2	6.3
	Pha	328	18	134	143	175	196	229	227
21	Amp	3.4	8.4	2.4	8.2	10.2	50.9	19.6	5.6
	Pha	328	27	154	163	191	212	244	242
22	Amp						51.0		
	Pha						213		
23	Amp	1.6	7.3	2.7	8.1	6.8	35.7	15.2	4.3
	Pha	321	38	134	144	157	177	213	212
24	Amp						36.0		
	Pha						177		
25	Amp						52.0		
	Pha						285		
26	Amp		7.0		9.0		73.0		
	Pha		12		147		207		
27	Amp	2.1	6.2	2.7	8.5	12.1	59.4	22.5	6.8
	Pha	323	7	130	141	203	225	257	255
28	Amp	2.7	7.2	2.7	9.4	14.5	72.8	27.7	7.9
	Pha	318	12	137	147	186	207	241	238
29	Amp	3.2	8.2	2.7	9.0	16.8	83.7	31.2	8.9
	Pha	310	8	138	147	206	228	261	259
30	Amp						52.0	35.0	
	Pha						285	238	
31	Amp	2.8	8.5	2.8	9.3	14.3	69.8	26.0	7.3
	Pha	326	16	138	154	232	252	287	282
32	Amp						56.0	21.0	
	Pha						255	293	

a: data from Hansen [1978]

b: from Cartwright et al. [1980a]

c: from Farvandsvæsenet [1998]

3.2 Validation of the elevation

Elevation amplitude and phase lags derived by the model at observation sites are compared in Table 7 and as scatter plots in Figures 8–6. In Table 7 mean and standard deviation of the difference between model and data derived amplitudes and phases are provided for each constituent. Note, that the harmonics in Tórshavn (Site 5) and Sørvág (Site 6) found in the different sources are treated as individual sites in the estimates of the mean and standard deviation just mentioned.

The model results are in general in good agreement with the data derived values, in particular for the semi diurnal tide. The largest amplitudes in the semidiurnal tide are on the western shelf with maximum amplitudes around Vágar, and minimum amplitudes in the area just north of Tórshavn. The gradient from the west to the east side of the islands are relatively steep for both amplitudes and phase lags, but it is captured to a fairly high degree of accuracy by the model, in spite that the model resolution is too coarse to resolve the gradients and topography in the coastal areas properly. The model ability to capture the strong gradients in the central regions of the Faroe Islands is documented through the comparison at Sites Sandur (Site 3), Kirkjubø (Site 4), and Tórshavn (Site 5), and north of Tórshavn also at Leirvík (Site 13) and Klakksvík (Site 12).

The largest deviation from the observed elevation data for the semidiurnal tide is around Vágoy (Sites 6, 7, 8, and 9). Including the advective and viscosity terms (Run C) better agreement is obtained in this area. Relative large deviations are also seen at some sites in areas with large gradients, but this is more a matter of model resolution. For the off-coastal sites relatively large disagreement for the M_2 occur for site 20 west of Suðuroy, which remains in the simulations including the non-linear terms. In general the semi diurnal tidal elevation is simulated to an accuracy comparable with the results obtained at same site with different analysis methods, with the all-over best agreement with measurement based data in Run C for the M_2 and S_2 constituents.

The simulation of the diurnal tide is less successful than for the semi diurnal tide, although the standard deviation between modelled and measured data based harmonics are comparable with the differences between the cited results from measured data in Tórshavn and Sørvág. The tidal charts shows structures, which indicate appearance of topographical trapped waves along the Scottish shelf and along the northern Faroe Shelf (Figures 12 and 13). Topographical waves along the European continent are discussed by Cartwright et al. [1980b], Huthnance [1992], and others, while topographical waves around the Faroe Plateau is rarely discussed in literature. Better understanding of the influence of the topographical trapped waves, and those increasing the accuracy of the simulation of the diurnal tide to the level of the semidiurnal tide, requires further research, which is beyond the present report.

Table 7: Elevation amplitudes (cm) and Greenwich phase lags ($^{\circ}$) estimated by the tidal model at tidal gauge sites listed in Table 4, and difference from the harmonic constants derived from measurements listed in Table 6. The mean and the standard deviation of the difference between modelled and 'observed' amplitude and phase lags are estimated for each constituent.

Site	Run: A-Q ₁				Run: D-Q ₁			
	Amplitude		Phase Lag		Amplitude		Phase Lag	
	Mod	Diff	Mod	Diff	Mod	Diff	Mod	Diff
	cm	cm	°	°	cm	cm	°	°
2	3.3	1.9	313	-37	3.2	1.8	324	-26
5a	1.5	-0.9	346	-23	1.3	-1.1	4	-5
5b	1.5	-1.1	346	-36	1.3	-1.3	4	-18
6a	1.6	-0.6	282	-24	1.7	-0.5	281	-25
6b	1.6	-0.9	282	-46	1.7	-0.8	281	-47
7	1.0	-0.7	312	-25	1.0	-0.7	304	-33
8	1.8	-0.1	310	-27	2.0	0.1	308	-29
9	2.3	-1.6	310	-1	2.5	-1.4	309	-2
11	2.1	0.0	341	60	2.5	0.4	342	61
20	2.5	0.5	340	12	2.5	0.5	343	15
21	2.5	-0.9	8	40	2.5	-0.9	8	40
23	1.8	0.2	347	26	1.8	0.2	347	26
27	3.0	0.9	270	-53	3.0	0.9	283	-40
28	2.4	-0.3	289	-29	2.6	-0.1	294	-24
29	2.8	-0.4	273	-37	2.9	-0.3	283	-27
31	3.1	0.3	318	-8	3.2	0.4	321	-5
Mean	-0.2		-13.0		-0.2		-8.7	
St. dev.	0.9		32.3		0.9		30.3	
Site	Run: A-O ₁				Run: C-O ₁			
	Amplitude		Phase Lag		Amplitude		Phase Lag	
	Mod	Diff	Mod	Diff	Mod	Diff	Mod	Diff
	cm	cm	°	°	cm	cm	°	°
1	7.4	1.7	47	22	6.2	0.5	27	2
2	8.9	4.4	24	-31	6.9	2.4	11	-44
3	3.7	-1.7	37	4	5.0	-0.4	28	-5
4	5.1	-1.1	46	1	6.2	0.0	37	-8
5a	6.3	-0.9	53	3	7.5	0.3	41	-9
5b	6.3	-3.7	53	-4	7.5	-2.5	41	-16
5c	6.3	-1.0	53	0	7.5	0.2	41	-12
6a	3.4	-1.9	354	-20	4.7	-0.6	21	7
6b	3.4	-3.6	354	-34	4.7	-2.3	21	-7
6c	3.4	-2.3	354	-21	4.7	-1.0	21	6
7	3.5	-2.4	25	-15	4.8	-1.1	28	-12
8	5.3	-0.4	6	-29	5.4	-0.3	20	-15
9	6.4	-2.1	359	-14	5.5	-3.0	14	1
10	8.2	0.5	8	-7	6.2	-1.5	12	-3
11	8.1	-1.6	26	6	7.3	-2.4	18	-2
12	6.8	-1.8	29	-1	6.8	-1.8	34	4
13	8.1	-0.2	29	8	7.9	-0.4	26	5
20	6.5	1.6	32	14	6.2	1.3	12	-6
21	8.6	0.2	40	13	9.3	0.9	28	1
23	6.7	-0.6	36	-2	6.7	-0.6	35	-3
27	8.2	2.0	351	-16	6.5	0.3	358	-9
28	8.2	1.0	356	-16	7.3	0.1	0	-12
29	8.5	0.3	354	-14	8.1	-0.1	3	-5
31	8.6	0.1	11	-5	8.0	-0.5	10	-6
Mean	-0.6		-6.6		-0.5		-6.2	
St. dev.	1.9		14.7		1.3		10.4	

Table 7: *continued.*
Run: A-P₁

Site	Amplitude		Phase Lag	
	Mod	Diff	Mod	Diff
	cm	cm	°	°
2	2.4	0.1	139	0
5a	2.3	0.7	121	-20
5b	2.3	0.9	121	5
6a	3.7	1.3	135	-2
6b	3.7	0.6	135	-14
8	3.0	0.6	142	16
20	2.7	0.7	137	3
21	1.7	-0.7	115	-39
23	2.2	-0.5	119	-15
27	2.4	-0.3	159	29
28	2.6	-0.1	150	13
29	3.1	0.4	155	17
31	2.1	-0.7	146	8
Mean		0.2		0.1
St. Dev.		0.6		18.3

Site	Run: A-K ₁				Run: C-K ₁				Run: D-K ₁			
	Amplitude		Phase Lag		Amplitude		Phase Lag		Amplitude		Phase Lag	
	Mod	Diff	Mod	Diff	Mod	Diff	Mod	Diff	Mod	Diff	Mod	Diff
	cm	cm	°	°	cm	cm	°	°	cm	cm	°	°
1	6.8	1.0	137	-3	6.9	1.1	139	-1	6.8	1.0	139	-1
2	7.3	1.4	150	23	7.6	1.7	143	16	7.5	1.6	144	17
3	8.6	1.6	130	-7	8.3	1.3	135	-2	8.4	1.4	134	-3
4	7.9	1.1	131	-6	8.3	1.5	134	-3	8.4	1.6	133	-4
5a	6.9	1.8	129	-14	8.0	2.9	131	-12	8.0	2.9	130	-13
5b	6.9	2.1	129	-1	8.0	3.2	131	1	8.0	3.2	130	0
5c	6.9	2.6	129	-13	8.0	3.7	131	-11	8.0	3.7	130	-12
6a	11.5	3.0	143	-2	9.6	1.1	147	2	10.1	1.6	147	2
6b	11.5	2.5	143	9	9.6	0.6	147	13	10.1	1.1	147	13
6c	11.5	2.0	143	0	9.6	0.1	147	4	10.1	0.6	147	4
7	9.5	0.0	135	4	8.9	-0.6	139	8	9.0	-0.5	139	8
8	9.2	0.3	152	16	8.0	-0.9	153	17	8.1	-0.8	152	16
9	9.5	-2.9	162	6	7.8	-4.6	161	5	8.0	-4.4	160	4
10	7.5	-2.0	174	11	5.7	-3.8	167	4	5.8	-3.7	167	4
11	4.2	-4.9	148	-16	4.6	-4.5	129	-35	4.6	-4.5	132	-32
12	5.9	-1.4	150	-21	6.2	-1.1	139	-32	6.1	-1.2	141	-30
13	5.0	-3.2	151	-18	5.0	-3.2	135	-34	5.3	-2.9	135	-34
20	8.2	1.1	146	3	7.3	0.2	140	-3	7.2	0.1	141	-2
21	4.8	-3.4	130	-33	5.2	-3.0	127	-36	5.2	-3.0	127	-36
23	6.5	-1.6	129	-15	6.6	-1.5	129	-15	6.6	-1.5	129	-15
27	7.8	-0.7	166	25	7.9	-0.6	149	8	7.9	-0.6	149	8
28	8.6	-0.8	162	15	8.3	-1.1	154	7	8.3	-1.1	154	7
29	9.4	0.4	165	18	8.5	-0.5	153	6	8.6	-0.4	153	6
31	7.6	-1.7	156	2	7.8	-1.5	154	0	7.9	-1.4	154	0
Mean		-0.1		-0.7		-0.4		-3.9		-0.3		-3.9
St. Dev.		2.2		14.8		2.3		15.9		2.3		15.6

Table 7: *continued.*
Run: A-N₂

Site	Amplitude		Phase Lag	
	Mod	Diff	Mod	Diff
	cm	cm	°	°
2	7.9	-0.4	191	19
5a	3.2	1.3	135	-36
5b	3.2	1.4	135	-40
6a	16.3	2.3	192	2
6b	16.3	2.1	192	12
7	13.2	1.6	175	-9
8	12.6	1.0	203	12
9	13.6	1.5	217	-7
11	9.0	-2.9	262	13
20	12.7	1.8	175	0
21	9.4	-0.8	192	1
23	6.4	-0.4	153	-4
27	11.7	-0.4	204	1
28	14.2	-0.3	187	1
29	16.3	-0.5	209	3
31	14.2	-0.1	233	1
Mean		0.5		-1.9
St. Dev.		1.4		16.0

Site	Run: A-M ₂				C-M ₂			
	Amplitude		Phase Lag		Amplitude		Phase Lag	
	Mod	Diff	Mod	Diff	Mod	Diff	Mod	Diff
	cm	cm	°	°	cm	cm	°	°
1	26.6	-0.6	193	1	26.9	-0.3	193	1
2	43.3	-1.4	210	11	43.5	-1.2	206	7
3	52.7	3.2	186	-6	52.6	3.1	189	-3
4	32.6	1.5	187	-4	29.5	-1.6	182	-9
5a	8.4	-1.9	182	-16	7.4	-2.9	188	-10
5b	8.4	-1.5	182	-14	7.4	-2.5	188	-8
5c	8.4	-2.0	182	-19	7.4	-3.0	188	-13
6a	78.8	12.3	205	-6	73.3	6.8	208	-3
6b	78.8	13.7	205	-2	73.3	8.2	208	1
6c	78.8	9.1	205	-6	73.3	3.6	208	-3
7	63.0	3.7	194	-1	63.7	4.4	196	1
8	61.4	6.2	221	9	62.2	7.0	221	9
9	68.4	7.9	231	-3	66.7	6.2	232	-2
10	64.1	2.8	250	-3	61.6	0.3	249	-4
11	48.6	0.8	272	-3	47.6	-0.2	272	-3
12	32.6	-2.8	264	-10	31.7	-3.7	265	-9
13	41.8	-2.0	271	-4	45.0	1.2	269	-6
20	64.3	8.4	194	-2	64.4	8.5	194	-2
21	50.5	-0.4	212	0	50.2	-0.7	212	0
22	47.3	-3.7	216	3	47.0	-4.0	216	3
23	36.0	0.3	179	2	35.9	0.2	180	3
24	33.8	-2.2	182	5	33.8	-2.2	182	5
27	58.9	-0.5	225	0	58.9	-0.5	225	0
28	70.7	-2.1	208	1	70.7	-2.1	208	1
29	81.6	-2.1	229	1	81.7	-2.0	229	1
31	71.8	2.0	254	2	72.1	2.3	254	2
32	52.0	-4.0	255	0	52.1	-3.9	255	0
Mean		1.7	-2.4		0.8		-1.5	
St. Dev.		4.9	6.7		3.9		5.2	

Table 7: *continued.*

Site	Run: A-S ₂				Run: C-S ₂			
	Amplitude		Phase Lag		Amplitude		Phase Lag	
	Mod	Diff	Mod	Diff	Mod	Diff	Mod	Diff
	cm	cm	°	°	cm	cm	°	°
1	12.3	1.0	223	1	11.8	0.5	229	7
2	16.6	-0.9	241	9	17.2	-0.3	242	10
3	21.8	1.4	220	-8	20.5	0.1	215	-13
4	15.1	2.5	219	-3	13.4	0.8	216	-6
5a	7.1	1.7	206	-11	5.7	0.3	204	-13
5b	7.1	1.3	206	-20	5.7	-0.1	204	-22
5c	7.1	1.5	206	-12	5.7	0.1	204	-14
6a	30.0	5.2	242	-3	28.4	3.6	238	-7
6b	30.0	3.3	242	-3	28.4	1.7	238	-7
6c	30.0	3.9	242	-3	28.4	2.3	238	-7
7	24.8	6.3	229	-12	23.9	5.4	224	-17
8	23.6	1.1	253	6	23.5	1.0	248	1
9	25.2	7.9	265	-15	26.2	8.9	260	-20
10	22.6	1.4	285	-1	24.4	3.2	282	-4
11	16.0	4.8	307	4	18.7	7.5	305	2
12	10.9	-0.3	290	-19	12.6	1.4	290	-19
13	13.0	-2.4	301	-6	15.4	0.0	300	-7
20	24.8	2.6	228	-1	24.1	1.9	227	-2
21	19.6	0.0	242	-2	19.6	0.0	241	-3
23	15.4	0.2	212	-1	15.4	0.2	212	-1
27	22.4	-0.1	257	0	22.1	-0.4	257	0
28	27.2	-0.5	241	0	27.1	-0.6	241	0
29	31.1	-0.1	262	1	31.0	-0.2	262	1
31	26.8	0.8	288	1	26.5	0.5	288	1
32	19.0	-2.0	287	-6	19.0	-2.0	288	-5
Mean		1.6		-4.2		1.4		-5.8
St. Dev.		2.5		7.3		2.6		8.3

Run: A-K₂

Site	Run: A-K ₂			
	Amplitude		Phase Lag	
	Mod	Diff	Mod	Diff
	cm	cm	°	°
2	4.5	1.0	239	37
5a	2.3	0.7	200	-13
5b	2.3	0.2	200	1
6a	8.3	1.2	245	3
6b	8.3	-1.1	245	19
8	6.6	-0.6	253	21
20	6.9	0.6	228	1
21	5.2	-0.4	241	-1
23	4.1	-0.2	208	-4
27	6.4	-0.4	255	0
28	7.8	-0.1	239	1
29	8.9	0.0	261	2
31	7.5	0.2	286	4
Mean		0.1		5.5
St. Dev.		0.7		12.9

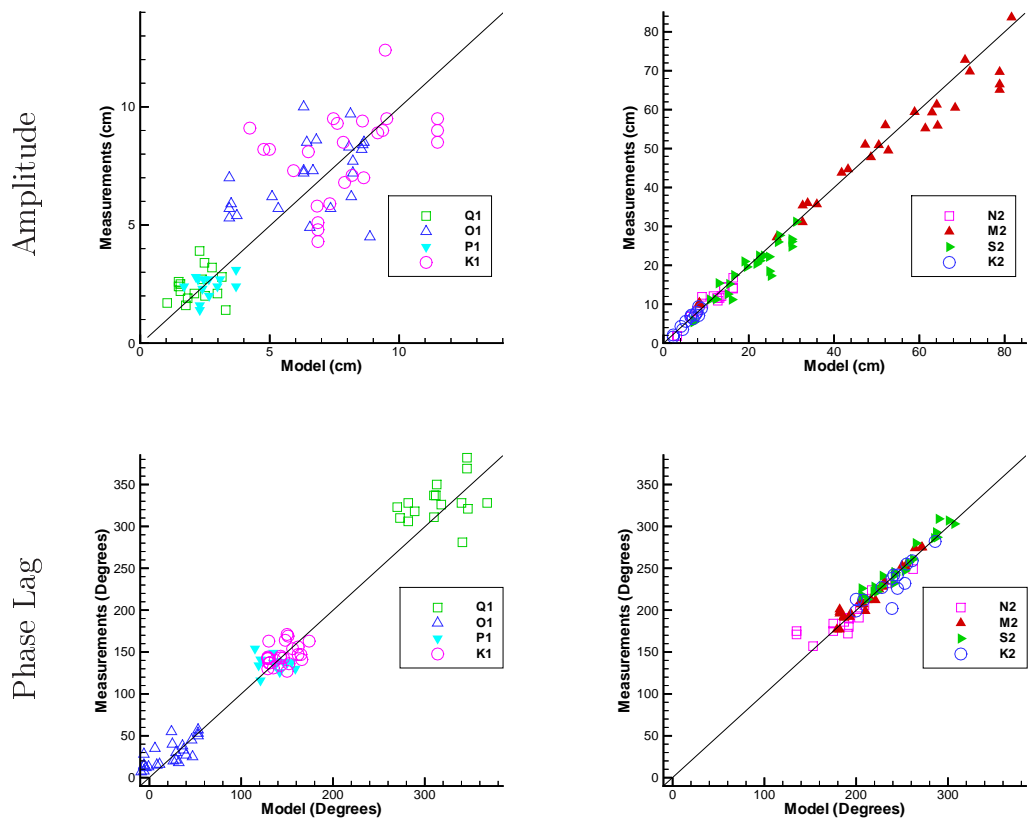


Figure 4: Scattering diagrams for comparison between observed and computed elevation amplitudes (upper) and phase lag (lower) for the diurnal- (left) and semidiurnal (right) constituents for run A. The line indicate 100% correlation.

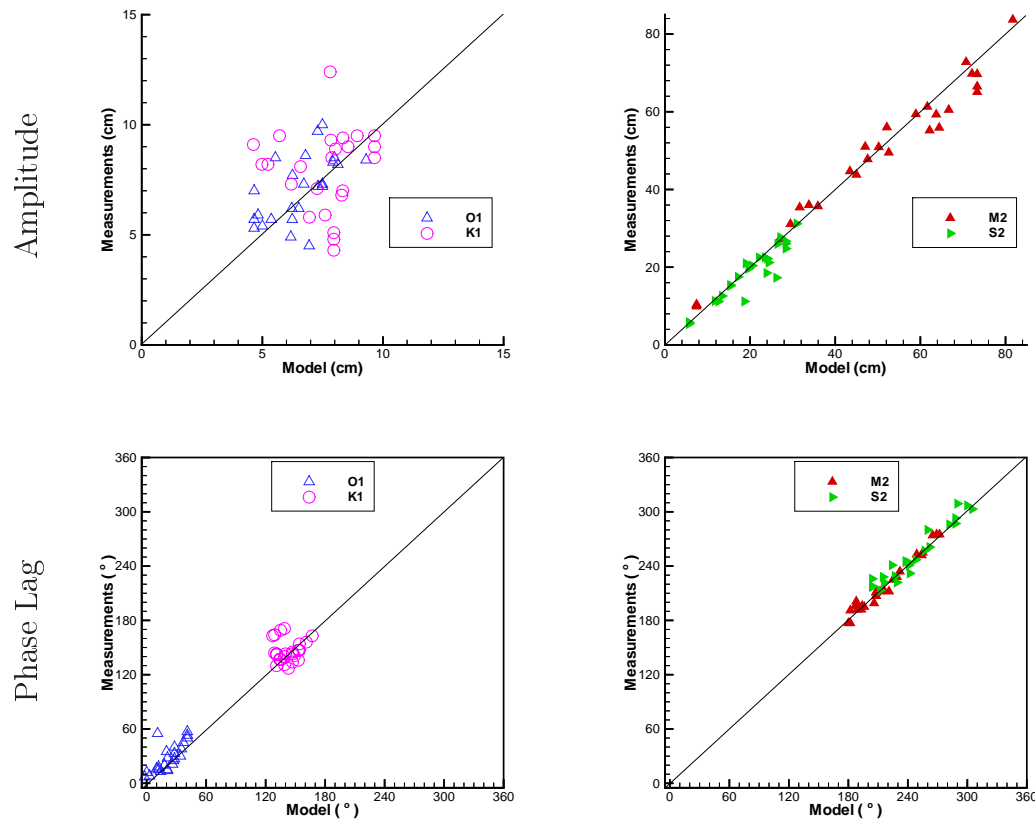


Figure 5: Scattering diagrams for comparison between observed and computed elevation amplitudes (upper) and phase lag (lower) for the diurnal- (left) and semidiurnal (right) constituents for run C. The line indicate 100% correlation.

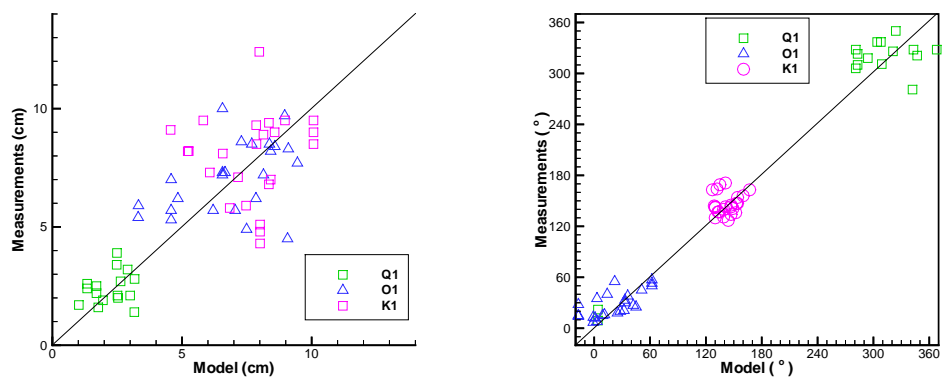


Figure 6: Scattering diagrams for comparison between observed and computed elevation amplitudes (left) and phase lag (right) for the diurnal constituents in run D. The line indicate 100% correlation.

3.3 Harmonic constants from measured current data

Tidal information derived from current meter data is adopted from Hansen and Larsen [1999] and some few stations (Sites Ve, No, S8, and S9) from other sources (Table 5). The data from Hansen and Larsen [1999] is all from series of a least 28 days length. For series where the duration is to short to resolve P_1 and K_2 (182.6 days), these constituents are inferred from K_1 and S_2 , respectively. At Sites S8 and S9 no attempt is done to estimate P_1 and K_2 , and for sites Ve and No it is referred to the respective sources for details. Barotropic tidal current constituents at fixed ADCP sites area adopted from Sherwin et al. [1999]. Current profile data from the ADCP measurements in the Nordic WOCE/VEINS project across the Faroe Shetland Channel, in the Faroe Bank Channel and north of the Faroes exist at the Fisheries Laboratory of the Faroes, and tidal analysis of these data are in progress, but unfortunately not completed in time to be included in the present report.

Hansen and Larsen [1999] provides tidal data from several time series at some of their sites. Although all time series are not from exactly the same position the spread in positions at one site is however of the same order as the resolution in the present model. At sites where several time series are available the mean and standard deviation is estimated for the sites as presented in Table 8.

Table 8: Harmonic constants derived from measured current data. Amplitude and Greenwich phase lag for east and north component, major- and minor semiaxis, inclination relative to east and Greenwich phase lag in the tidal ellipses, and number of time series included. Negative minor semi axis indicate anticyclonic (clockwise) rotation. At sites where more than one timeseries exist [Hansen and Larsen, 1999] the cited values are the mean of the analysed series on the site and standard deviation is given in the brackets below.

Site	East		North		Major	Minor	Incl.	Grpl	Series
	Amp $mm s^{-1}$	Grpl °	Amp $mm s^{-1}$	Grpl °					
<i>Constituent: Q1</i>									
Ve	0	63	0	131	63	0	90	131	1
No	12	18	198	216	21	3	56	210	1
S1	88	290	62	169	96	-48	152	125	1
S2	47	293	19	205	47	19	59	233	6
	(8)	(5)	(4)	(14)	(8)	(4)	(86)	(90)	
S3	17	322	23	123	28	5	125	129	1
S8	8	3	258	209	8	-2	14	253	1
S9	15	11	261	70	18	1	143	77	1
W1	8	156	11	236	13	-3	106	181	7
	(2)	(176)	(4)	(50)	(3)	(1)	(39)	(76)	
W2	27	340	25	227	30	-20	141	188	1
N1	40	330	12	262	40	-11	6	328	4
	(8)	(9)	(6)	(9)	(8)	(5)	(2)	(9)	
N2	42	261	29	232	50	-11	32	253	2
	(0)	(12)	(7)	(2)	(4)	(2)	(7)	(12)	
N3	39	343	27	182	47	-8	147	169	1
N5	12	40	6	10	13	-3	26	34	1
E1	8	226	11	209	13	-2	53	215	1
E2	9	253	16	240	19	-1	61	243	14
	(3)	(12)	(3)	(9)	(3)	(1)	(9)	(9)	
F1	15	196	12	146	17	-8	34	179	1
F2	29	142	28	62	31	-26	37	110	1

To be continued on the following page

Table 8: *continued from previous page*

Site	East		North		Major $mm s^{-1}$	Minor $mm s^{-1}$	Incl. °	Grpl	Series
	Amp $mm s^{-1}$	Grpl °	Amp $mm s^{-1}$	Grpl °					
<i>Constituent: O1</i>									
Ve	0	161	0	169	161	0	90	169	1
No	25	38	268	252	45	-5	57	256	1
S1	154	326	122	217	164	-108	153	165	1
S2	123	322	69	232	123	-69	59	263	6
	(13)	(3)	(8)	(4)	(13)	(7)	(89)	(91)	
S3	90	327	108	142	140	6	130	144	1
S8	37	19	285	193	37	-18	178	105	1
S9	42	22	313	130	47	1	152	132	1
W1	17	72	23	252	26	-12	120	240	7
	(3)	(127)	(9)	(16)	(8)	(6)	(15)	(16)	
W2	62	36	90	254	104	-33	122	243	1
N1	92	350	31	276	92	-30	6	348	4
	(5)	(4)	(7)	(6)	(5)	(7)	(3)	(4)	
N2	77	286	53	262	92	-18	33	278	2
	(7)	(1)	(14)	(1)	(13)	(6)	(4)	(2)	
N3	70	30	49	244	83	-24	147	220	1
N5	17	67	9	323	17	-9	170	253	1
E1	18	264	40	253	44	-3	66	255	1
E2	24	277	38	264	45	-5	57	267	14
	(3)	(6)	(5)	(4)	(5)	(2)	(3)	(4)	
F1	53	237	55	166	63	-44	48	198	1
F2	76	183	85	113	94	-64	55	139	1
B1	7	294	8	333	10	4	50	317	1
B2	5	340	7	276	8	-4	64	291	1
B3	18	73	18	323	21	-15	135	288	1

To be continued on the following page

Table 8: *continued from previous page*

Site	East		North		Major	Minor	Incl.	Grpl	Series
	Amp $mm s^{-1}$	Grpl °	Amp $mm s^{-1}$	Grpl °					
<i>Constituent: P1</i>									
Ve	0	47	0	36	47	0	90	36	1
No	9	12	143	138	14	0	53	139	1
S1	37	176	32	62	41	-26	145	19	1
S2	32	172	19	82	32	-19	89	262	6
	(4)	(3)	(1)	(3)	(4)	(1)	(95)	(103)	
S3	14	208	15	18	20	2	131	22	1
W1	4	191	7	72	7	-3	107	65	7
	(1)	(35)	(1)	(25)	(1)	(0)	(12)	(25)	
W2	17	236	19	95	24	-8	130	79	1
N1	31	218	10	136	31	-10	2	217	4
	(0)	(4)	(2)	(7)	(0)	(2)	(2)	(4)	
N2	30	161	17	125	33	-9	26	154	2
	(5)	(7)	(7)	(1)	(7)	(5)	(5)	(2)	
N3	17	275	10	113	20	-3	150	100	1
N5	3	274	3	167	3	-2	132	134	1
E1	7	139	12	111	13	-3	61	118	1
E2	9	138	11	117	14	-2	50	126	14
	(1)	(7)	(1)	(10)	(1)	(1)	(5)	(8)	
F1	16	80	12	1	17	-12	16	69	1
F2	40	54	42	335	45	-37	52	7	1
<i>Constituent: K1</i>									
Ve	0	175	0	25	174	0	90	25	1
No	26	35	143	138	43	-1	53	139	1
S1	114	194	92	81	124	-78	150	34	1
S2	96	189	58	103	96	-57	33	157	6
	(13)	(4)	(4)	(3)	(13)	(4)	(70)	(70)	
S3	44	221	43	32	62	5	136	37	1
S8	24	18	138	70	25	-15	26	121	1
S9	23	12	182	51	24	-8	158	9	1
W1	12	212	21	89	23	-9	111	80	7
	(5)	(31)	(3)	(27)	(5)	(2)	(13)	(26)	
W2	54	254	54	112	72	-25	135	93	1
N1	94	234	34	163	94	-32	7	231	4
	(1)	(4)	(6)	(7)	(1)	(7)	(2)	(4)	
N2	83	171	56	144	98	-21	31	163	2
	(9)	(1)	(21)	(0)	(17)	(7)	(7)	(4)	
N3	55	288	27	128	61	-9	154	112	1
N5	8	293	8	186	10	-7	136	148	1
E1	18	157	37	127	40	-9	65	132	1
E2	24	154	35	136	42	-6	55	142	14
	(4)	(6)	(2)	(9)	(3)	(1)	(4)	(7)	
F1	49	98	37	21	50	-35	20	83	1
F2	120	73	129	353	136	-112	57	22	1
B1	27	190	19	91	27	-19	168	18	1
B2	16	187	13	111	17	-12	25	169	1
B3	29	192	25	105	29	-25	10	184	1

To be continued on the following page

Table 8: *continued from previous page*

Site	East		North		Major	Minor	Incl.	Grpl	Series
	Amp mm s^{-1}	Grpl °	Amp mm s^{-1}	Grpl °					
<i>Constituent: N2</i>									
Ve	0	311	0	120	310	0	90	120	1
No	82	132	189	190	155	1	58	189	1
S1	190	251	113	162	190	-113	1	250	1
S2	136	252	68	180	138	-64	11	247	6
	(9)	(6)	(5)	(6)	(9)	(6)	(1)	(5)	
S3	67	247	79	59	104	7	130	62	1
S8	59	19	203	130	59	-18	5	201	1
S9	47	28	233	206	53	-11	29	226	1
W1	46	245	60	158	61	-44	85	161	7
	(5)	(6)	(8)	(6)	(8)	(6)	(14)	(16)	
W2	36	259	59	137	63	-29	113	126	1
N1	99	274	34	214	101	-28	10	271	4
	(13)	(7)	(9)	(21)	(13)	(9)	(4)	(7)	
N2	116	245	84	203	134	-48	32	232	2
	(15)	(2)	(21)	(2)	(21)	(16)	(3)	(1)	
N3	86	301	79	161	110	-40	138	138	1
N5	29	317	24	251	32	-20	32	296	1
E1	35	214	60	181	67	-17	62	189	1
E2	50	224	59	198	76	-17	50	208	14
	(6)	(7)	(5)	(7)	(6)	(2)	(3)	(6)	
F1	69	243	68	162	74	-63	42	205	1
F2	63	258	73	171	74	-63	81	178	1
B1	38	228	10	223	39	-1	15	228	1
B2	20	243	33	235	39	-2	59	237	1
B3	43	211	8	189	44	-3	10	210	1
<i>Constituent: M2</i>									
Ve	0	1823	0	159	1822	0	90	159	1
No	358	559	220	222	663	10	57	221	1
S1	777	274	498	196	789	-479	12	266	1
S2	660	275	360	204	674	-334	13	269	6
	(40)	(1)	(19)	(2)	(42)	(15)	(1)	(1)	
S3	342	263	567	82	662	8	121	82	1
S8	264	118	246	198	276	-83	18	240	1
S9	188	127	264	241	222	-41	33	257	1
W1	247	272	305	184	307	-244	87	185	7
	(36)	(6)	(34)	(3)	(34)	(37)	(10)	(8)	
W2	264	290	339	166	383	-194	123	148	1
N1	495	298	195	231	503	-174	10	294	4
	(27)	(2)	(19)	(8)	(24)	(15)	(4)	(2)	
N2	536	266	441	225	651	-242	37	250	2
	(75)	(4)	(131)	(1)	(117)	(91)	(4)	(0)	
N3	328	323	298	196	396	-198	140	166	1
N5	116	328	79	272	127	-59	28	314	1
E1	214	257	347	216	387	-126	62	226	1
E2	253	255	308	221	383	-111	51	234	14
	(30)	(1)	(23)	(1)	(32)	(14)	(2)	(1)	
F1	262	272	277	189	288	-250	56	219	1
F2	323	275	352	194	365	-308	60	219	1
B1	189	245	43	232	194	-9	13	244	1
B2	127	254	89	249	155	-6	35	252	1
B3	182	230	53	224	189	-5	16	230	1

To be continued on the following page

Table 8: *continued from previous page*

Site	East		North		Major	Minor	Incl.	Grpl	Series
	Amp	Grpl	Amp	Grpl					
<i>Constituent: S2</i>									
Ve	0	581	0	194	581	0	90	194	1
No	154	226	281	280	273	-2	55	280	1
S1	256	311	146	232	258	-142	9	306	1
S2	230	311	111	239	233	-104	10	306	6
	(13)	(1)	(3)	(3)	(13)	(4)	(1)	(1)	
S3	116	304	191	113	223	19	121	116	1
S8	108	41	279	259	114	-13	19	276	1
S9	79	48	307	285	91	-15	30	301	1
W1	80	304	100	221	102	-77	76	231	7
	(9)	(11)	(6)	(8)	(6)	(9)	(10)	(11)	
W2	86	327	133	207	143	-70	114	194	1
N1	171	334	60	267	174	-53	9	331	4
	(5)	(3)	(7)	(8)	(5)	(5)	(4)	(4)	
N2	186	301	141	263	221	-74	35	288	2
	(18)	(4)	(39)	(0)	(31)	(26)	(5)	(0)	
N3	117	7	108	237	144	-67	139	209	1
N5	43	12	18	333	45	-11	19	7	1
E1	67	285	111	256	126	-29	60	263	1
E2	89	285	105	259	134	-30	50	270	14
	(9)	(2)	(6)	(2)	(9)	(3)	(3)	(2)	
F1	85	311	97	229	100	-83	68	247	1
F2	93	310	102	232	108	-86	57	259	1
B1	55	274	17	280	58	2	17	275	1
B2	50	286	24	288	55	1	26	286	1
B3	56	259	18	273	59	4	17	260	1
<i>Constituent: K2</i>									
Ve	0	186	0	180	186	0	90	180	1
No	51	75	281	280	90	0	55	280	1
S1	70	311	40	232	70	-38	9	306	1
S2	62	311	30	239	63	-28	10	306	6
	(3)	(1)	(1)	(4)	(3)	(1)	(1)	(1)	
S3	31	304	52	113	61	5	121	116	1
W1	21	303	27	220	27	-20	76	230	7
	(2)	(11)	(1)	(8)	(1)	(2)	(10)	(11)	
W2	23	327	36	207	39	-19	114	194	1
N1	46	334	16	267	47	-14	9	331	4
	(1)	(3)	(1)	(8)	(1)	(1)	(4)	(3)	
N2	53	305	42	265	63	-23	36	291	2
	(8)	(10)	(15)	(2)	(13)	(11)	(7)	(2)	
N3	32	12	29	242	39	-18	139	214	1
N5	12	12	5	333	12	-3	19	7	1
E1	18	285	30	256	34	-8	60	263	1
E2	25	285	28	259	37	-8	49	270	14
	(3)	(2)	(2)	(2)	(3)	(1)	(3)	(2)	
F1	23	311	26	229	27	-22	68	247	1
F2	25	310	28	232	29	-23	57	259	1

3.4 Validation of the current simulation

The tidal current ellipse parameters are compared in Tables 9–11 and as scatter plots in Figures 8–9. Mean and standard deviation of the difference between model and data derived ellipse parameters, and also the ratio of the model to the data derived axis lengths are provided for each constituent in Tables 9–11. In the estimates of the mean and standard deviations the results from the coastal sites (No, Ve and S3) are not included.

When comparing the model results with data from moored current meters the origin of the data must be included in the considerations. The model provides a depth averaged current, while the current meter provides the current at a particular depth. However, in strong currents the mooring may be pushed deeper by the current, which influence the depth and possibly also the angle between the current direction and anemometer on the instrument. Although the tidal current at least theoretically may be considered as barotropic when the depth exceeds 50 m [Prandle, 1997] local baroclinic effects may influence the measured data in particular in areas with steep topography. Areas with changing bathymetry may not be properly represented in the model due to insufficient resolution, which implies that the model derived inclination and phase of the current motion differ considerably from the values derived from measured data.

In the linear simulation (Run A) the length of the major axis is generally in good agreement with the data based axis lengths for the semidiurnal current, while it is roughly twice the data based lengths for the diurnal current. Including the advective terms and viscosity (Run C) the semidiurnal major axis are slightly below data based values, while the diurnal major axis are reduced to be roughly 130% of the data based values. In general the modelled semi diurnal major axis, inclination and phase are in excellent agreement with the data based parameters, while minor axis are larger at nearly all sites. To large minor axis may partly be explained by coarse resolution. The diurnal tidal currents differ more from the data based values, which is not unexpected from the deviation between data time series at the same site, in particular at Sites S2 and W1 (Table 8), and the appearance of topographically trapped waves mentioned in Section 3.2.

Better simulation of the diurnal tide may be obtained by improving the representation of friction felt by the diurnal tide, which partly arise from the semi diurnal tide. This may be mimicked by increasing the friction coefficient for the diurnal tide [Kowalik, 1994] as done in Run D, but this seems not to improve the agreement between model and data derived current parameters. Other model approaches is to use the calculated semidiurnal current in the estimate of the friction felt by the diurnal tide through a linear bottom friction (Eq. 5) or more sophisticated friction tensors [Sinha and Pingree, 1997], but these options are not explored for the present report.

Table 9: Length of major and minor semi axis, inclination, and net phase of current ellipses at measurements sites derived by a linear model with quadratic friction terms. The difference from the corresponding variable derived from measured data (Table 5) and for the lengths also the ratio between model derived and data based values is also provided. Negative minor semi axis indicate anticyclonic (clockwise) rotation, and negative ratio indicate different rotation directions.

Site	Major			Minor			Inclination		Phase	
	Mod mm s ⁻¹	Diff mm s ⁻¹	Ratio %	Mod mm s ⁻¹	Diff mm s ⁻¹	Ratio %	Mod °	Diff °	Mod °	Diff °
<i>Constituent: Q₁</i>										
Ve	213	150	338	-16	16	0	126	36	207	76
No	6	-15	29	-1	-2	-33	97	41	245	35
S1	150	54	156	-119	71	248	111	-41	134	9
S2	99	52	211	-84	65	-442	137	78	111	-122
S3	110	82	393	9	4	180	135	10	123	-6
S8	53	45	663	-42	40	2100	5	-9	247	-6
S9	33	15	183	-5	4	-500	160	17	133	56
W1	19	6	146	-7	4	233	160	54	208	27
W2	131	101	437	-103	83	515	141	0	160	-28
N1	26	-14	65	-7	-4	64	38	32	40	72
N2	56	6	112	-35	24	318	157	-55	147	74
N3	54	7	115	-46	38	575	132	-15	208	39
N5	15	2	115	1	-2	-33	64	38	205	171
E1	24	11	185	-16	14	800	6	-47	138	-77
E2	38	19	200	-29	28	2900	179	-62	14	-49
F1	124	107	729	-100	92	1250	40	6	144	-35
F2	51	20	165	-24	-2	92	122	85	281	171
Mean	30.8	248.7		32.5	719.3			5.8		21.6
St.dev.	36.6	208.3		33.4	834.4			47.7		84.7
<i>Constituent: O₁</i>										
Ve	559	398	347	-24	24	0	126	36	223	54
No	135	90	300	-29	24	580	93	36	287	31
S1	304	140	185	-244	136	226	120	-33	212	47
S2	192	69	156	-163	94	236	148	89	186	-77
S3	221	81	158	6	0	100	134	4	193	49
S8	82	45	222	-61	43	339	11	-167	317	-148
S9	40	-7	85	-8	7	-800	161	9	205	73
W1	32	6	123	-10	-2	83	25	-95	90	-150
W2	229	125	220	-171	138	518	143	21	242	-1
N1	119	27	129	-50	20	167	8	2	25	37
N2	111	19	121	-77	59	428	164	-49	175	77
N3	103	20	124	-71	47	296	158	11	250	30
N5	14	-3	82	5	-4	-56	33	-137	297	44
E1	46	2	105	-5	2	167	39	-27	254	-1
E2	77	32	171	-42	37	840	29	-28	277	10
F1	210	147	333	-165	121	375	47	-1	232	34
F2	103	9	110	-69	5	108	166	-69	36	77
B1	56	46	560	7	3	175	121	71	107	150
B2	29	21	363	27	23	-675	104	40	102	171
B3	62	41	295	-15	0	100	125	-10	132	-156
Mean	43.5	199.1		42.9	328.7			-21.9		12.8
St.dev.	49.0	126.0		49.8	248.0			67.3		96.3

continue on the following page ...

Table 9: *continued from previous page.*

Site	Major			Minor			Inclination		Phase	
	Mod mm s ⁻¹	Diff mm s ⁻¹	Ratio %	Mod mm s ⁻¹	Diff mm s ⁻¹	Ratio %	Mod °	Diff °	Mod °	Diff °
<i>Constituent: P₁</i>										
Ve	201	154	428	-14	14	0	127	37	128	92
No	21	7	150	-4	4	0	94	41	172	33
S1	39	-2	95	-36	10	138	119	-26	146	127
S2	24	-8	75	-23	4	121	138	49	116	-146
S3	27	7	135	3	1	150	135	4	67	45
W1	19	12	271	-12	9	400	106	-1	67	2
W2	20	-4	83	-11	3	138	23	-107	347	-92
N1	72	41	232	-43	33	430	2	0	298	81
N2	31	-2	94	-23	14	256	167	141	89	-65
N3	82	62	410	-74	71	2467	15	-135	355	-105
N5	21	18	700	9	7	-450	65	-67	273	139
E1	12	-1	92	-6	3	200	179	-62	331	33
E2	15	1	107	-9	7	450	1	-49	188	62
F1	28	11	165	-26	14	217	68	52	171	102
F2	31	-14	69	-25	-12	68	97	45	339	-28
Mean		9.5	199.5		13.6	444.5		-13.3		9.2
St.dev.		22.0	188.4		20.8	651.8		77.4		96.4
<i>Constituent: K₁</i>										
Ve	626	452	360	-23	23	0	126	36	128	103
No	82	39	191	-15	14	1500	94	41	179	40
S1	141	17	114	-126	48	162	123	-27	142	108
S2	90	-6	94	-82	25	144	140	107	117	-40
S3	104	42	168	7	2	140	135	-1	76	39
S8	45	20	180	-32	17	213	12	-14	227	106
S9	21	-3	88	-4	-4	50	173	15	90	81
W1	54	31	235	-28	19	311	107	-4	75	-5
W2	62	-10	86	-28	3	112	8	-127	346	-107
N1	227	133	241	-133	101	416	4	-3	304	73
N2	102	4	104	-76	55	362	172	141	86	-77
N3	242	181	397	-220	211	2444	16	-138	2	-110
N5	64	54	640	27	20	-386	72	-64	290	142
E1	39	-1	98	-19	10	211	14	-51	156	24
E2	51	9	121	-32	26	533	13	-42	189	47
F1	57	7	114	-56	21	160	176	156	116	33
F2	85	-51	63	-80	-32	71	104	47	4	-18
B1	67	40	248	-10	-9	53	128	-40	15	-3
B2	36	19	212	18	6	-150	127	-78	25	36
B3	84	55	290	-45	20	180	125	-65	35	31
Mean		29.4	195.5		31.6	350.5		-11.0		18.9
St.dev.		54.9	146.3		54.5	556.8		83.9		73.5

continue on the following page ...

Table 9: *continued from previous page.*

Site	Major			Minor			Inclination		Phase	
	Mod mm s ⁻¹	Diff mm s ⁻¹	Ratio %	Mod mm s ⁻¹	Diff mm s ⁻¹	Ratio %	Mod °	Diff °	Mod °	Diff °
<i>Constituent: N₂</i>										
Ve	738	428	238	-16	16	0	127	37	181	61
No	261	106	168	-25	24	-2500	92	34	238	49
S1	150	-40	79	-97	-16	86	14	13	254	4
S2	122	-16	88	-65	1	102	25	14	246	-1
S3	172	68	165	5	-2	71	132	2	103	41
S8	61	2	103	-21	3	117	31	26	235	34
S9	48	-5	91	-11	0	100	32	3	234	8
W1	64	3	105	-50	6	114	110	25	167	6
W2	80	17	127	-44	15	152	143	30	129	3
N1	120	19	119	-45	17	161	15	5	290	19
N2	130	-4	97	-81	33	169	63	31	231	-1
N3	108	-2	98	-66	26	165	139	1	157	19
N5	18	-14	56	-10	-10	50	10	-22	288	-8
E1	86	19	128	-27	10	159	66	4	227	38
E2	89	13	117	-31	14	182	56	6	232	24
F1	63	-11	85	-56	-7	89	68	26	209	4
F2	83	9	112	-69	6	110	58	-23	215	37
B1	34	-5	87	4	3	-400	14	-1	228	0
B2	32	-7	82	3	1	-150	30	-29	241	4
B3	41	-3	93	-3	0	100	3	-7	220	10
Mean	-1.5	98.2		6.0	141.4		6.0		11.8	
St.dev.	14.9	18.8		12.4	76.0		18.7		14.2	
<i>Constituent: M₂</i>										
Ve	2633	811	145	7	7	0	128	38	171	12
No	1102	439	166	-104	94	-1040	90	33	235	14
S1	735	-54	93	-449	-30	94	8	-4	266	0
S2	596	-78	88	-290	-44	87	20	7	258	-11
S3	785	123	119	-30	22	-375	130	9	93	11
S8	295	19	107	-92	9	111	24	6	246	6
S9	234	12	105	-46	5	112	27	-6	248	-9
W1	282	-25	92	-232	-12	95	104	17	173	-12
W2	381	-2	99	-196	2	101	142	19	132	-16
N1	557	54	111	-182	8	105	14	4	294	0
N2	582	-69	89	-341	99	141	56	19	243	-7
N3	476	80	120	-288	90	145	140	0	159	-7
N5	97	-30	76	-42	-17	71	7	-21	297	-17
E1	371	-16	96	-96	-30	76	64	2	232	6
E2	395	12	103	-110	-1	99	52	1	238	4
F1	287	-1	100	-258	8	103	65	9	211	-8
F2	386	21	106	-327	19	106	47	-13	225	6
B1	175	-19	90	16	7	-178	4	-9	236	-8
B2	154	-1	99	21	15	-350	24	-11	252	0
B3	222	33	117	-31	26	620	174	-22	50	0
Mean	-3.8	99.6		9.1	152.6		-0.1		-4.3	
St.dev.	41.2	11.1		37.3	136.4		12.6		7.6	

continue on the following page ...

Table 9: continued from previous page.

Site	Major			Minor			Inclination		Phase	
	Mod mm s ⁻¹	Diff mm s ⁻¹	Ratio %	Mod mm s ⁻¹	Diff mm s ⁻¹	Ratio %	Mod °	Diff °	Mod °	Diff °
<i>Constituent: S₂</i>										
Ve	1114	533	192	-14	14	0	127	37	229	35
No	413	140	151	-38	36	1900	91	36	289	9
S1	238	-20	92	-141	-1	99	13	4	304	-2
S2	194	-39	83	-92	-12	88	23	13	298	-8
S3	268	45	120	3	-16	16	132	11	149	33
S8	96	-18	84	-26	13	200	28	9	287	11
S9	80	-11	88	-13	-2	87	30	0	287	-14
W1	95	-7	93	-78	1	101	108	32	217	-14
W2	121	-22	85	-66	-4	94	145	31	174	-20
N1	205	31	118	-75	22	142	15	6	339	8
N2	209	-12	95	-123	49	166	59	24	283	-5
N3	181	37	126	-117	50	175	141	2	207	-2
N5	39	-6	87	-19	8	173	8	-11	337	-30
E1	135	9	107	-38	9	131	66	6	282	19
E2	139	5	104	-42	12	140	54	4	286	16
F1	87	-13	87	-78	-5	94	51	-17	268	21
F2	117	9	108	-96	10	112	45	-12	267	8
B1	59	1	102	12	10	600	7	-10	275	0
B2	54	-1	98	10	9	1000	27	1	292	6
B3	74	15	125	-2	-2	-50	175	-22	87	7
Mean	-2.5	98.9		9.8	203.0			3.5		0.1
St.dev.	19.2	14.0		17.1	238.8			15.5		14.1
<i>Constituent: K₂</i>										
Ve	333	147	179	-11	11	0	127	37	243	63
No	120	30	133	-10	10	0	92	37	298	18
S1	65	-5	93	-39	1	103	17	8	308	2
S2	53	-10	84	-25	-3	89	27	17	301	-5
S3	72	11	118	3	-2	60	132	11	161	45
W1	27	0	100	-21	1	105	105	29	230	0
W2	33	-6	85	-19	0	100	146	32	183	-11
N1	58	11	123	-23	9	164	15	6	343	12
N2	57	-6	90	-33	10	143	62	26	286	-5
N3	53	14	136	-35	17	194	140	1	215	1
N5	11	-1	92	-6	3	200	11	-8	338	-29
E1	40	6	118	-12	4	150	68	8	288	25
E2	41	4	111	-13	5	163	58	9	293	23
F1	24	-3	89	-20	-2	91	64	-4	271	24
F2	29	0	100	-22	-1	96	57	0	272	13
Mean	0.3	101.7		3.7	133.2			10.3		4.2
St.dev.	7.2	16.7		5.8	40.9			13.1		16.1

continue on the following page ...

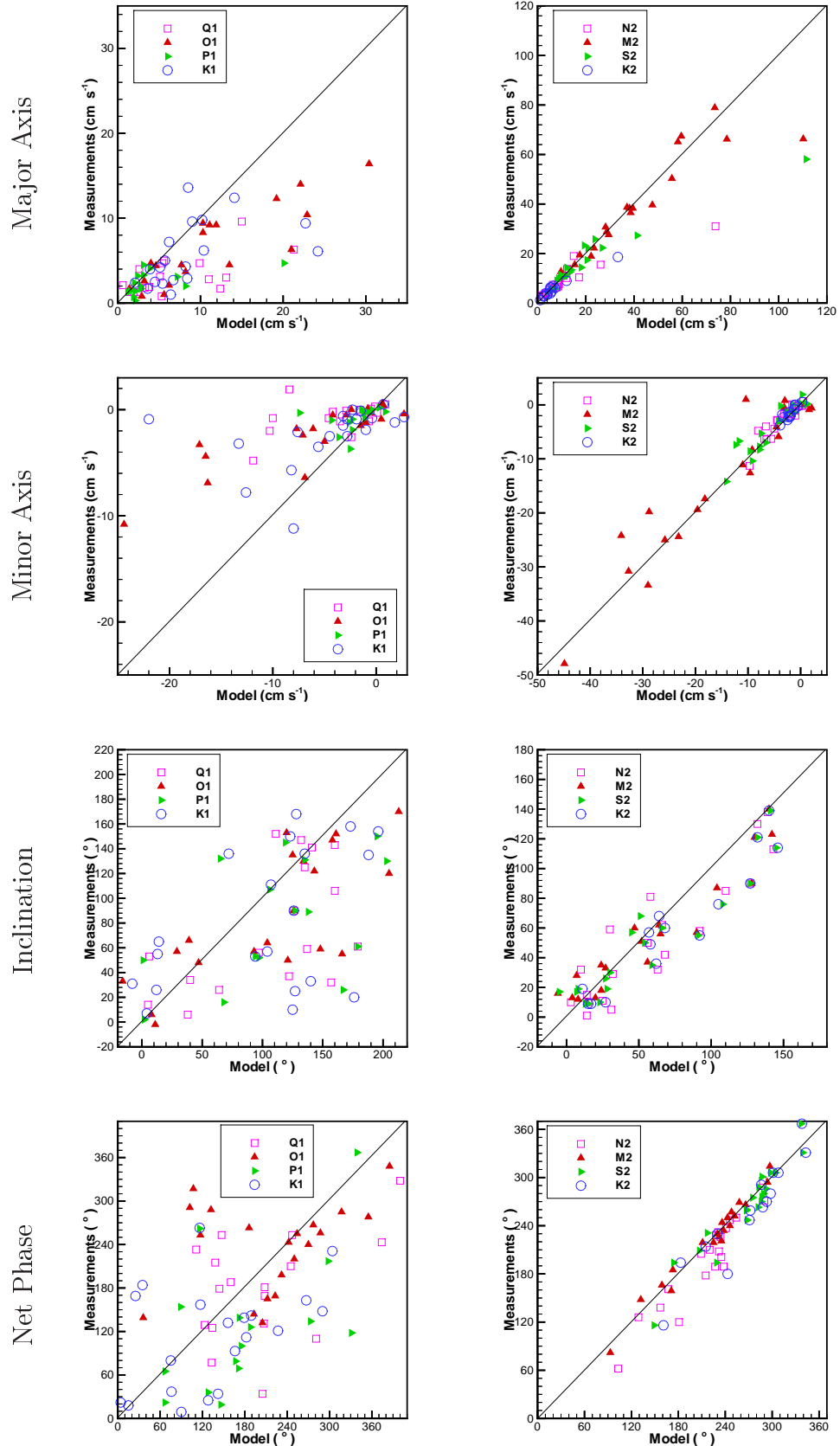


Figure 7: Scattering diagrams for comparison between observed and computed length of major (top) and minor semi ellipse axis, inclination, and net phase (bottom) for the diurnal (left) and semi diurnal (right) constituents in run A. The line indicate 100% correlation.

Table 10: Length of major and minor semi axis, inclination, and net phase of current ellipses at measurements sites derived by a non-linear model with quadratic friction terms (Run C). The difference from the corresponding variable derived from measured data (Table 5) and for the lengths also the ratio between model derived and data based values is provided. Negative minor semi axis indicate anticyclonic (clockwise) rotation, and negative ratio indicate different rotation directions.

Site	Major			Minor			Inclination		Phase	
	Mod mm s ⁻¹	Diff mm s ⁻¹	Ratio %	Mod mm s ⁻¹	Diff mm s ⁻¹	Ratio %	Mod °	Diff °	Mod °	Diff °
<i>Constituent: O1</i>										
Ve	415	254	258	-6	6	0	125	35	190	21
No	144	99	320	-42	37	840	88	31	252	-4
S1	183	19	112	-132	24	122	117	-36	204	39
S2	108	-15	88	-80	11	116	140	81	185	-78
S3	141	1	101	-3	-3	-50	134	4	147	3
S8	32	-5	86	-17	-1	94	17	19	296	11
S9	24	-23	51	3	2	300	12	40	357	45
W1	34	8	131	-23	11	192	119	-1	207	-33
W2	125	21	120	-73	40	221	153	31	232	-11
N1	79	-13	86	-21	-9	70	166	-20	150	-18
N2	62	-30	67	-45	27	250	179	-34	144	46
N3	110	27	133	-80	56	333	151	4	207	-13
N5	32	15	188	19	10	-211	105	-65	297	44
E1	54	10	123	-11	8	367	64	-2	249	-6
E2	60	15	133	-24	19	480	53	-4	260	-7
F1	190	127	302	-134	90	305	41	-7	259	61
F2	115	21	122	-57	-7	89	37	-18	266	127
B1	19	9	190	-6	2	-150	156	106	240	-77
B2	11	3	138	-3	-1	75	23	-41	47	116
B3	24	3	114	-17	2	113	74	-61	340	52
Mean		11.3	128.5		16.7	205.2		-0.5		17.5
St.dev.		34.0	57.6		25.4	119.0		45.8		57.2
<i>Constituent: K1</i>										
Ve	357	183	205	-18	18	0	122	32	130	105
No	46	3	107	-6	5	600	91	38	264	125
S1	46	-78	37	-34	-44	44	155	5	45	11
S2	42	-54	44	-31	-26	54	172	-41	26	49
S3	45	-17	73	2	-3	40	133	-3	65	28
S8	32	7	128	-21	6	140	180	-26	5	64
S9	22	-2	92	-1	-7	13	166	8	44	35
W1	19	-4	83	0	-9	0	75	-36	61	-19
W2	65	-7	90	-51	26	204	112	-23	105	12
N1	167	73	178	-93	61	291	6	-1	326	95
N2	90	-8	92	-65	44	310	174	-37	163	100
N3	167	106	274	-145	136	1611	158	4	216	104
N5	27	17	270	11	4	-157	58	-78	275	127
E1	19	-21	48	-7	-2	78	122	57	332	-160
E2	19	-23	45	-6	0	100	137	82	15	-127
F1	92	42	184	-71	36	203	35	15	122	39
F2	71	-65	52	-65	-47	58	53	-4	115	93
B1	74	47	274	2	-17	-11	132	-36	339	-39
B2	36	19	212	19	7	-158	132	-73	360	11
B3	85	56	293	-41	16	164	135	-55	5	1
Mean		6.2	140.9		10.8	211.4		-14.1		23.3
St.dev.		48.8	93.7		43.1	372.5		42.0		78.5

continue on the following page ...

Table 10: *continued from previous page.*

Site	Major			Minor			Inclination		Phase	
	Mod mm s ⁻¹	Diff mm s ⁻¹	Ratio %	Mod mm s ⁻¹	Diff mm s ⁻¹	Ratio %	Mod °	Diff °	Mod °	Diff °
<i>Constituent:M2</i>										
Ve	1527	-295	84	-33	33	0	122	32	153	-6
No	980	317	148	-19	9	-190	92	35	218	-3
S1	735	-54	93	-442	-37	92	6	-6	266	0
S2	592	-82	88	-273	-61	82	19	6	257	-12
S3	792	130	120	-12	4	-150	125	4	90	8
S8	295	19	107	-94	11	113	23	5	244	4
S9	235	13	106	-47	6	115	26	-7	247	-10
W1	277	-30	90	-213	-31	87	96	9	178	-7
W2	387	4	101	-193	-1	99	138	15	133	-15
N1	481	-22	96	-126	-48	72	15	5	294	0
N2	566	-85	87	-324	82	134	56	19	247	-3
N3	416	20	105	-216	18	109	137	-3	159	-7
N5	76	-51	60	-31	-28	53	3	-25	294	-20
E1	336	-51	87	-70	-56	56	62	0	227	1
E2	367	-16	96	-82	-29	74	51	0	233	-1
F1	268	-20	93	-237	-13	95	51	-5	226	7
F2	383	18	105	-323	15	105	45	-15	226	7
B1	176	-18	91	17	8	-189	3	-10	232	-12
B2	155	0	100	25	19	-417	23	-12	249	-3
B3	227	38	120	-27	22	540	173	-23	47	-3
Mean		-18.6	95.5		-7.2	143.0		-2.8		-4.4
St.dev.		36.4	12.8		36.0	131.9		12.2		7.6
<i>Constituent:S2</i>										
Ve	1106	525	190	-7	7	0	127	37	206	12
No	423	150	155	-41	39	2050	91	36	280	0
S1	209	-49	81	-115	-27	81	8	-1	302	-4
S2	169	-64	73	-73	-31	70	21	11	295	-11
S3	263	40	118	1	-18	5	132	11	138	22
S8	77	-37	68	-12	-1	92	30	11	285	9
S9	74	-17	81	-5	-10	33	30	0	290	-11
W1	91	-11	89	-70	-7	91	134	58	173	-58
W2	109	-34	76	-45	-25	64	145	31	159	-35
N1	257	83	148	-89	36	168	14	5	327	-4
N2	208	-13	94	-132	58	178	46	11	272	-16
N3	218	74	151	-143	76	213	149	10	191	-18
N5	49	4	109	-26	15	236	8	-11	337	-30
E1	139	13	110	-41	12	141	66	6	279	16
E2	138	4	103	-39	9	130	56	6	284	14
F1	61	-39	61	-54	-29	65	43	-25	244	-3
F2	99	-9	92	-88	2	102	14	-43	253	-6
B1	40	-18	69	29	27	1450	30	13	297	22
B2	49	-6	89	14	13	1400	44	18	305	19
B3	43	-16	73	24	20	600	161	-36	71	-9
Mean		-7.9	92.2		8.1	301.0		3.8		-7.4
St.dev.		38.2	25.9		30.0	442.2		23.8		20.8

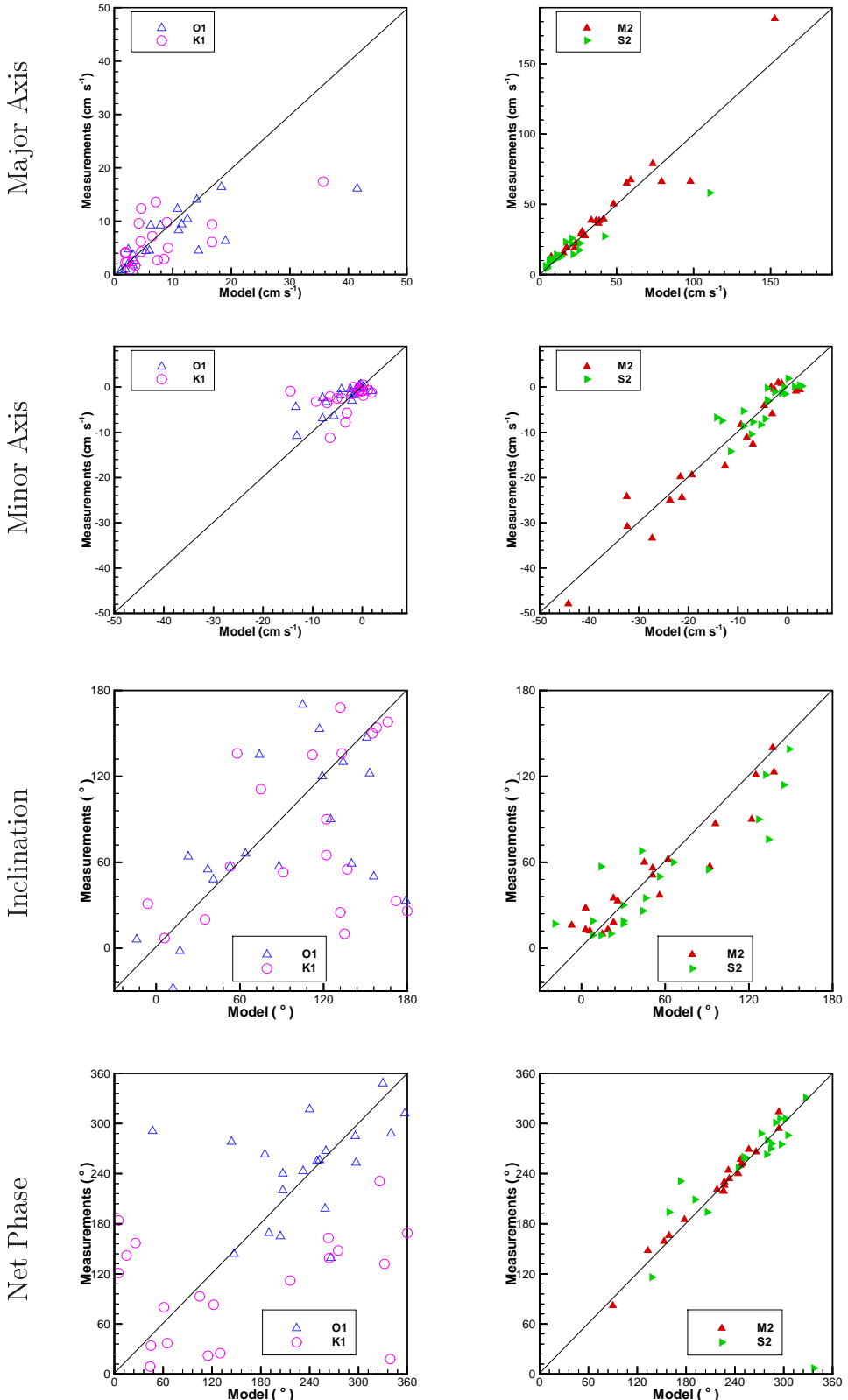


Figure 8: Scattering diagrams for comparison between observed and computed length of major (top) and minor semi ellipse axis, inclination, and net phase (bottom) for the diurnal (left) and semi diurnal (right) constituents in run C. The line indicate 100% correlation.

Table 11: Length of major and minor semi axis, inclination, and net phase of current ellipses at measurements sites derived by a linear model with quadratic friction terms with increased friction coefficient (Run D). The difference from the corresponding variable derived from measured data (Table 5) and for the lengths also the ratio between model derived and data based values is also provided. Negative minor semi axis indicate anticyclonic (clockwise) rotation, and negative ratio indicate different rotation directions.

Site	Major			Minor			Inclination		Phase	
	Mod mm s ⁻¹	Diff mm s ⁻¹	Ratio %	Mod mm s ⁻¹	Diff mm s ⁻¹	Ratio %	Mod °	Diff °	Mod °	Diff °
<i>Constituent: Q1</i>										
Ve	249	186	395	-16	16	0	126	36	209	78
No	35	14	167	-7	4	-233	96	40	282	72
S1	120	24	125	-96	48	200	113	-39	146	21
S2	80	33	170	-69	50	-363	139	80	121	-112
S3	99	71	354	8	3	160	135	10	139	10
S8	43	35	538	-33	31	1650	8	-6	247	-6
S9	26	8	144	-4	3	-400	163	20	130	53
W1	21	8	162	-8	5	267	169	63	215	34
W2	111	81	370	-85	65	425	133	-8	173	-15
N1	35	-5	88	-6	-5	55	17	11	10	42
N2	48	-2	96	-31	20	282	161	-51	154	81
N3	72	25	153	-60	52	750	135	-12	216	47
N5	16	3	123	2	-1	-67	60	34	221	-173
E1	16	3	123	-5	3	250	161	108	341	126
E2	26	7	137	-15	14	1500	175	-66	35	-28
F1	89	72	524	-74	66	925	38	4	148	-31
F2	28	-3	90	-10	-16	38	138	-79	303	13
Mean	20.6	203.0		23.9	512.2			4.2		3.7
St.dev.	27.1	154.9		27.7	515.3			54.4		76.1
<i>Constituent: O1</i>										
Ve	663	502	412	-16	16	0	126	36	232	63
No	194	149	431	-44	39	880	91	34	301	45
S1	249	85	152	-200	92	185	123	-30	221	56
S2	157	34	128	-129	60	187	150	91	196	-67
S3	244	104	174	-2	-4	-33	134	4	190	46
S8	62	25	168	-49	31	272	4	-174	337	-128
S9	28	-19	60	-4	3	-400	149	-3	232	100
W1	53	27	204	-31	19	258	164	44	239	-1
W2	152	48	146	-80	47	242	140	18	246	3
N1	142	50	154	-56	26	187	4	-2	25	37
N2	125	33	136	-90	72	500	168	-45	183	85
N3	71	-12	86	-20	-4	83	157	10	257	37
N5	35	18	206	13	4	-144	88	-82	68	175
E1	57	13	130	-6	3	200	58	-8	285	30
E2	78	33	173	-32	27	640	35	-22	295	28
F1	109	46	173	-86	42	195	26	-22	209	11
F2	109	15	116	-77	13	120	0	-55	226	87
B1	37	27	370	8	4	200	121	71	99	142
B2	18	10	225	16	12	-400	56	-8	56	125
B3	39	18	186	-7	-8	47	125	-10	138	-150
Mean	26.5	165.3		26.1	250.7			-13.4		33.5
St.dev.	24.0	67.7		28.3	153.6			59.6		87.7

continue on the following page ...

Table 11: *continued from previous page.*

Site	Major			Minor			Inclination		Phase	
	Mod mm s ⁻¹	Diff mm s ⁻¹	Ratio %	Mod mm s ⁻¹	Diff mm s ⁻¹	Ratio %	Mod °	Diff °	Mod °	Diff °
<i>Constituent:K1</i>										
Ve	441	267	253	-18	18	0	126	36	150	125
No	56	13	130	-9	8	900	94	41	264	125
S1	47	-77	38	-35	-43	45	154	4	48	14
S2	42	-54	44	-32	-25	56	171	-42	29	52
S3	54	-8	87	6	1	120	134	-2	72	35
S8	32	7	128	-21	6	140	0	-26	185	64
S9	22	-2	92	-1	-7	13	167	9	42	33
W1	16	-7	70	4	-5	-44	85	-26	67	-13
W2	69	-3	96	-54	29	216	109	-26	105	12
N1	165	71	176	-94	62	294	7	0	322	91
N2	90	-8	92	-65	44	310	174	143	83	-80
N3	166	105	272	-142	133	1578	166	12	203	91
N5	26	16	260	11	4	-157	54	-82	268	120
E1	20	-20	50	-6	-3	67	126	61	324	-168
E2	20	-22	48	-4	-2	67	143	88	9	-133
F1	89	39	178	-73	38	209	36	16	117	34
F2	68	-68	50	-62	-50	55	43	-14	119	97
B1	73	46	270	1	-18	-5	132	-36	338	-40
B2	35	18	206	19	7	-158	133	-72	359	10
B3	84	55	290	-39	14	156	134	-56	4	0
Mean	5.6	138.7		10.8	209.9		-2.8		10.8	
St.dev.	48.3	91.7		42.9	364.5		57.3		79.8	

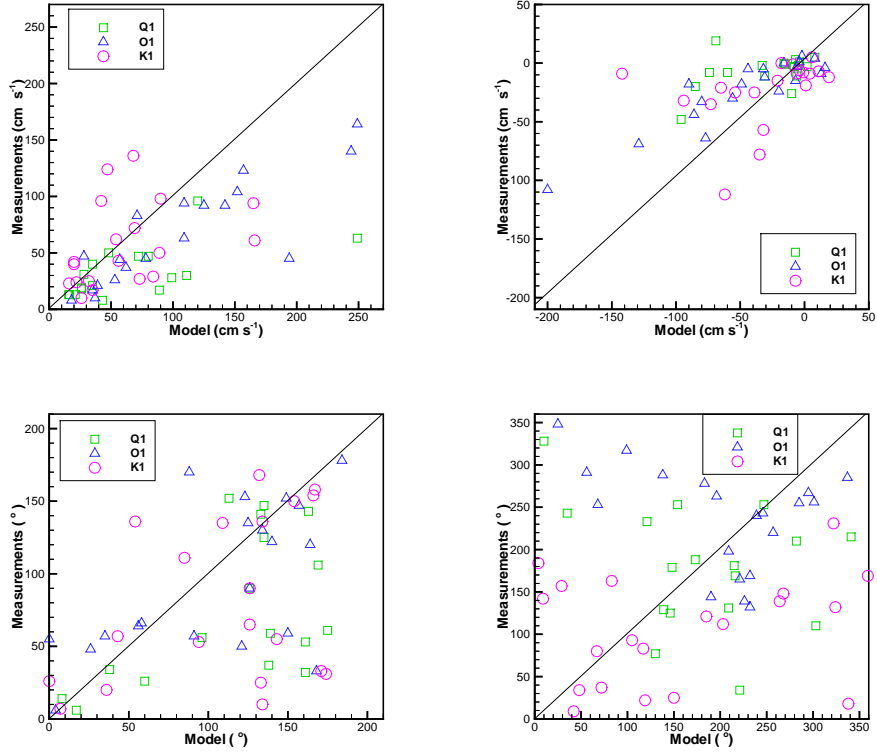


Figure 9: Scattering diagrams for comparison between observed and computed length of major (top left) and minor (top right) semi ellipse axis, inclination (lower left), and net phase (lower right) for the constituents in run D. The line indicate 100% correlation.

3.5 Conclusion

Based on the comparison between model and data derived tidal constituents the runs listed in Table 12 are concluded to be in the best overall agreement with the measurement based data. The mean and standard deviation of the difference between model and data derived parameters from Tables 7–10 are included in Table 12. If nothing else is stated data from these runs are used in the graphically presentation of model results and in the database.

Table 12: Runs found to be in best agreement with measurement based parameters. The mean and standard deviation of the difference between model and data derived parameters from Tables 7–10 are included for brevity, and number of sites (N) used in the estimates are included as well. Note, that the data based elevation values from more than one source are included for Sites 5 and 6, while the coastal current sites (No, Ve, and S3) are excluded in the estimates of mean and standard deviation of the current parameters. If nothing else is stated data from these runs are used in the graphically presentation of model results and in the database.

Run	Elevation			Current					
	Amp cm	Pha °	N	Maj mm s ⁻¹	Min mm s ⁻¹	Incl °	Pha °	N	
A-Q ₁	Mean	-0.2	-13.0	16	30.8	31.5	5.8	21.6	14
	St. dev.	0.9	32.3		36.6	33.4	47.7	84.7	
C-O ₁	Mean	-0.5	-6.2	24	11.3	16.7	-0.5	17.5	17
	St. dev.	1.3	10.4		34.0	25.4	45.8	57.2	
A-P ₁	Mean	0.2	0.1	13	9.5	13.6	-13.3	9.2	12
	St. dev.	0.6	18.3		22.0	20.8	77.4	96.4	
C-K ₁	Mean	-0.4	-3.9	24	6.2	10.8	-14.1	23.3	17
	St. dev.	2.3	15.9		48.8	43.1	42.0	78.5	
A-N ₂	Mean	0.5	-1.9	16	-1.5	6.0	6.0	11.8	17
	St. dev.	1.4	16.0		14.9	12.4	18.7	14.2	
C-M ₂	Mean	0.8	-1.5	27	-18.6	-7.2	-2.8	-4.4	17
	St. dev.	3.9	5.2		36.4	36.0	12.2	7.6	
C-S ₂	Mean	1.4	-5.8	25	-7.9	8.1	3.8	-7.4	17
	St. dev.	2.6	8.3		38.2	30.0	23.8	20.6	
A-K ₂	Mean	0.1	5.5	13	0.3	3.7	10.3	4.2	12
	St. dev.	0.7	12.9		7.2	5.8	13.1	16.1	

4 Model results

4.1 Tidal Charts

Tidal charts for each constituents are presented on the following pages (Figures 10–13). Definitions are given in Section 2.2. The plots are provided in the model grid, i.e. Mercator relative to the 7°W Median. Color version are included in the electronic version.

All four included semi diurnal constituents included shows a pronounced minimum in amplitude in the area north of Tórshavn, and larger amplitudes on the western shelf with maximum amplitudes around Vágoy. This results in relatively large gradients from the west to the east of the islands.

The area is to small to resolve the wave of the diurnal wave, and the variations in amplitude are largely due to local effects on the tidal wave. The tidal charts shows structures, which indicate appearance of topographical trapped waves along the Scottish shelf and along the northern Faroe Shelf (Figures 12 and 13). Topographical waves along the European continent are discussed by Cartwright et al. [1980b], Huthnance [1992], and others, while topographical waves around the Faroe Plateau is rarely discussed in literature. Further, enhancement of the diurnal constituents are also seen on the Bill Baily Bank and on the Faroe Bank. O_1 and K_1 shows a dipole pattern on the Bill Baily Bank, with a minimum and a maximum in amplitude with centers on the edge of the Bank. Further, the axis of the dipole of these two constituents are normal to each other.

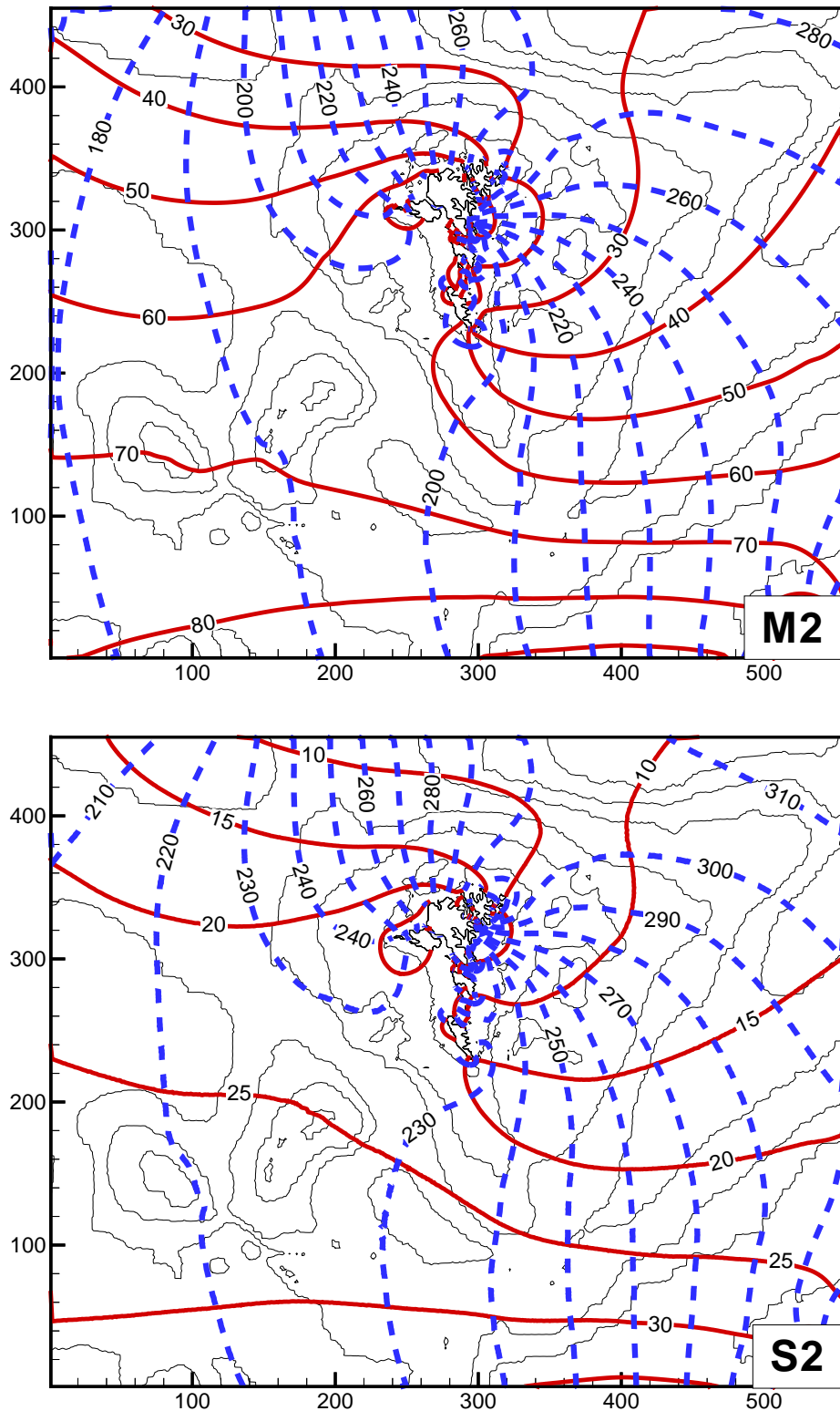
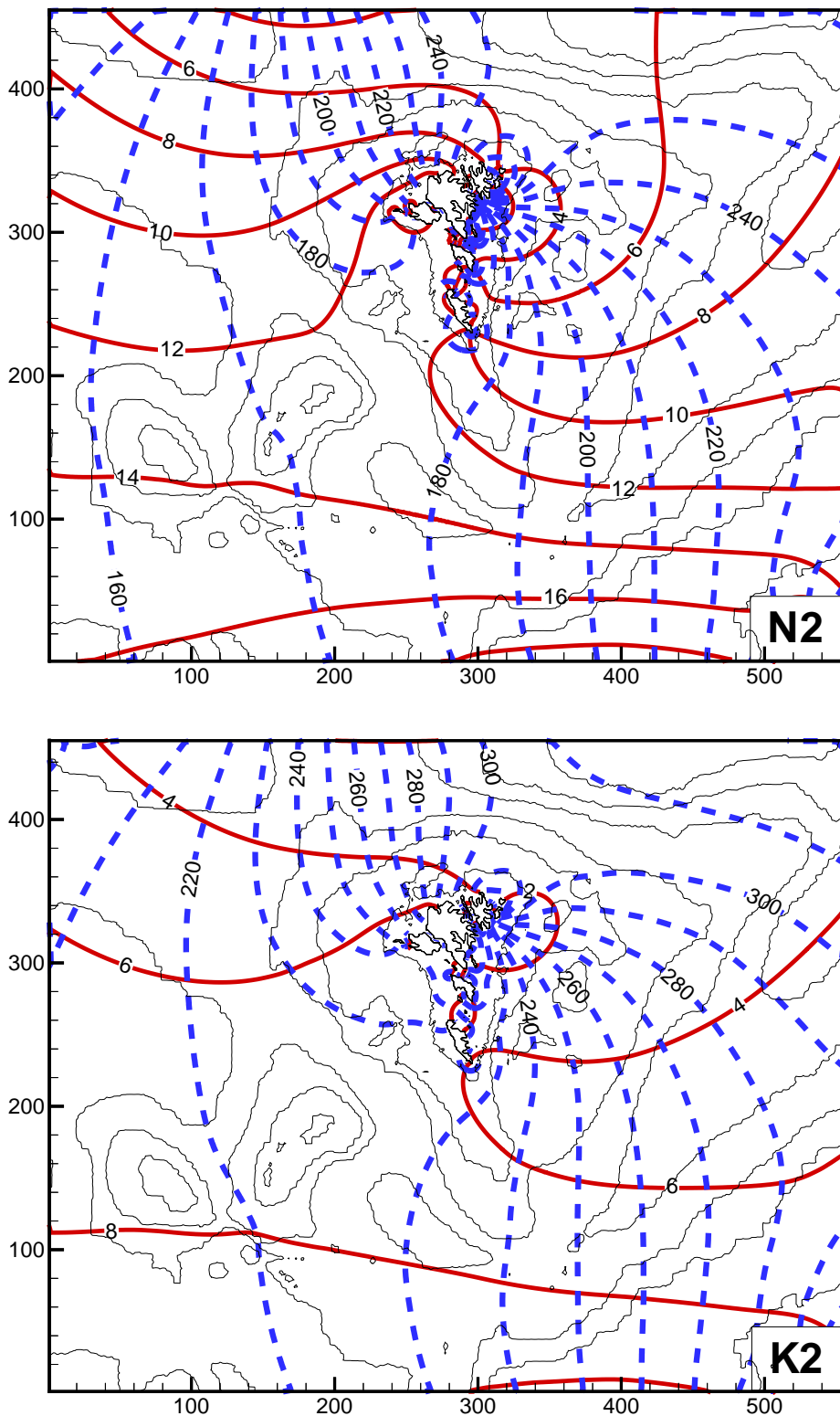


Figure 10: Tidal chart for M_2 and S_2 showing amplitude (cm) (solid line) and Greenwich phase lag ($^\circ$) (broken line). Thin lines shows 100 m, 200 m, 500 m, 1000 m and 1500 m depth contours.



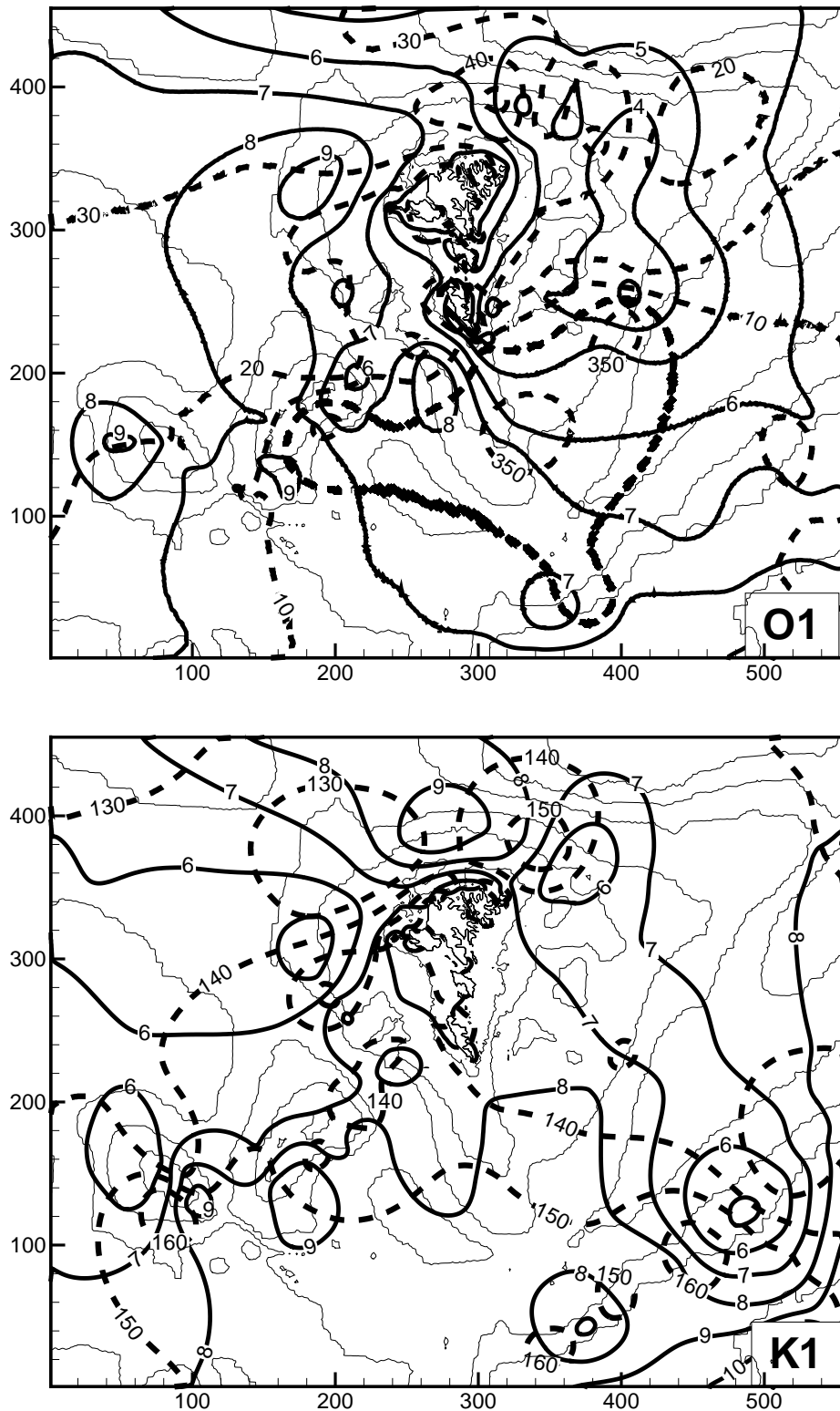


Figure 12: Tidal chart for O₁ and K₁ showing amplitude (cm) (solid line) and Greenwich phase lag (°) (broken line). Thin lines shows 100 m, 200 m, 500 m, 1000 m and 1500 m depth contours.

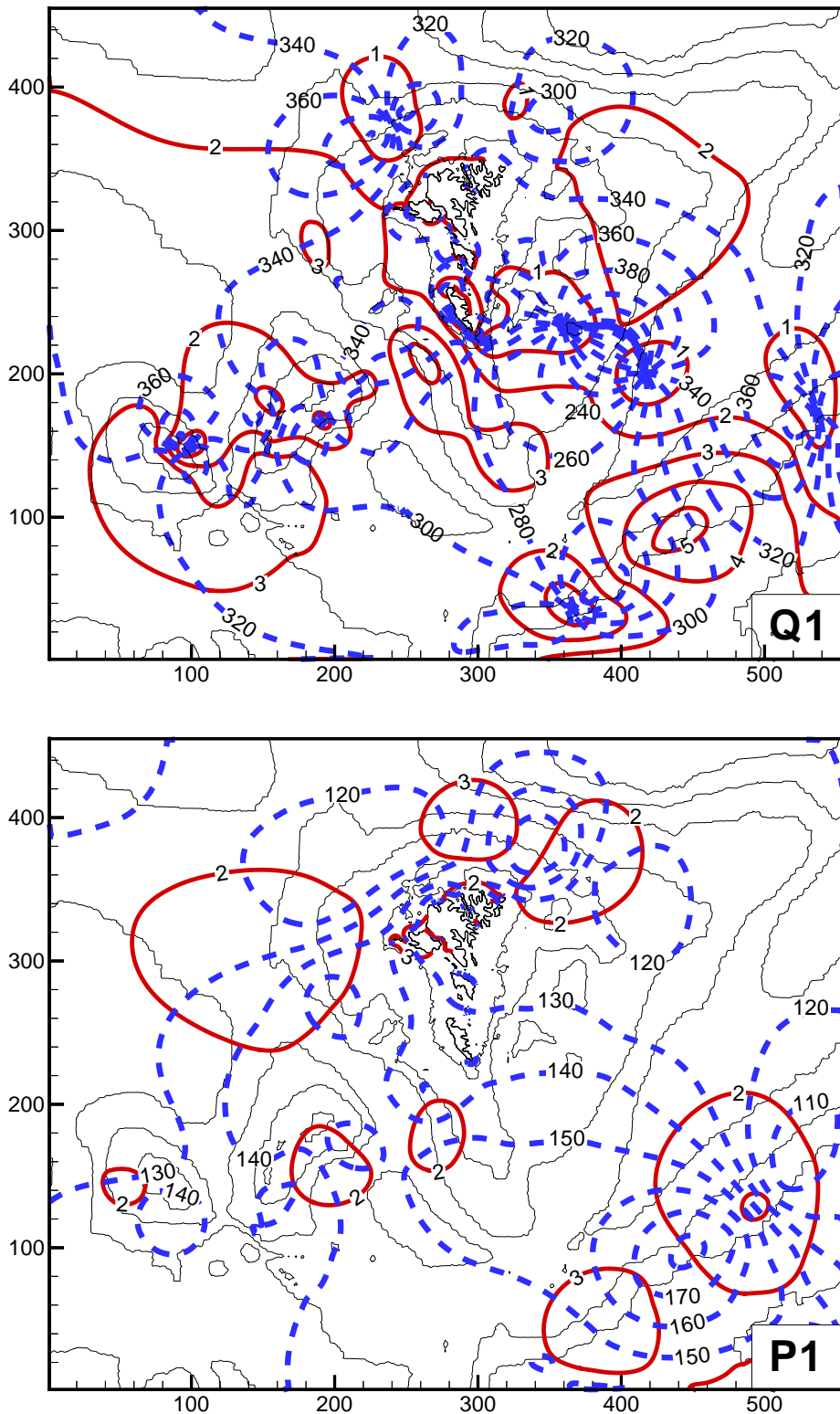


Figure 13: Tidal chart for Q_1 and P_1 showing amplitude (cm) (solid line) and Greenwich phase lag ($^{\circ}$) (broken line). Thin lines shows 100 m, 200 m, 500 m, 1000 m and 1500 m depth contours.

4.2 Tidal Currents

The tidal current derived by the model is presented as

- Plots of the major and minor axis for each of tidal constituents in Section 4.2.1.
- Plots of extreme currents presented as contour plots of the major semi axis lengths for each constituent, and plots presenting the sum of the major semi axis lengths for more than one constituent in Section 4.2.2.
- Vector plots of the residual tidal currents in Section 4.2.3.
- Tidal current maps for every hour, approximately, through a semidiurnal tidal cycle for the entire model domain and two sub domains in Section 4.2.4.

4.2.1 Tidal current ellipses

Plot of the major and minor axis for each of tidal constituents are shown in Figures 14 – 17. Please consult Section 2.2 for definitions of the ellipse parameters. The length of the axis is provided by a reference axis in the upper right corner in the maps.

The semidiurnal tidal current is generally strong on all shallow areas and is dominating the tidal currents. The strongest current occurs in coastal regions mainly due to the large gradient in elevation amplitude from the west to the east side of the islands. On Munkagrunnunum on the southern Faroe Shelf it may be noted that the semidiurnal current is relatively strong out to deeper water than in most other areas.

As for the elevation the current picture is more complicated for the diurnal tide. Relative strong diurnal currents are seen where structures of topographical trapped waves are seen in the elevation, i.e. on the northern Faroe Shelf, west of Suðuroy and on Munkagrunnunum. Indications of trapped topographical waves from measurements are previously provided by Hansen [1978] on Munkagrunnunum and by Cartwright et al. [1980a] west of Suðuroy. Some enhancement is also seen on the slope into the FSC just NE of Suðuroyar Bank. As seen in the elevation relative strong diurnal tides are also on the banks west of the Faroes.

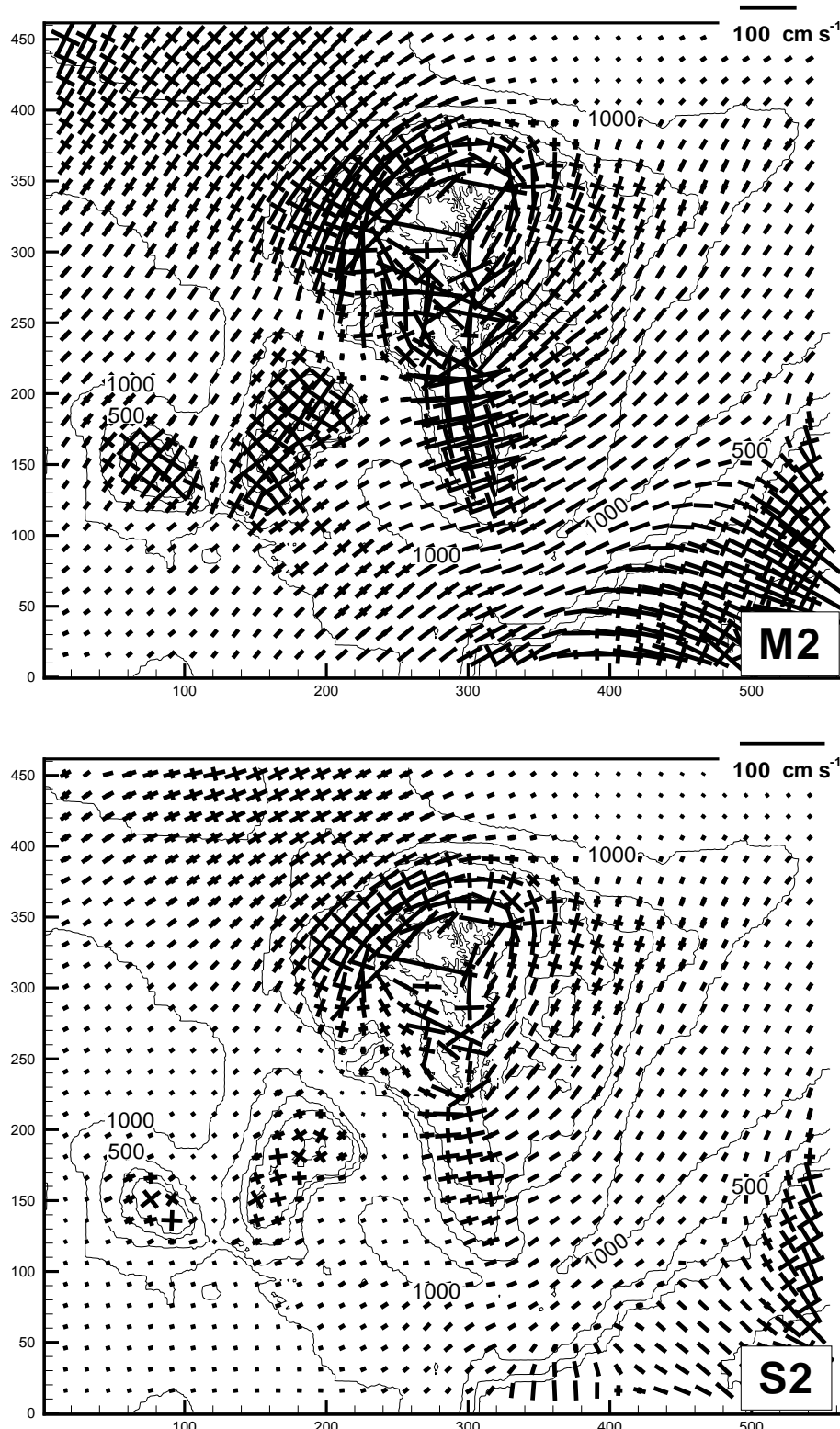


Figure 14: Tidal current ellipse axis for M_2 and S_2 drawn in every 15'th grid point. Note the different magnitude of the axis in the two plots.

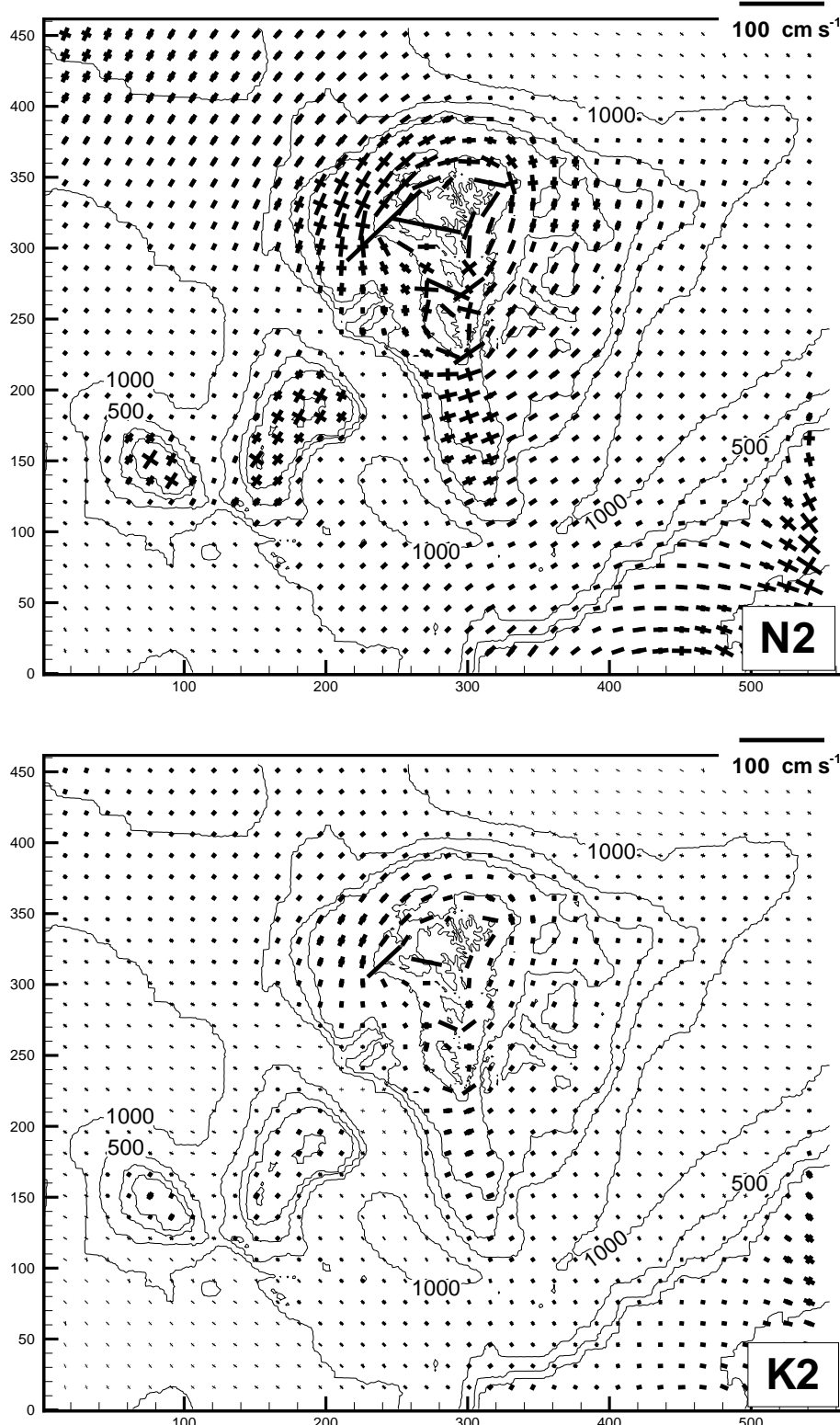


Figure 15: Tideal current ellipse axis for N_2 and K_2 drawn in every 15'th grid point.

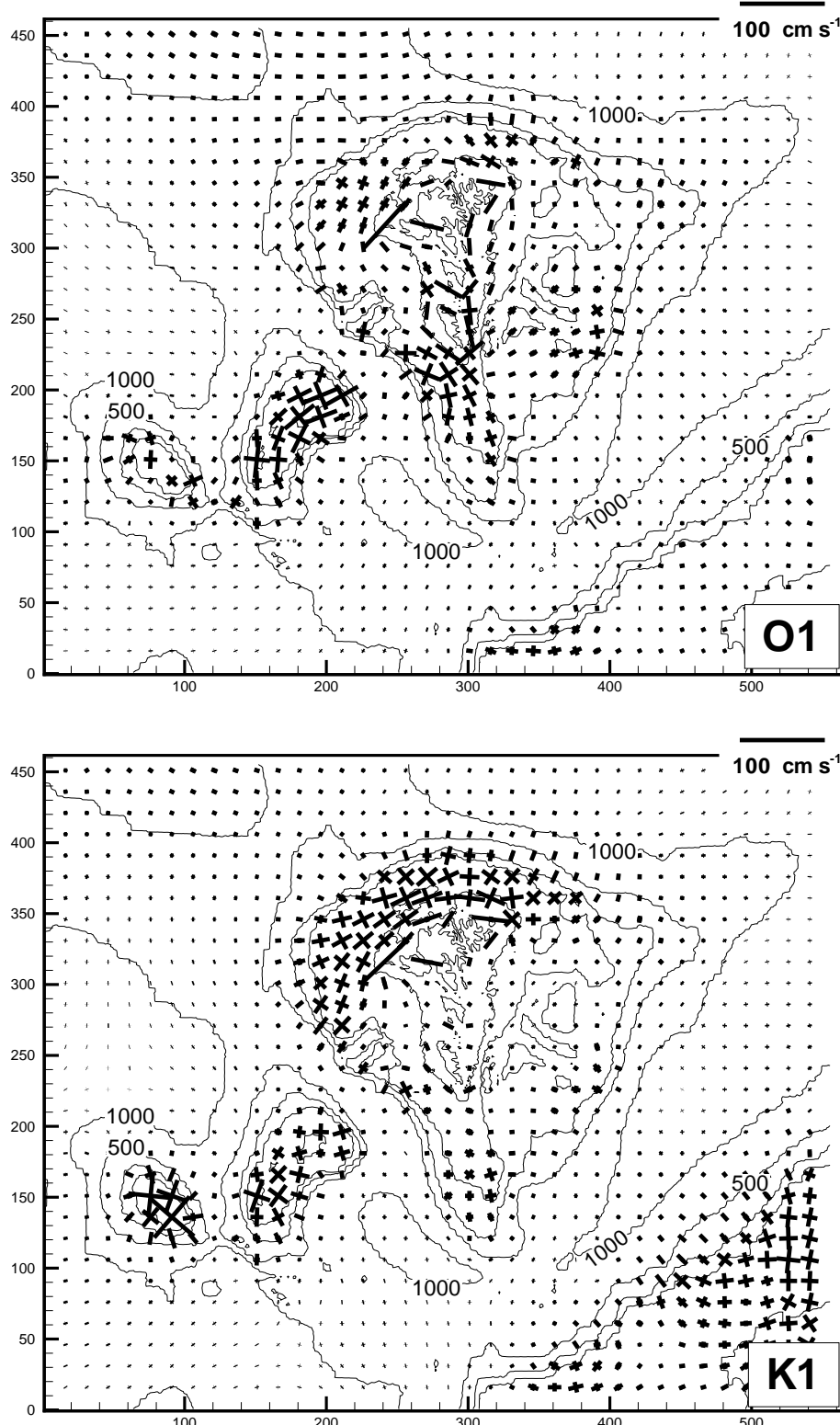


Figure 16: Tideal current ellipse axis for O_1 and K_1 drawn in every 15'th grid point.

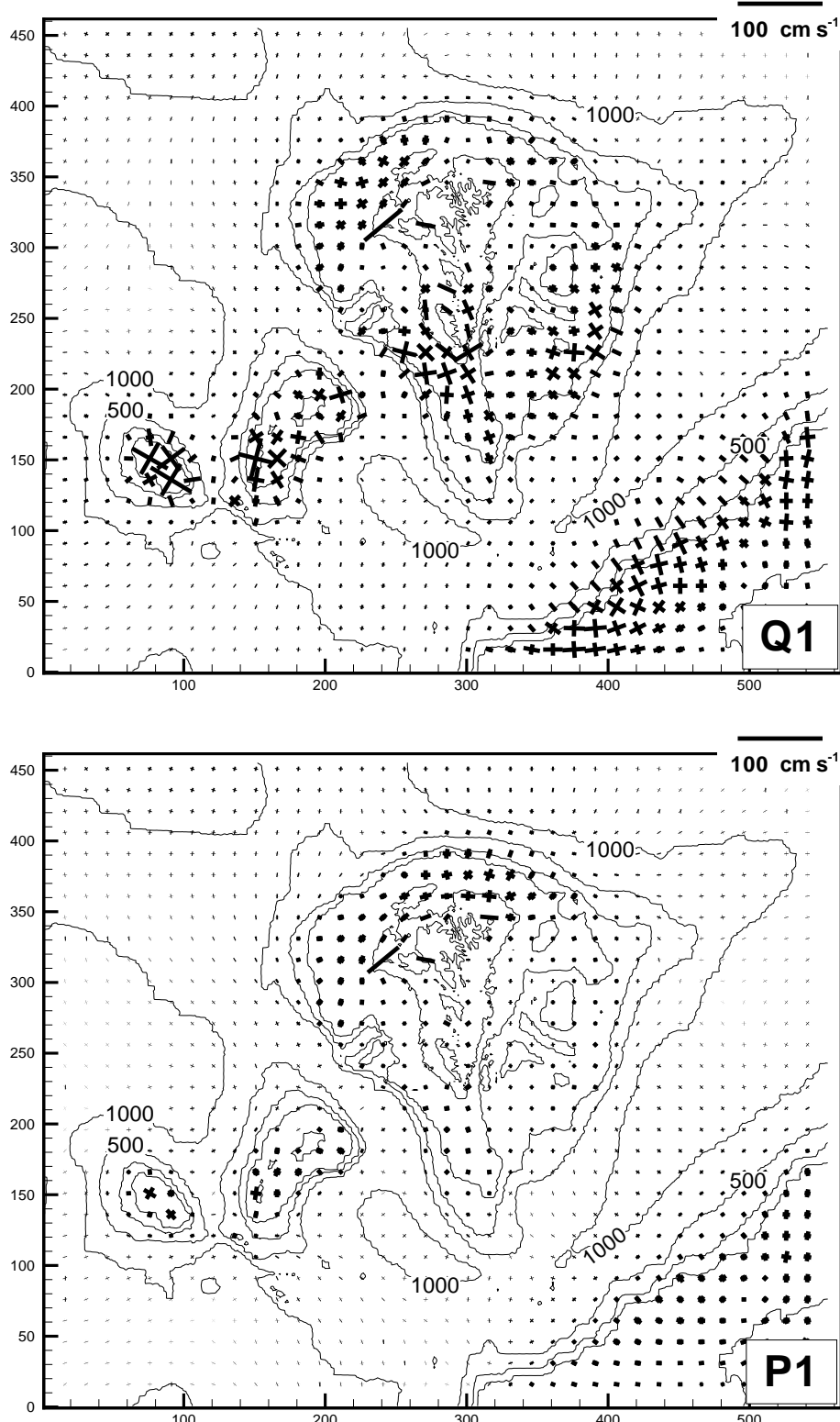


Figure 17: Tideal current ellipse axis for Q_1 and P_1 drawn in every 15'th grid point.

4.2.2 Extreme tidal current speed

Contour plots of the major semi axis length for M_2 and S_2 and for O_1 and K_1 are shown in Figures 18 and 19, respectively, and sum of major semi axis length for

- $M_2 + S_2$
- $O_1 + K_1$
- $M_2 + S_2 + O_1 + K_1$
- $M_2 + S_2 + N_2 + K_2 + O_1 + K_1 + Q_1 + P_1$

are shown in Figures 20 and 21. These estimates may be considered as extreme currents, which may occur if the current for all constituents are in phase and the major axis has the same inclination for all constituents. Since the inclination for the involved constituents generally are not identical, although it is the case at some locations, the extremes may be overestimated in some regions. It may however be noted that other constituents not included here may significantly contribute to the resulting tide at some locations.

The resulting motion of combining M_2 and S_2 has an amplitude which oscillates with a period of 14.76 days, while the motion arising from combination of O_1 and K_1 oscillates with a period of 13.66 days. These motions dominates the fortnightly tides at a particular site. The resulting motion from these four constituents leads to a 'variation' of the 'fortnightly amplitude' of a period of approximately half year, and adding additional constituents to the motion leads to additional long periodic oscillations. The practical importance of these motions depends however on the contribution from each constituents, and those on the harmonic constants at the particular location.

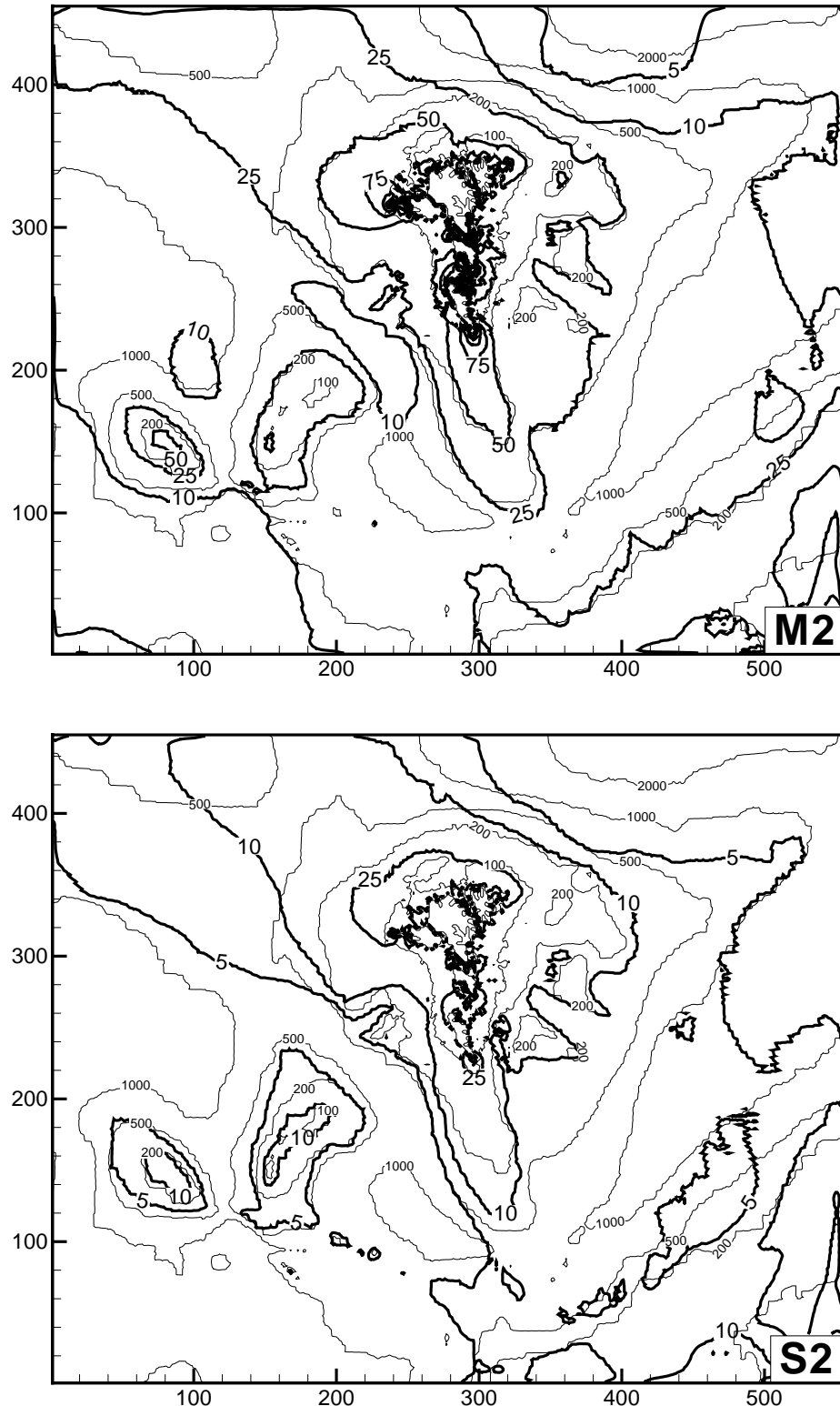


Figure 18: Contour plot of semimajor axis lengths estimated for M_2 , and S_2 . Contours (thick lines) are drawn for 5, 10, 25, 50, 75, 100, 125, 150, 200, 250, and 300 cm s^{-1} , while thin lines indicate depth contours at 100, 200, 500, and 1000 m.

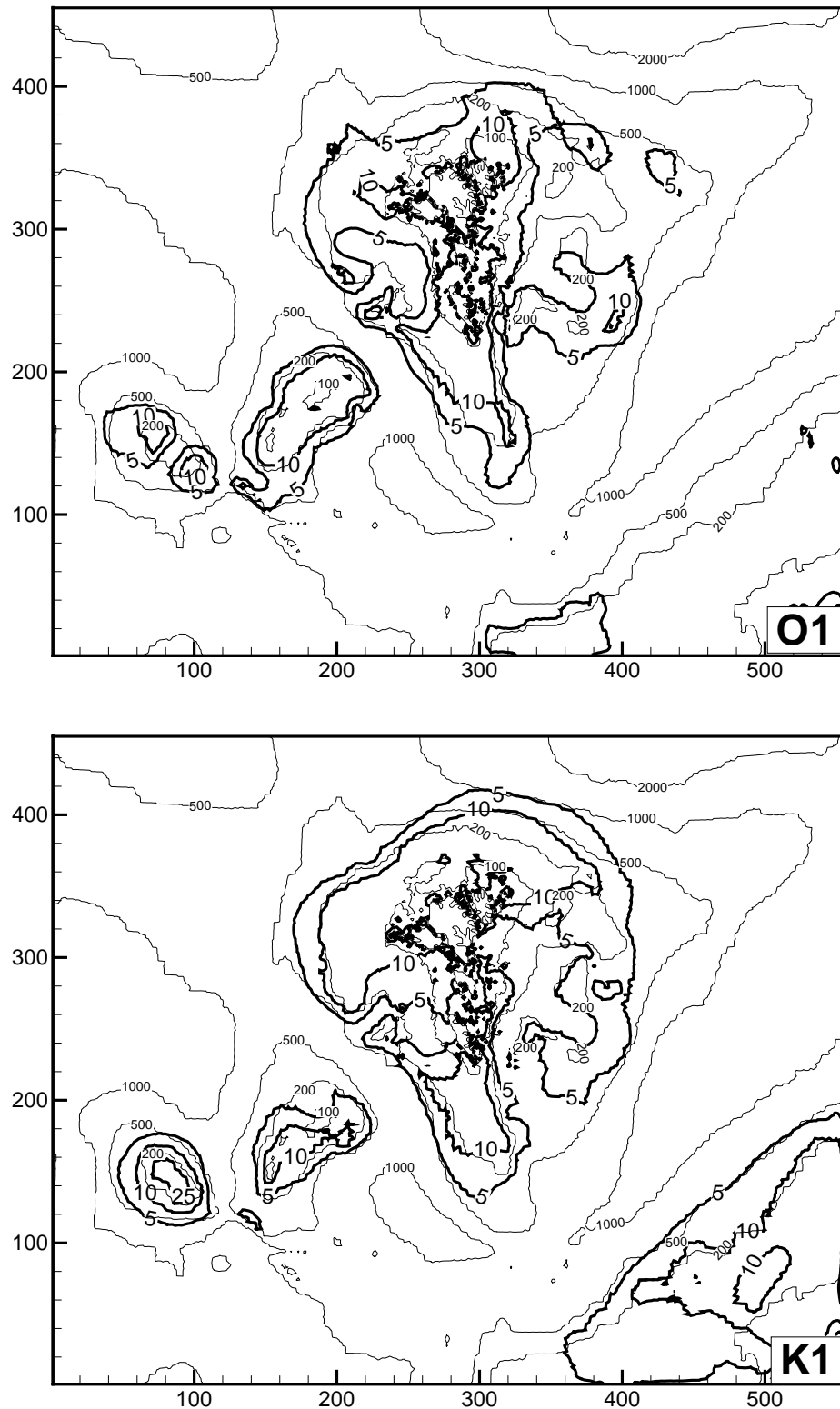


Figure 19: As Figure 18, but for O_1 and K_1 .

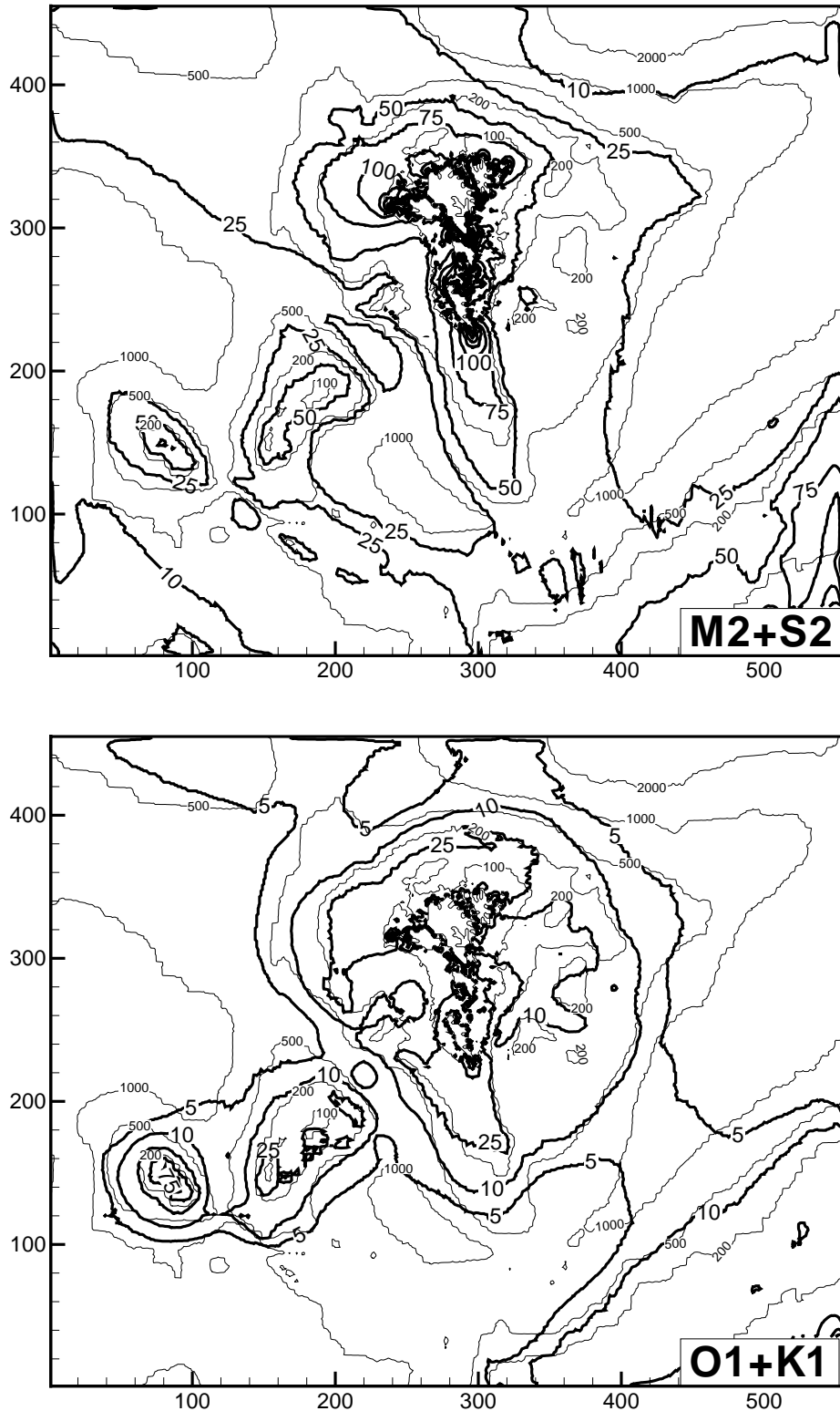


Figure 20: As Figure 18, but for the sum of M_2 , and S_2 and of O_1 and K_1 .

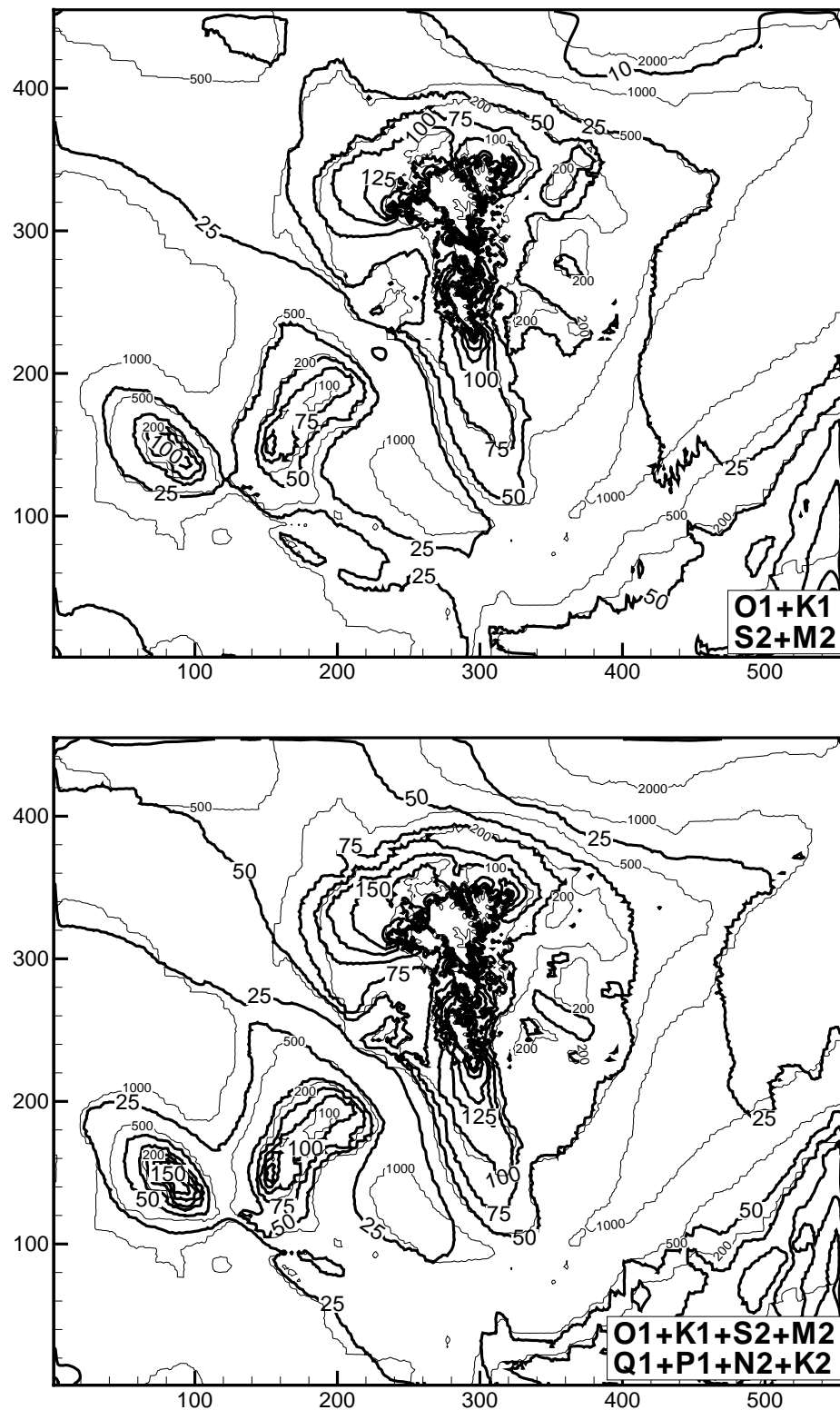


Figure 21: As Figure 18, but for the sums of $M_2 + S_2 + O_1 + K_1$, and all eighth constituents included in the simulation.

4.2.3 Residual tidal currents

The sum of the residual from the harmonic analysis of the current components for each of the constituents included in Run C are presented in Figure 22 and the contribution from each constituent in Figures 23 and 24. It may be noted, that some contribution may be from higher harmonics generated by the non-linearity in the model, which is not extracted by the harmonic analysis. These results are, however, in fairly good qualitative agreement with the results derived from measured data by Hansen and Larsen [1999].

The major contribution to the residual circulation is from the M_2 tide as concluded from measurements by Hansen [1992]. M_2 generates an inner anticyclonic circulation in waters shallower than 100 m, which largely is confirmed by measurements [Hansen, 1992, Hansen and Larsen, 1999], but also a stronger flow along the shelf slope. This flow may be confirmed by some current meter measurements, but unfortunately no measurements are available to confirm the slack residual current between the inner and the slope residual currents. Interesting features are the anticyclonic residuals on the Faroe Bank and on the Bill Bailey Bank, and in particular the relatively strong residuals on each flank of the Faroe Bank Channel. The bifurcations north of Faroe Bank Channel and on the eastern Faroe Shelf may be noted. It may be speculated if the on-shore branches and also the onshore flow south of Suðuroy Bank may be important path ways for import of off-shelf substances to the shelf area. On the Wyville Thompson Ridge, Ymer Ridge and south of Munkagrunnium eddy like structures seems to appear.

The contribution from S_2 , K_1 , and O_1 are weaker than the M_2 -contribution, but they make a significant contribution to the total residual at several locations. It is in particular significant in the flow on the northwestern shelf, where a relative strong current is seen onto the shelf north of the Faroes. It may be speculated if this flow is responsible for transports of nutrients and zooplankton (E. Gaard, pers. comm.) from the off shelf water to the spawning areas north of the Faroe Islands.

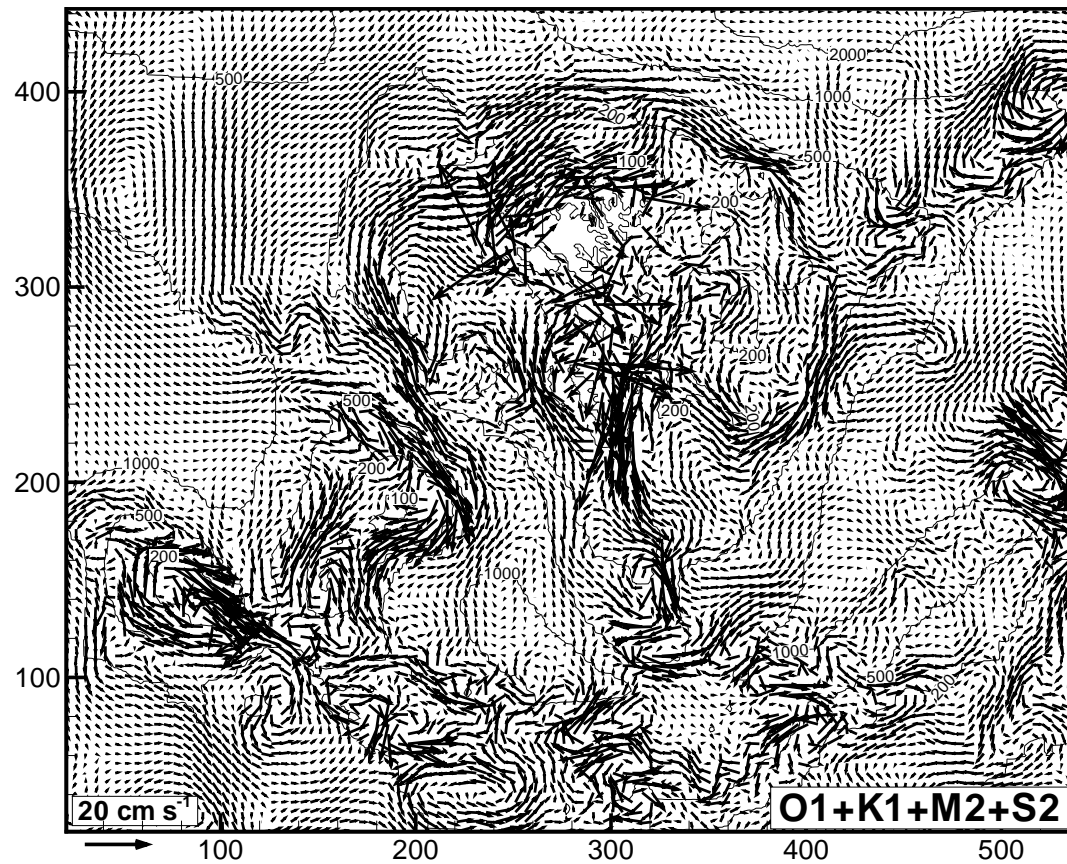
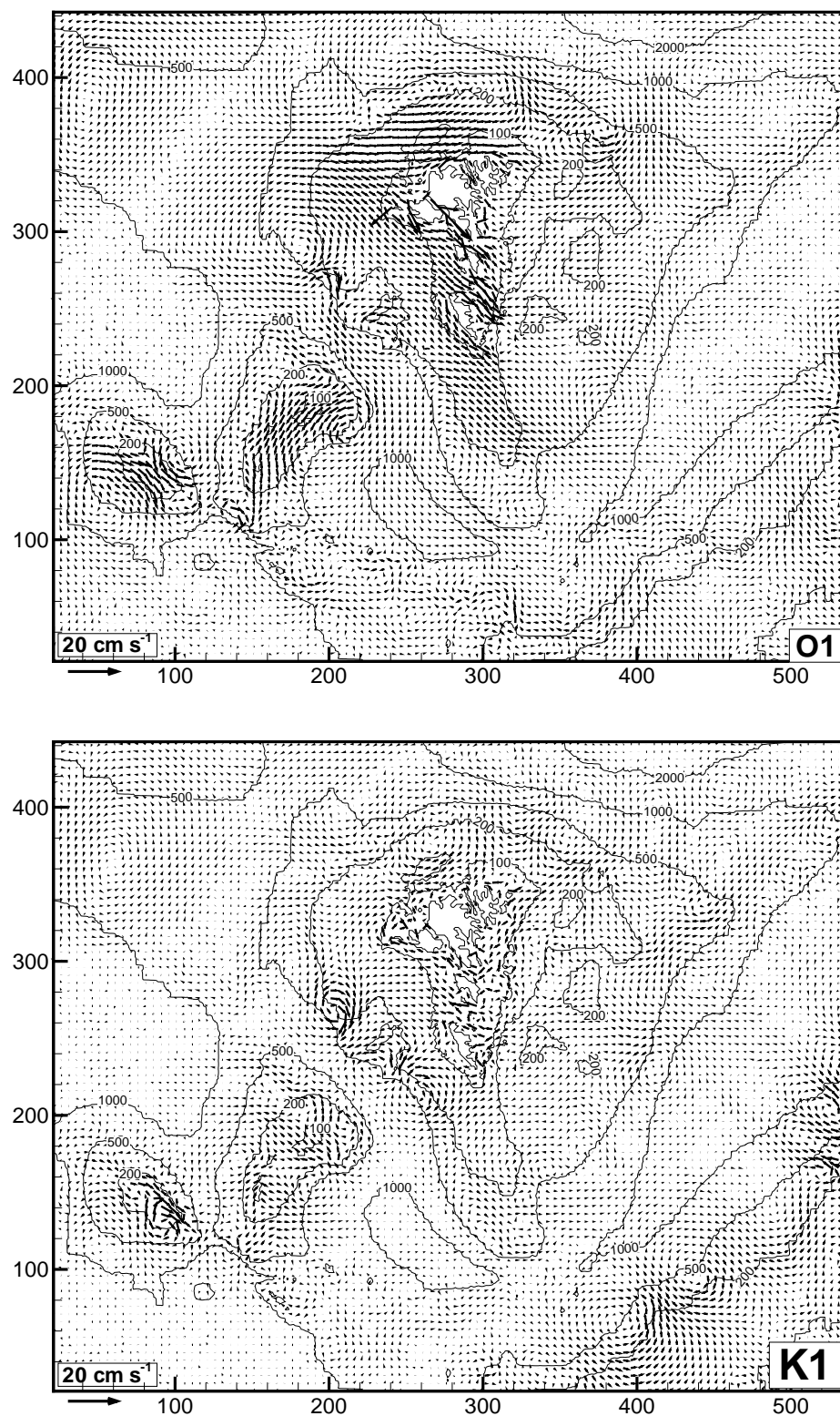


Figure 22: Sum of the residual current derived from the four constituents in Run C.

Figure 23: Residual current generated by O_1 and K_1 in Run C.

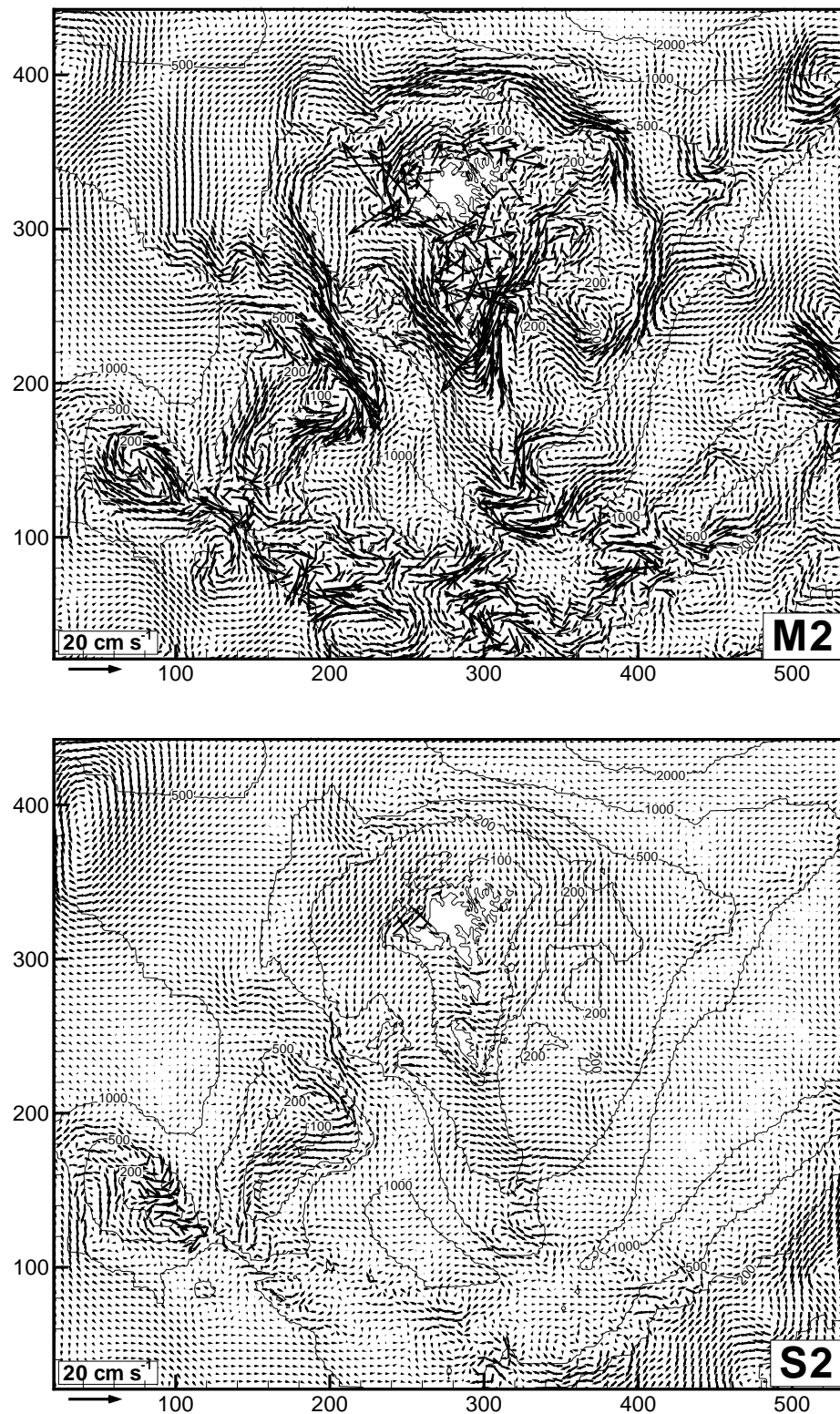


Figure 24: Residual current generated by M_2 and S_2 in Run C.

4.2.4 Tidal current maps

Tidal current maps for every hour, approximately, through a semidiurnal tidal cycle are shown in the following figures for:

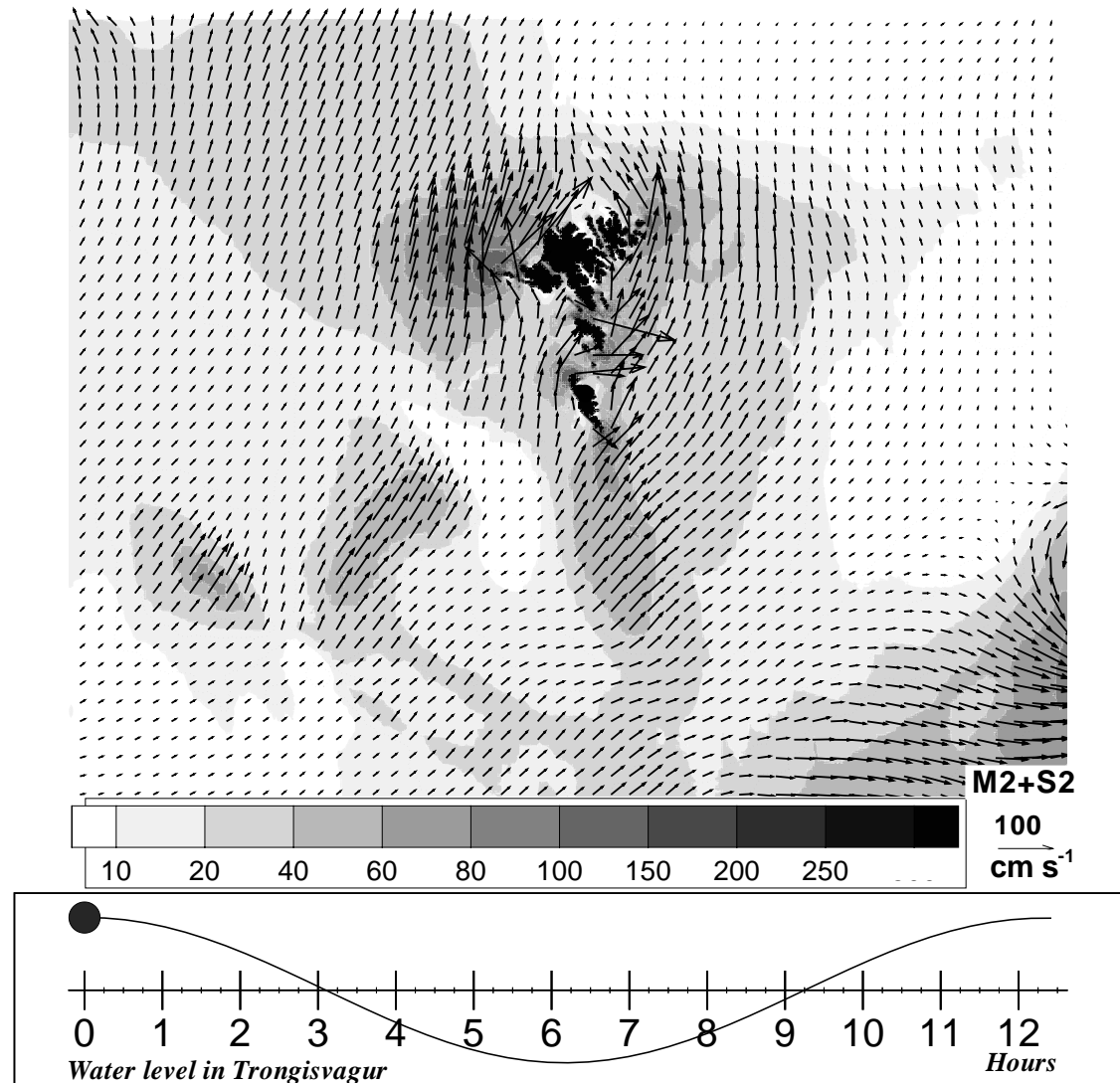
- Entire model domain
- Coastal regions of the Faroe Islands
- Munkagrunninum on the southern Faroe Shelf.

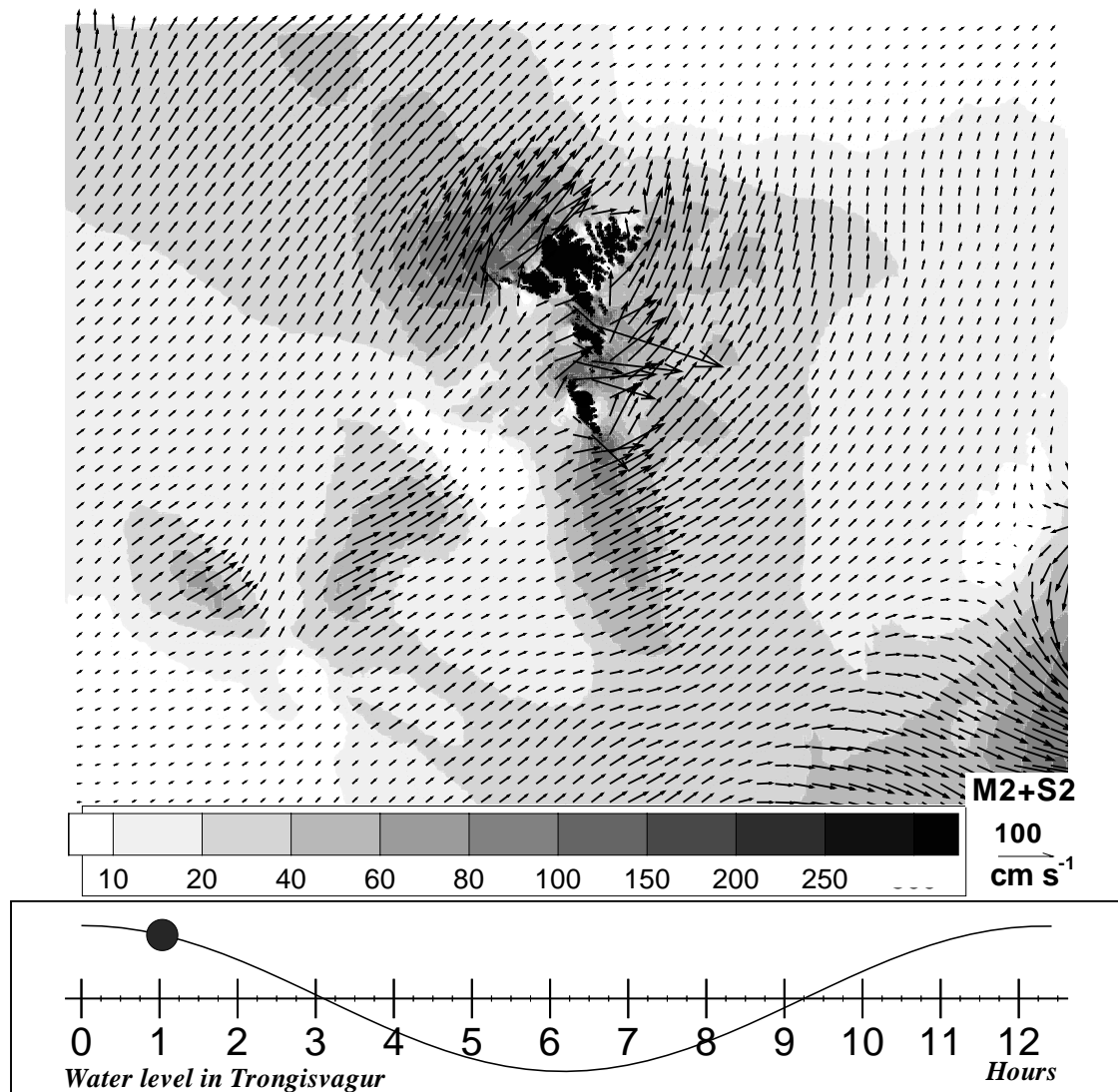
These maps are derived from the result of the harmonic analysis of the model simulation for M_2 and S_2 at a time where these constituents are in phase, i.e. at average spring tide, for the elevation at the reference site, which is Trongisvági on Suðuroy following traditional current maps [Farvandsvæsenet, 1998, Heinesen, 1985]. The reference site is indicated by a bullet on the current maps for the coastal regions.

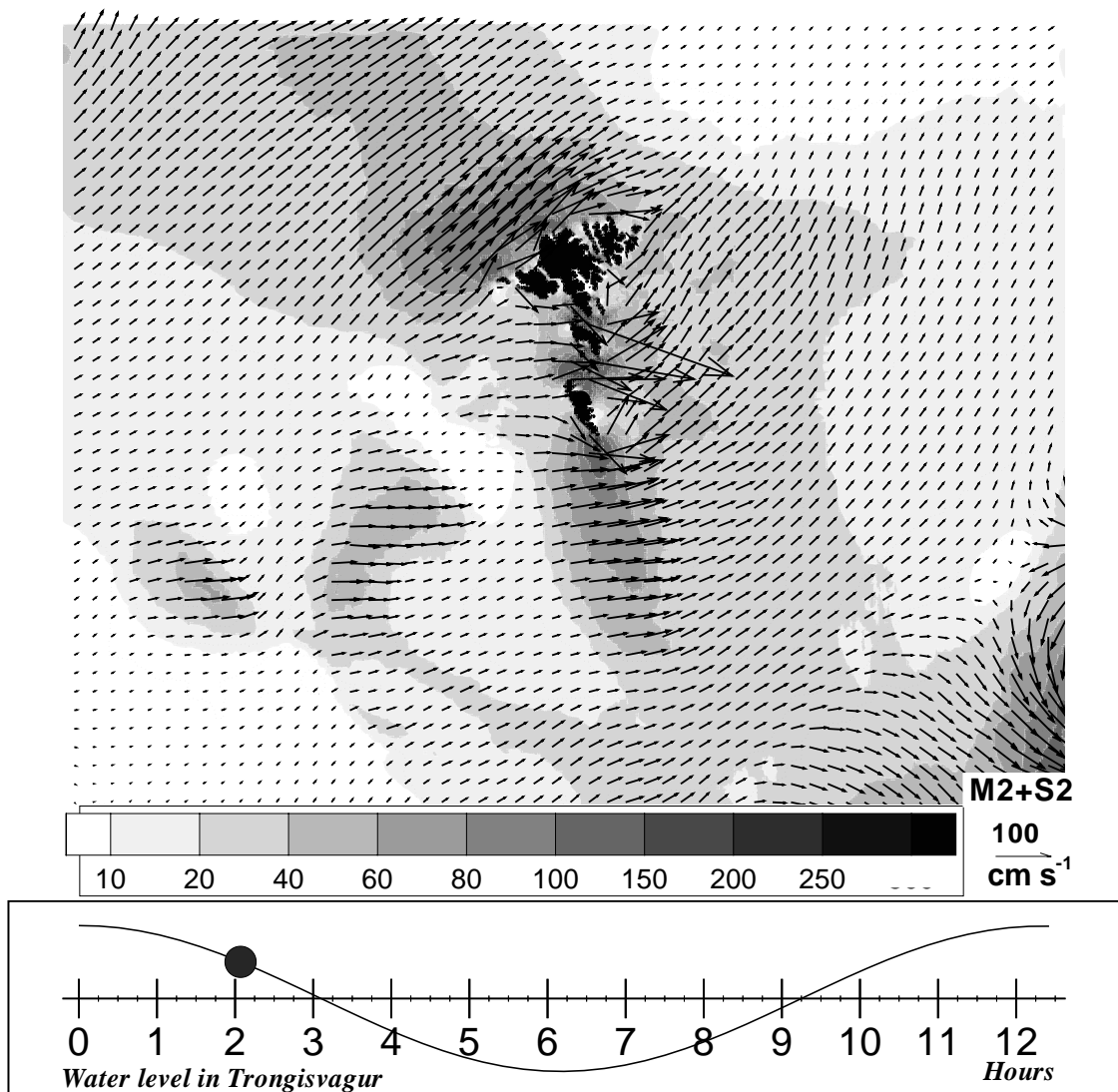
The time is given relative to the model derived surface elevation at the reference site which is shown graphically in the panel below the current map. The speed is indicated by the gray scale and the length of the vectors. A reference vector is included in the lower right corner in the maps.

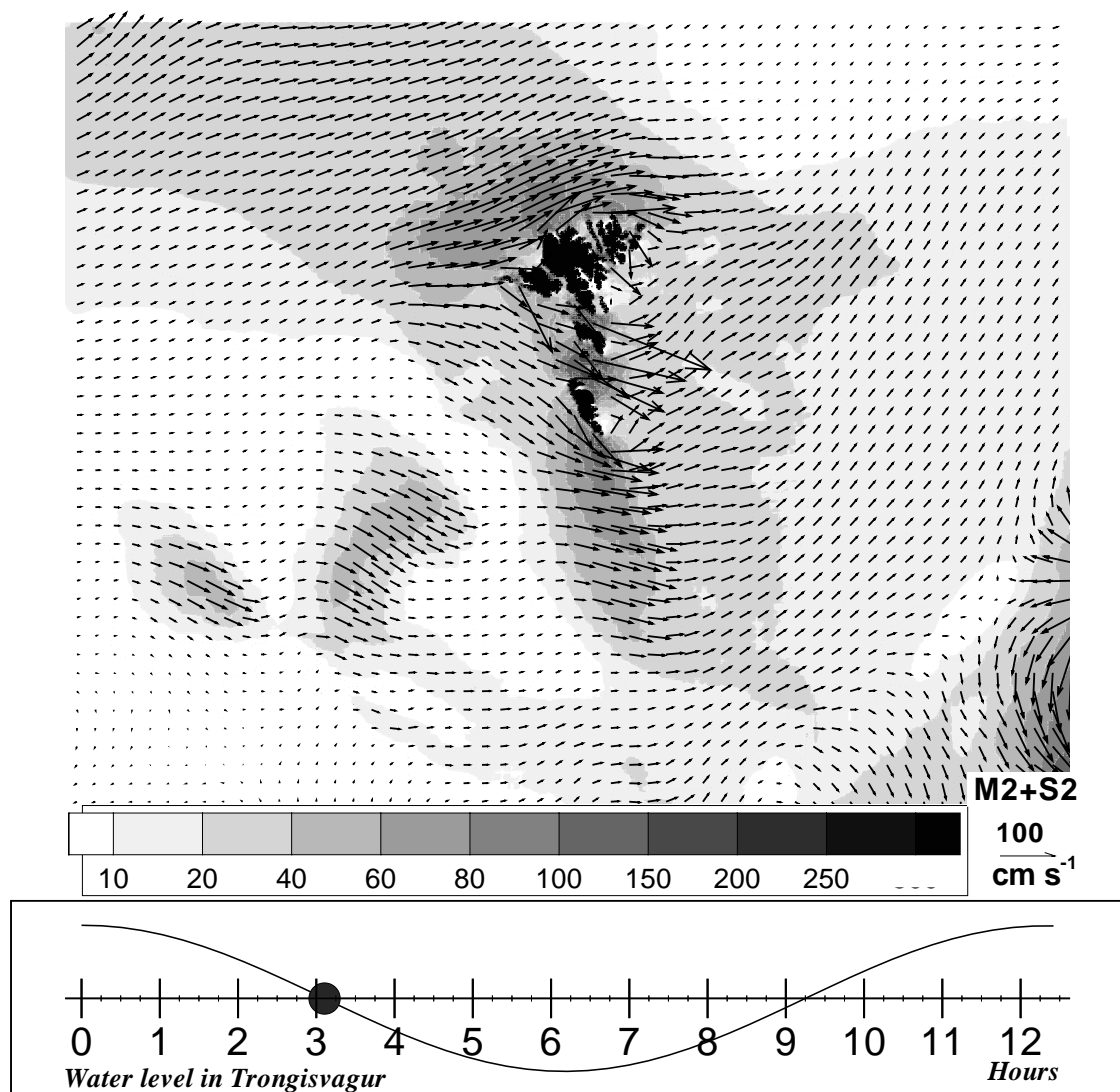
Color version of these maps and similar maps of the surface elevation are provided with roughly 0.25 hour intervals on the CD-ROM.

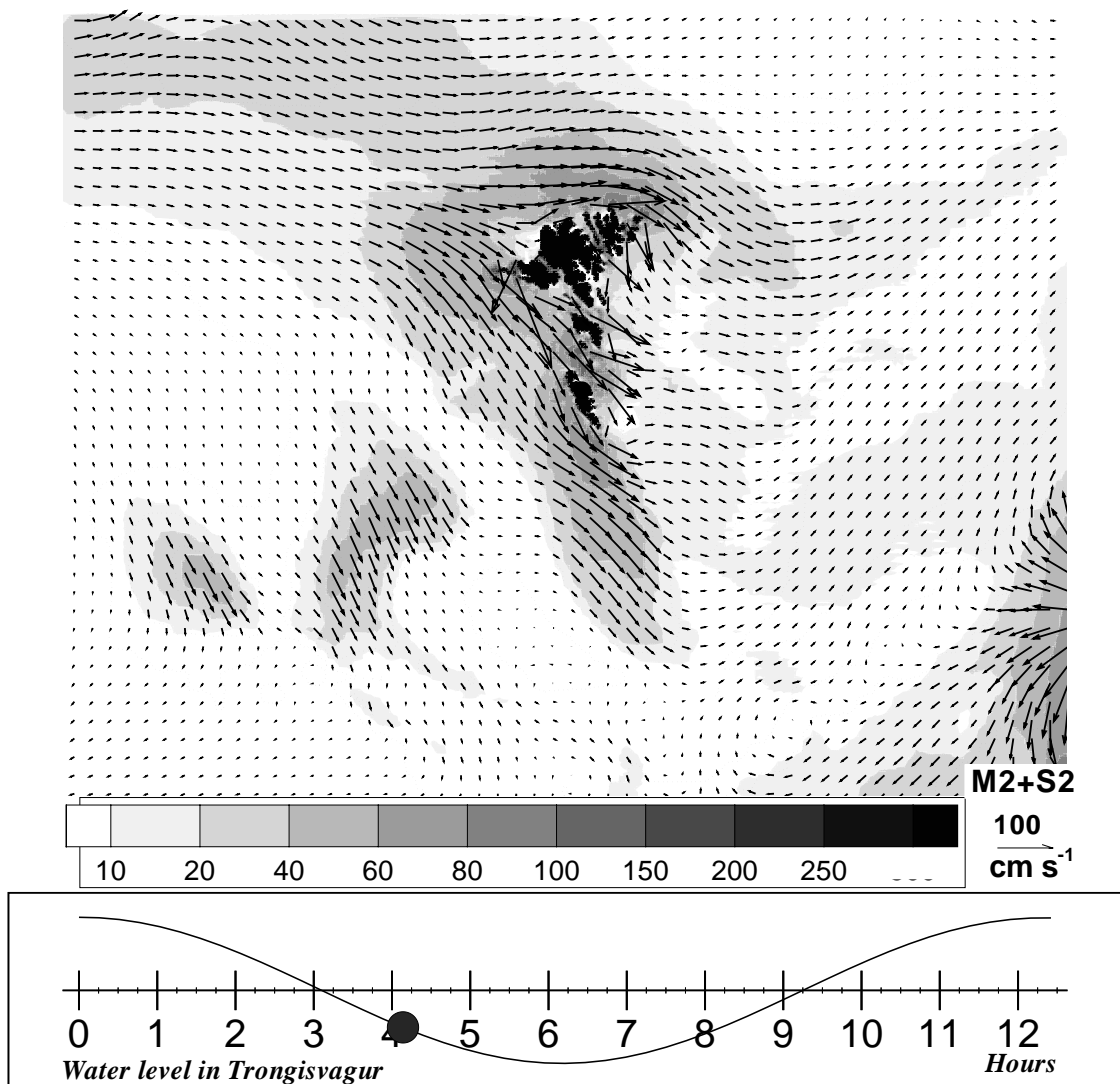
Entire model domain

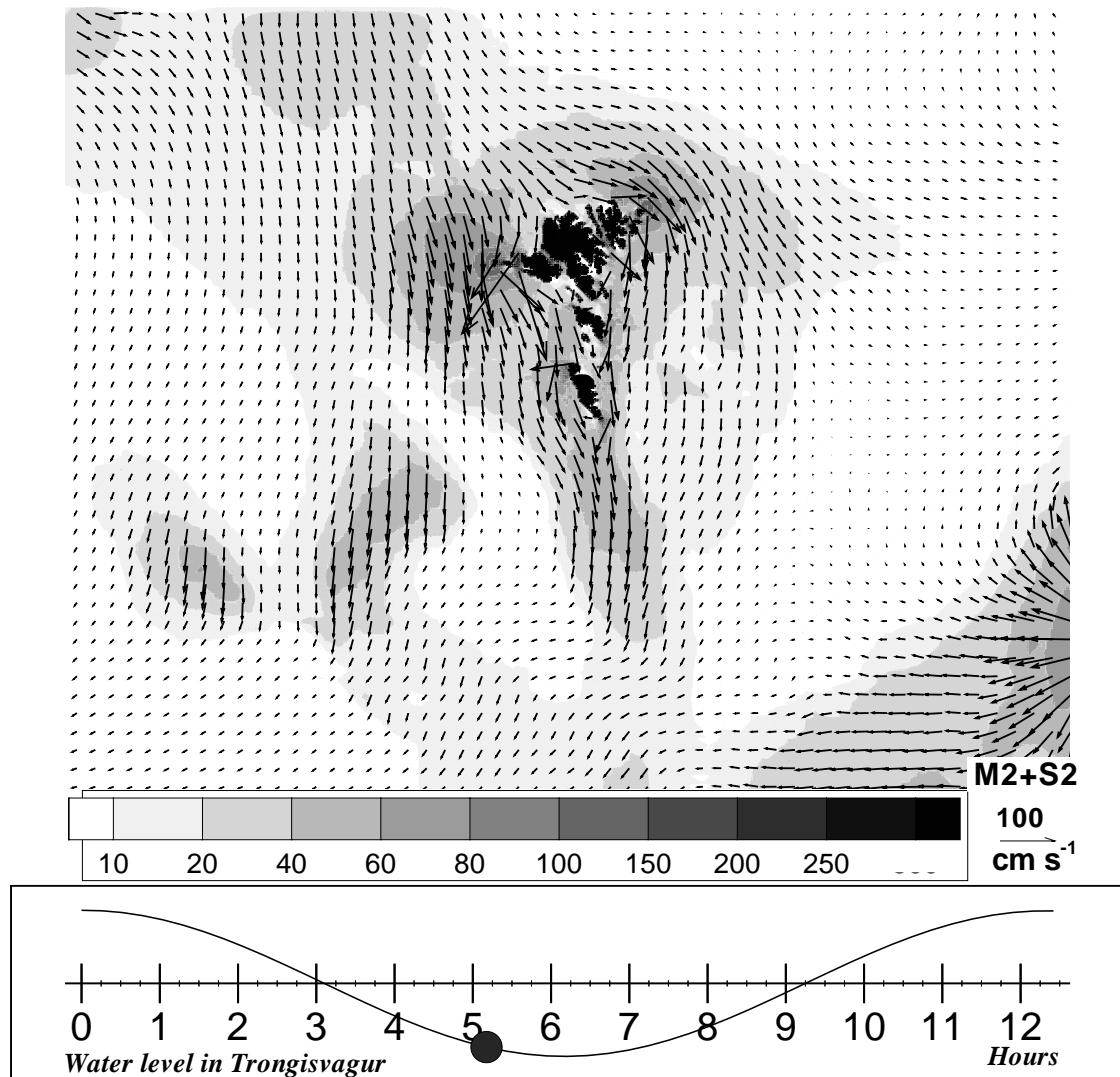


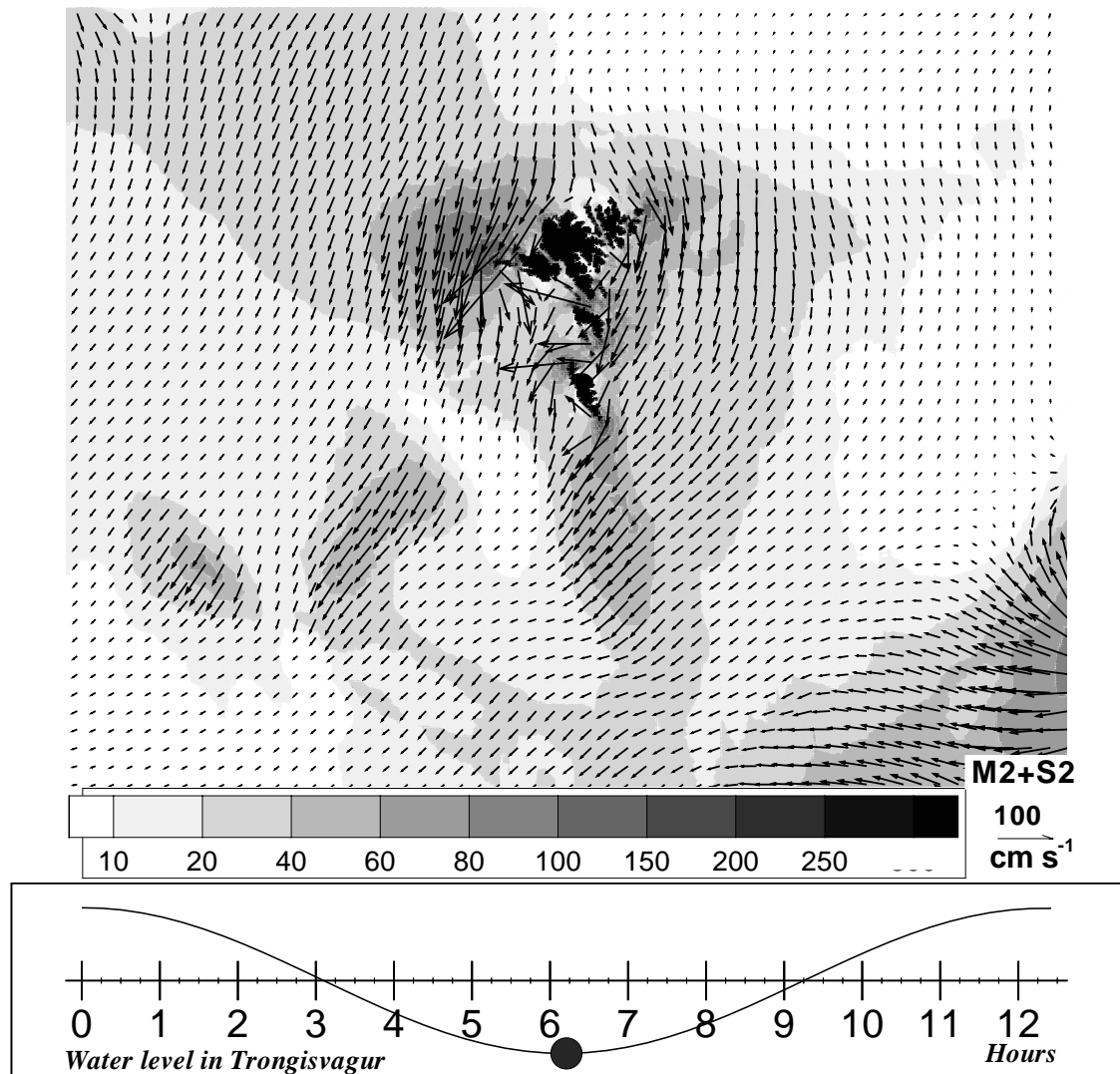


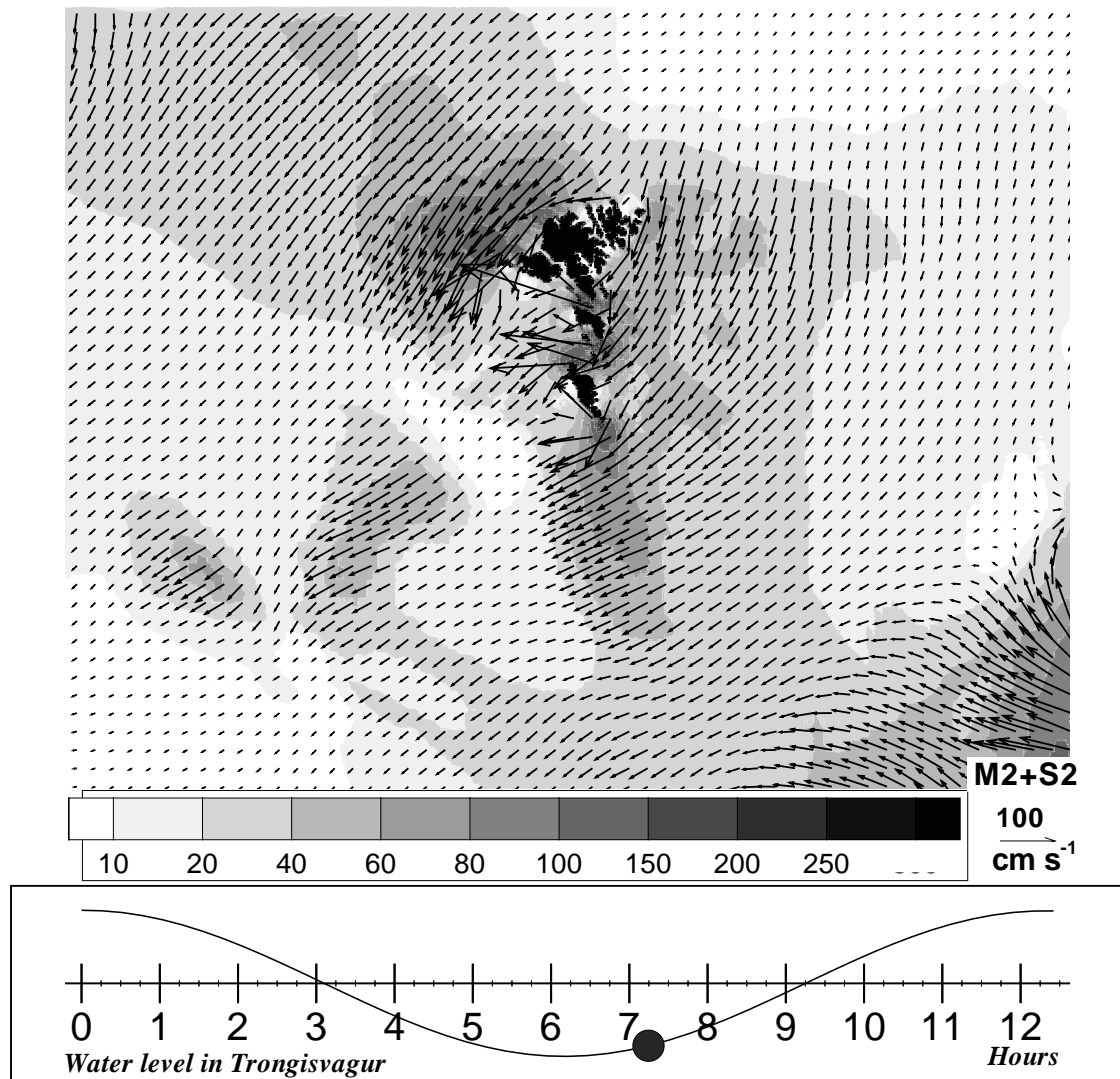


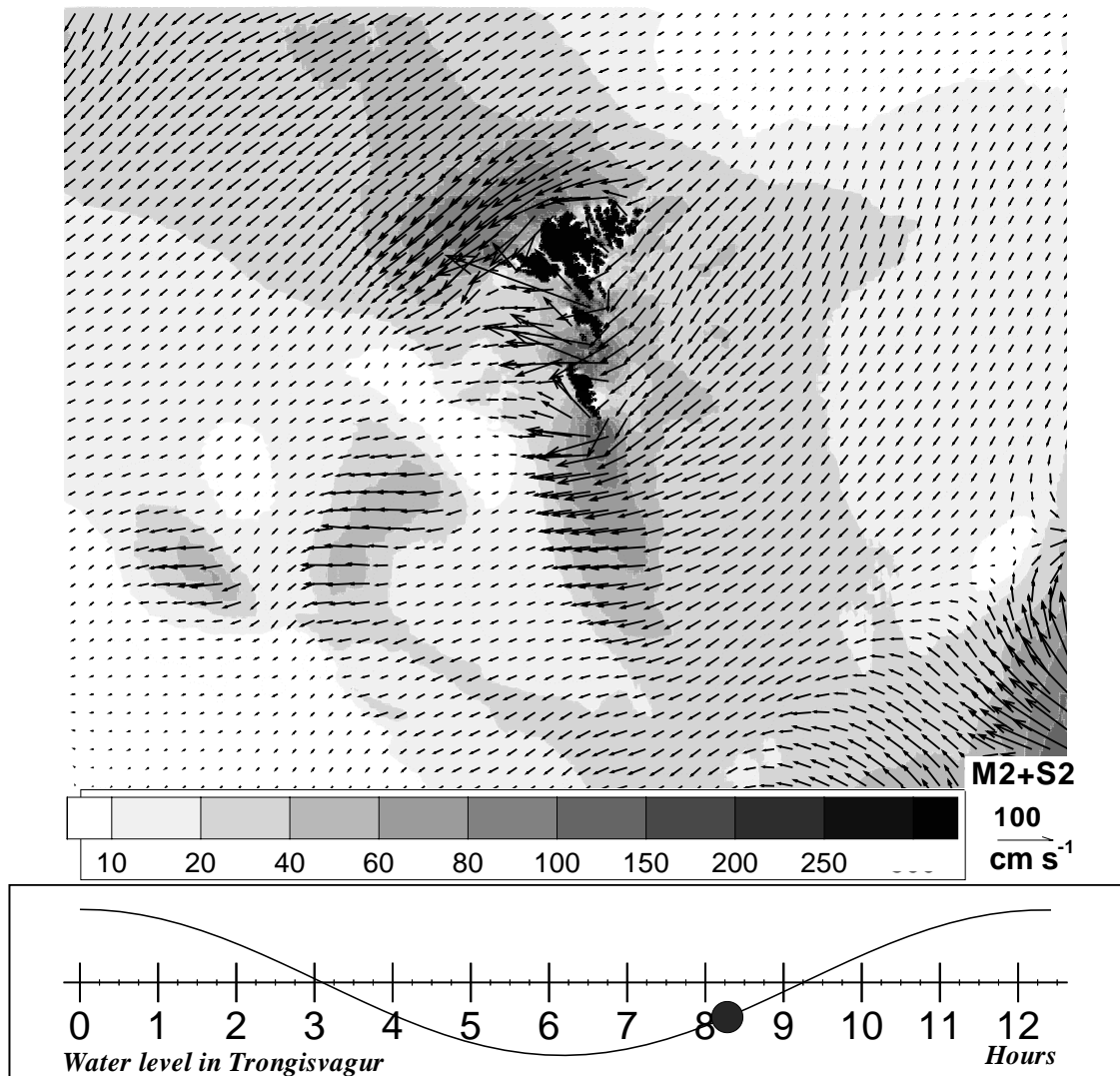


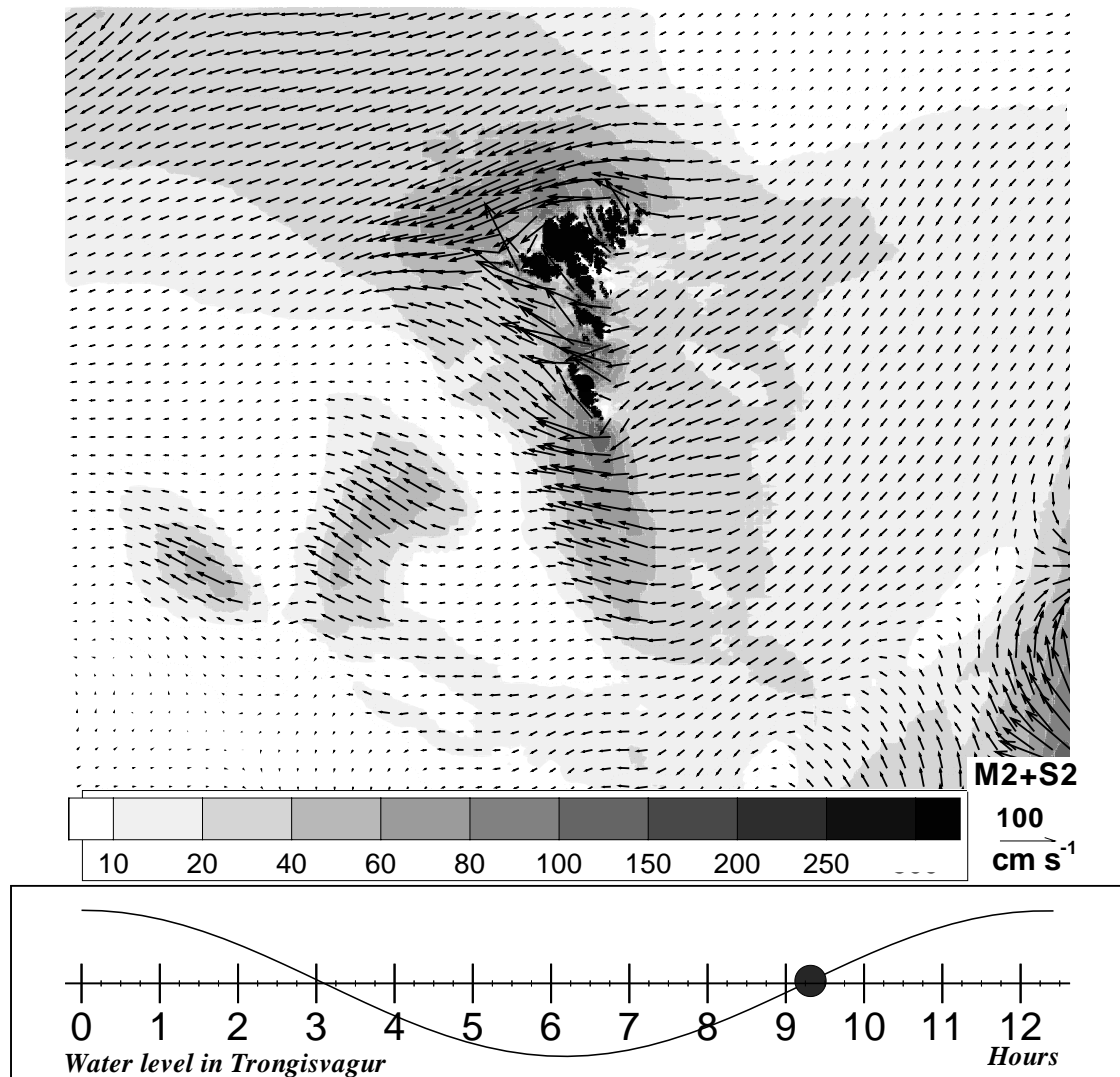


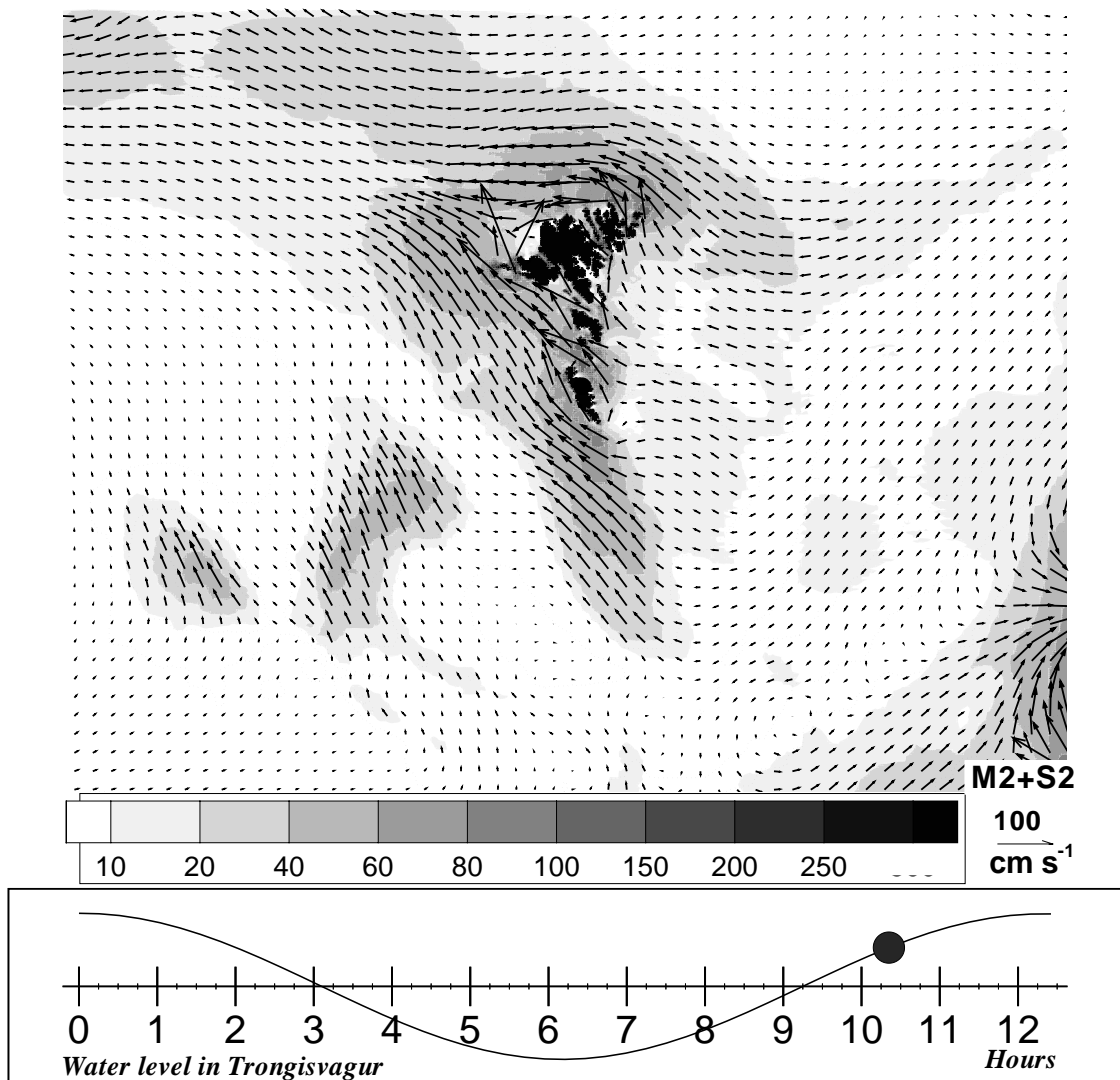


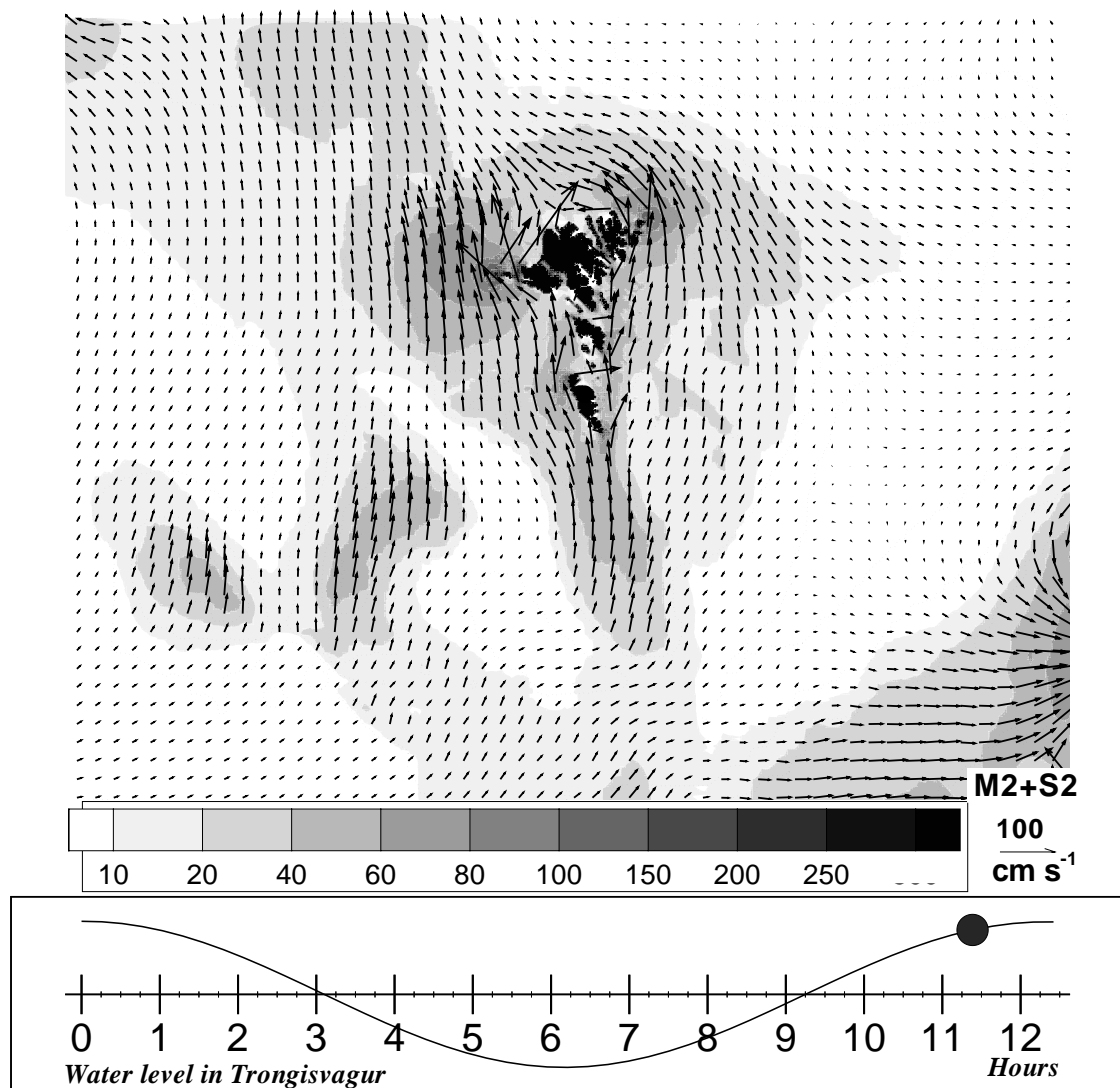




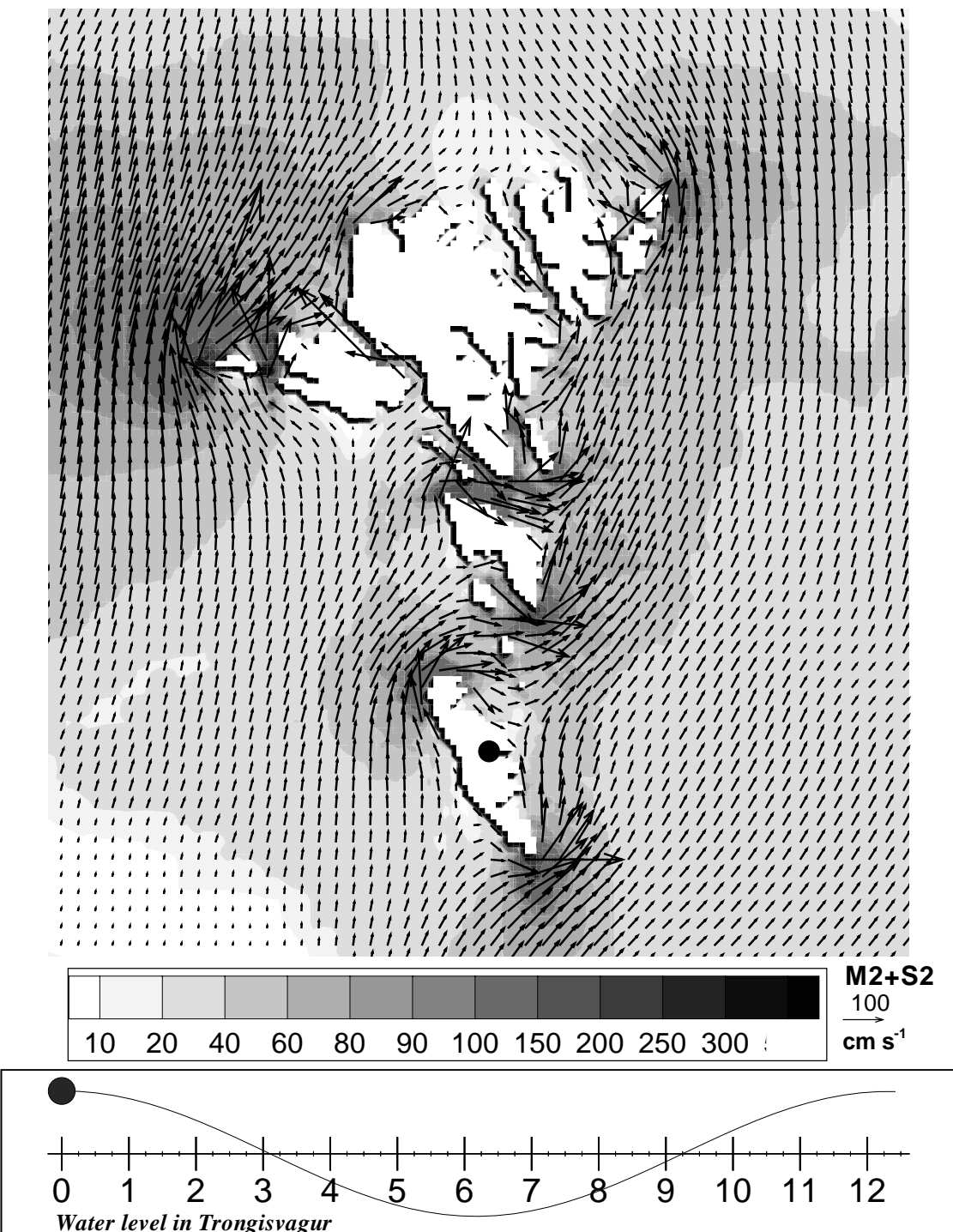


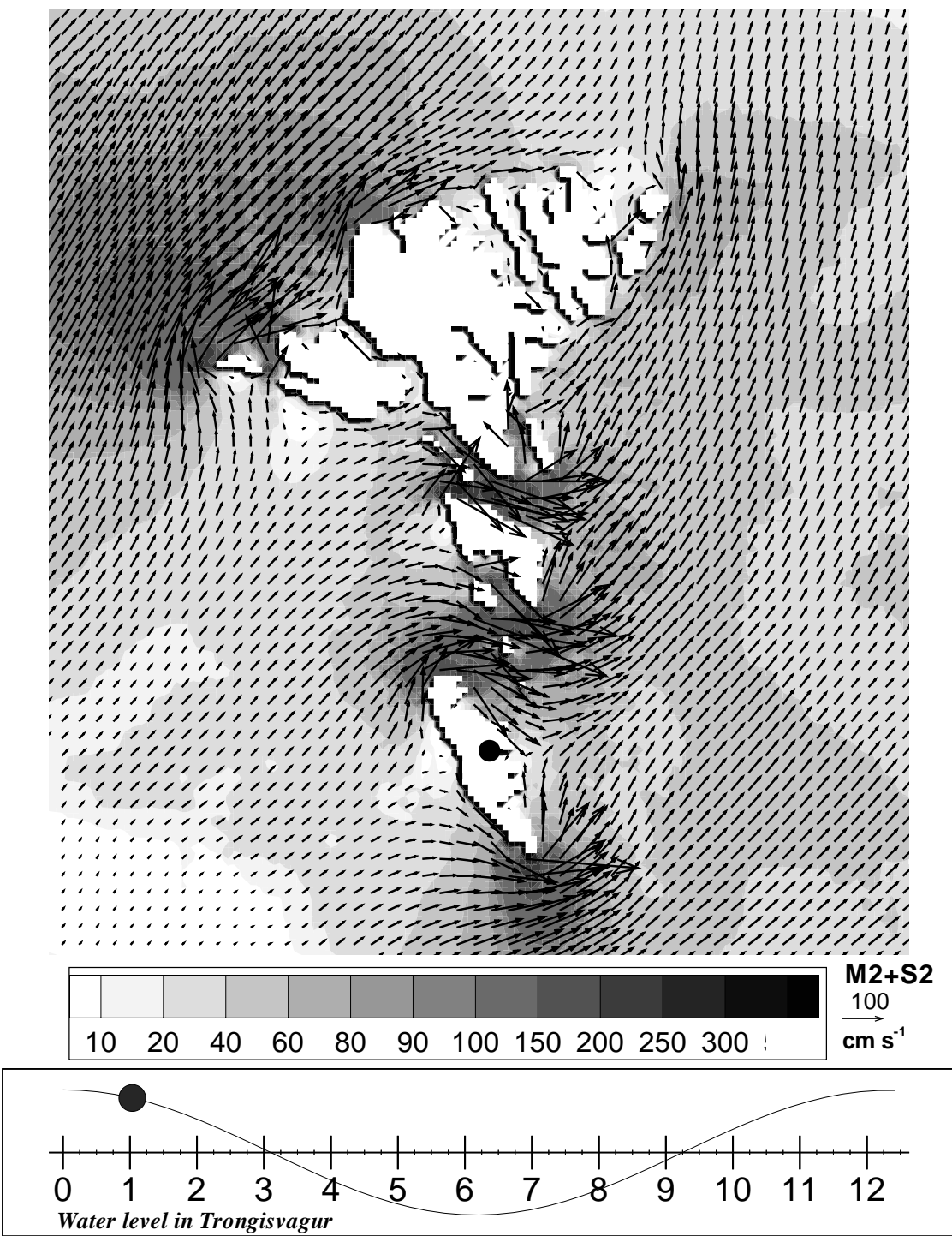


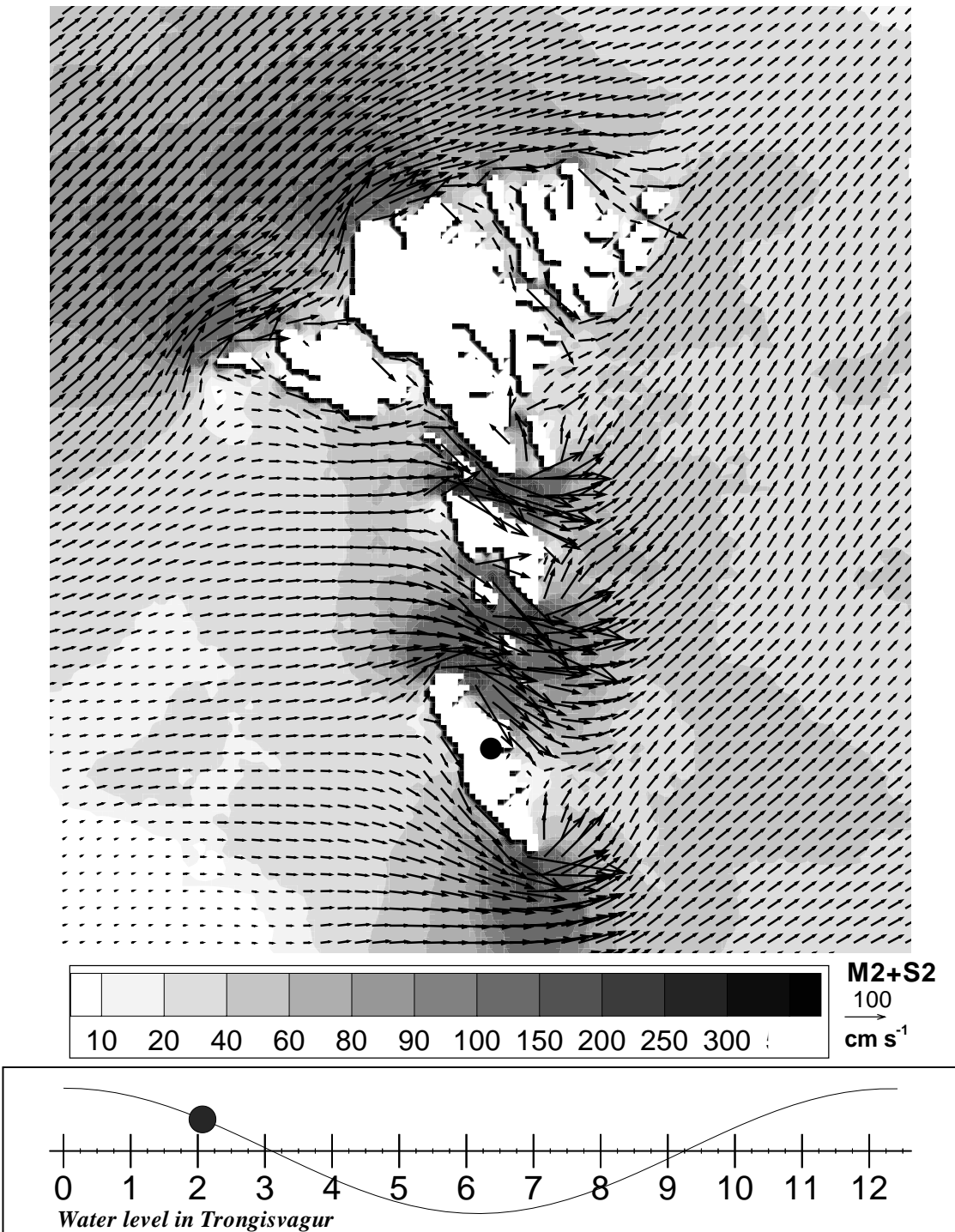


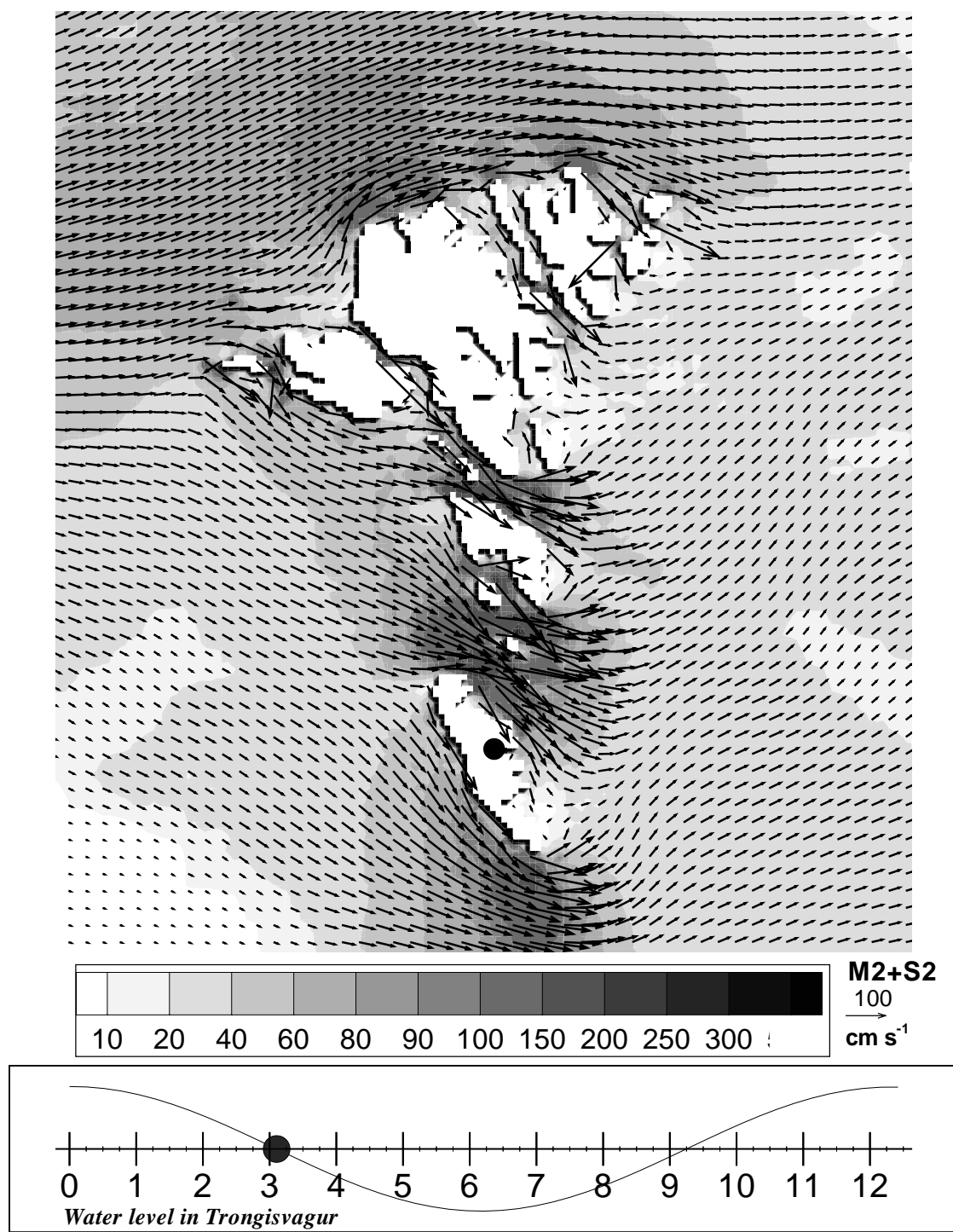


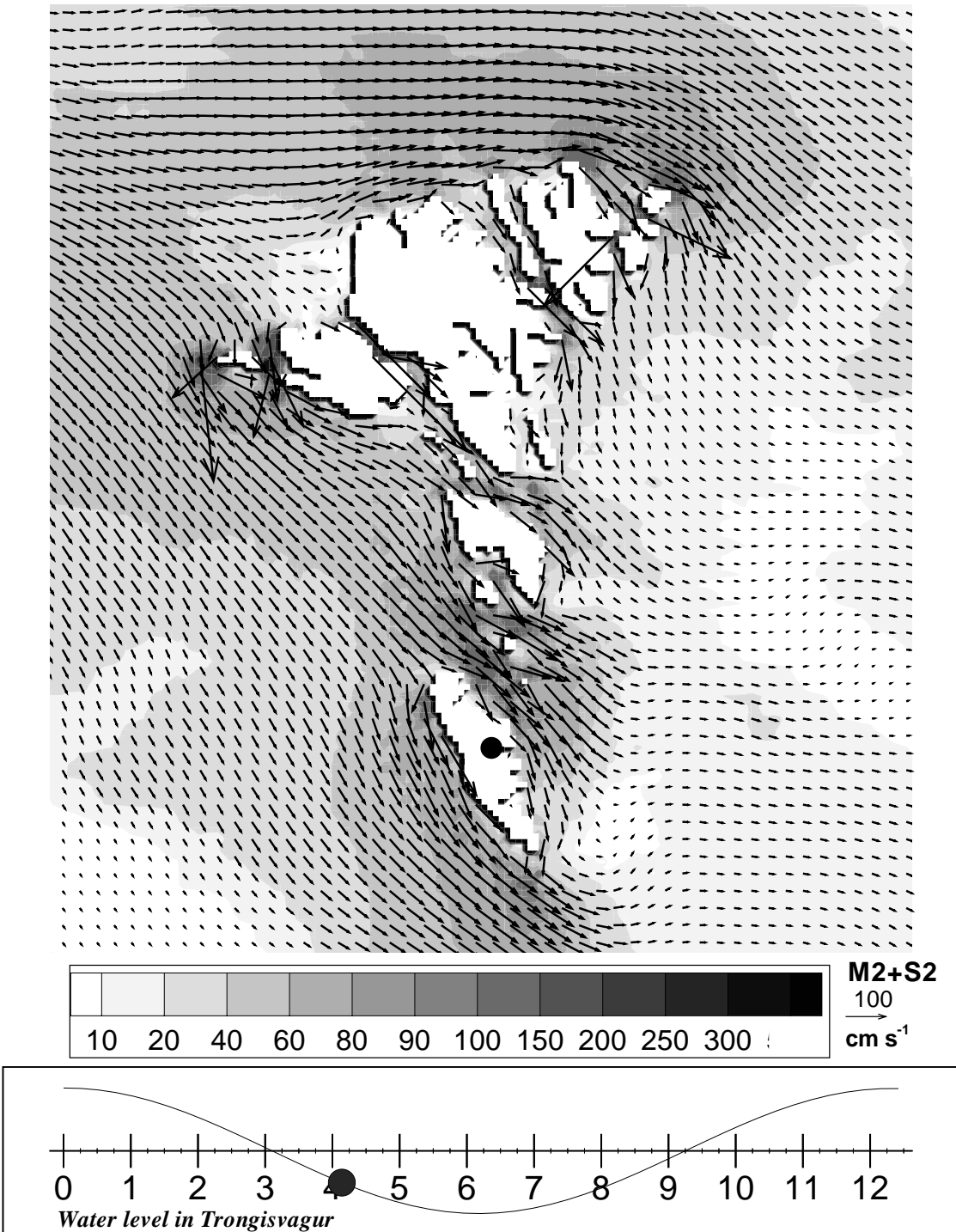
Coastal regions of the Faroe Islands

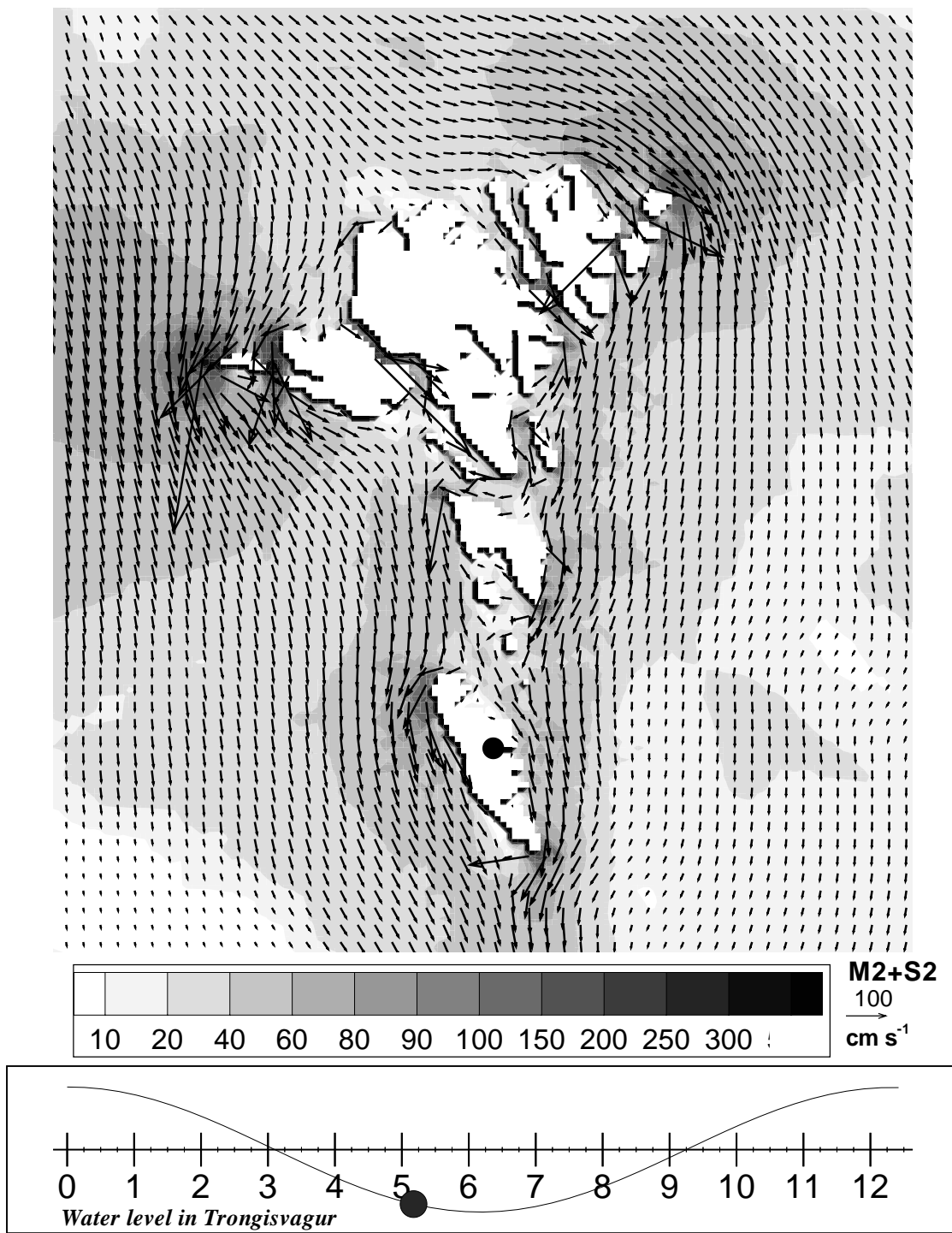


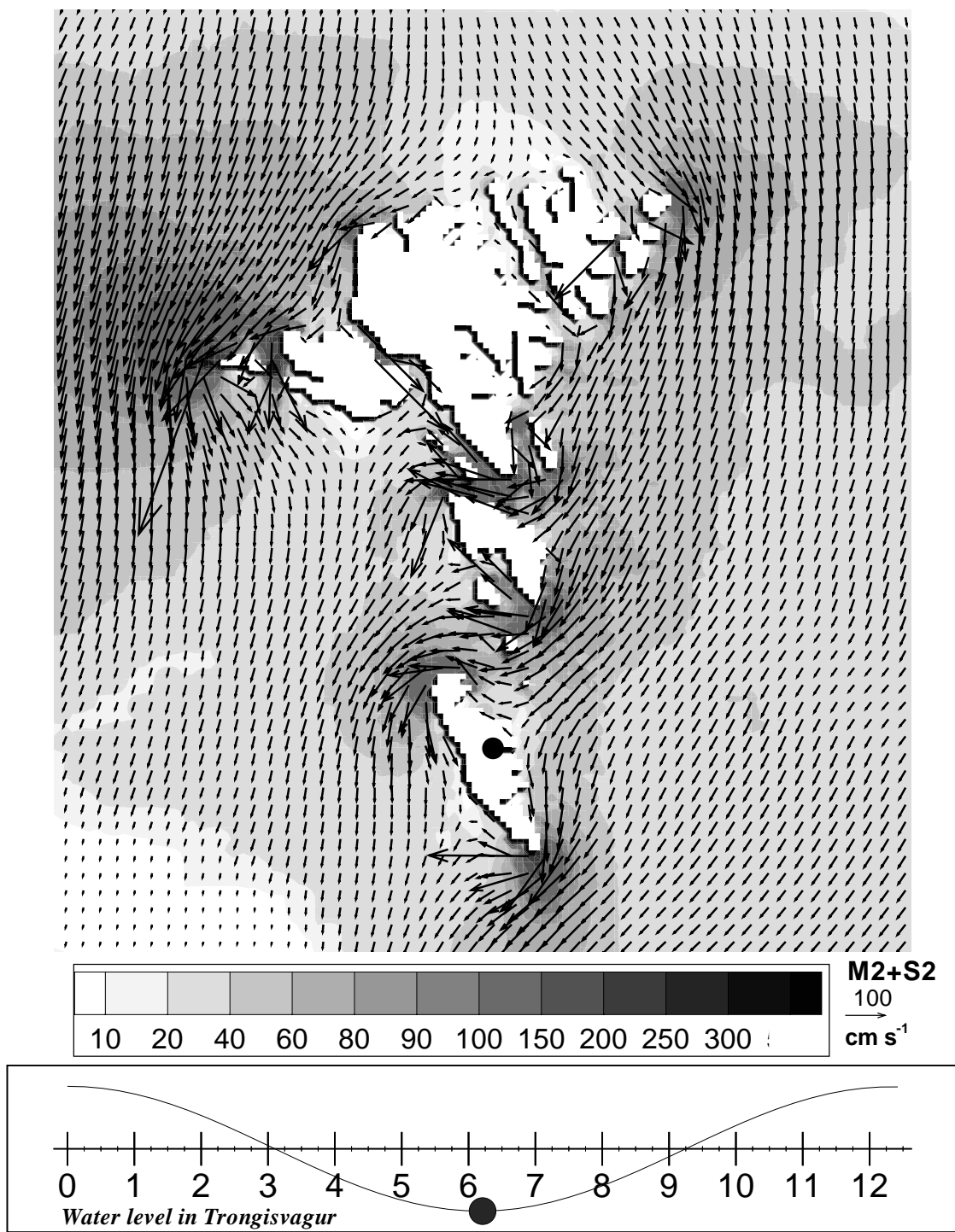


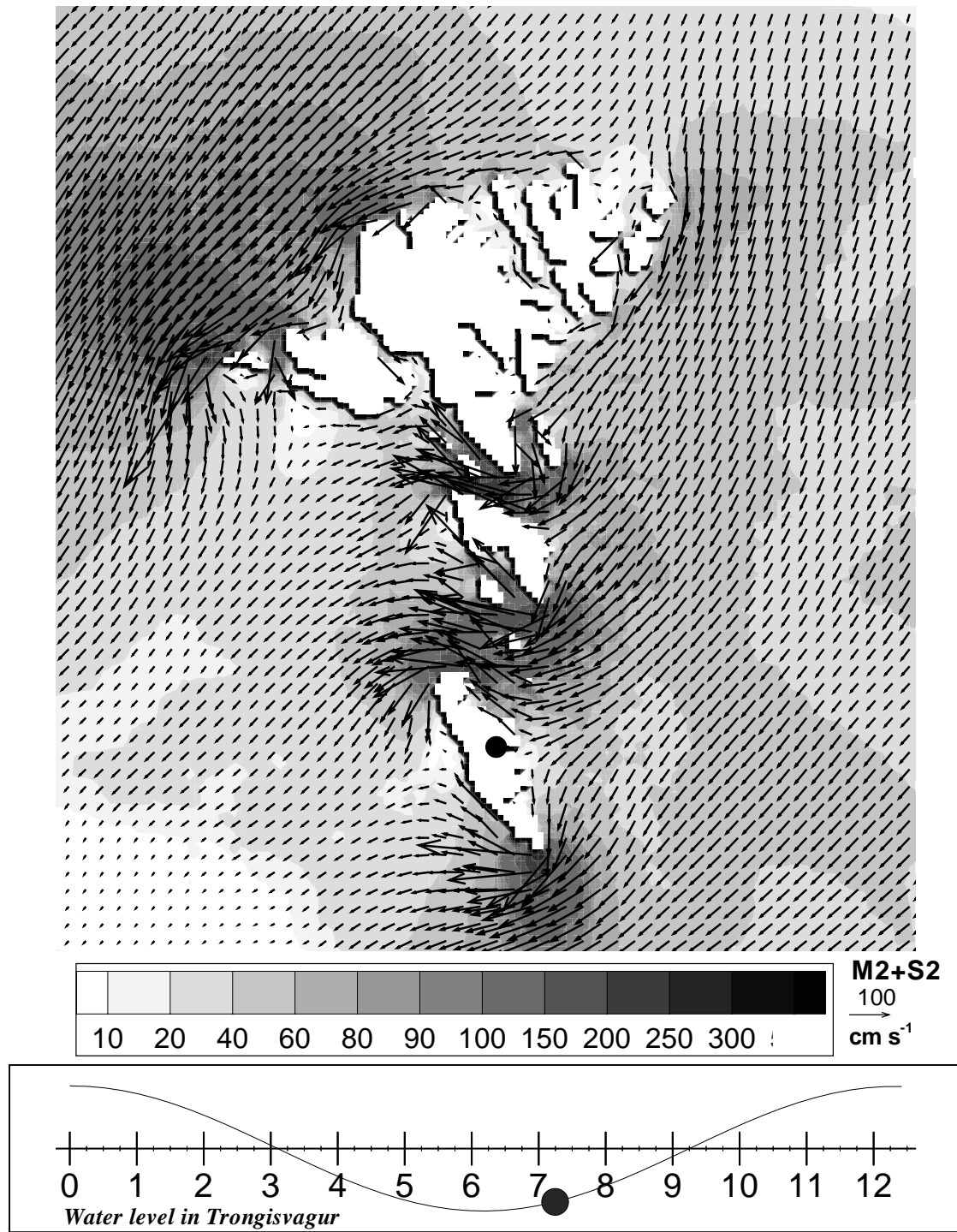


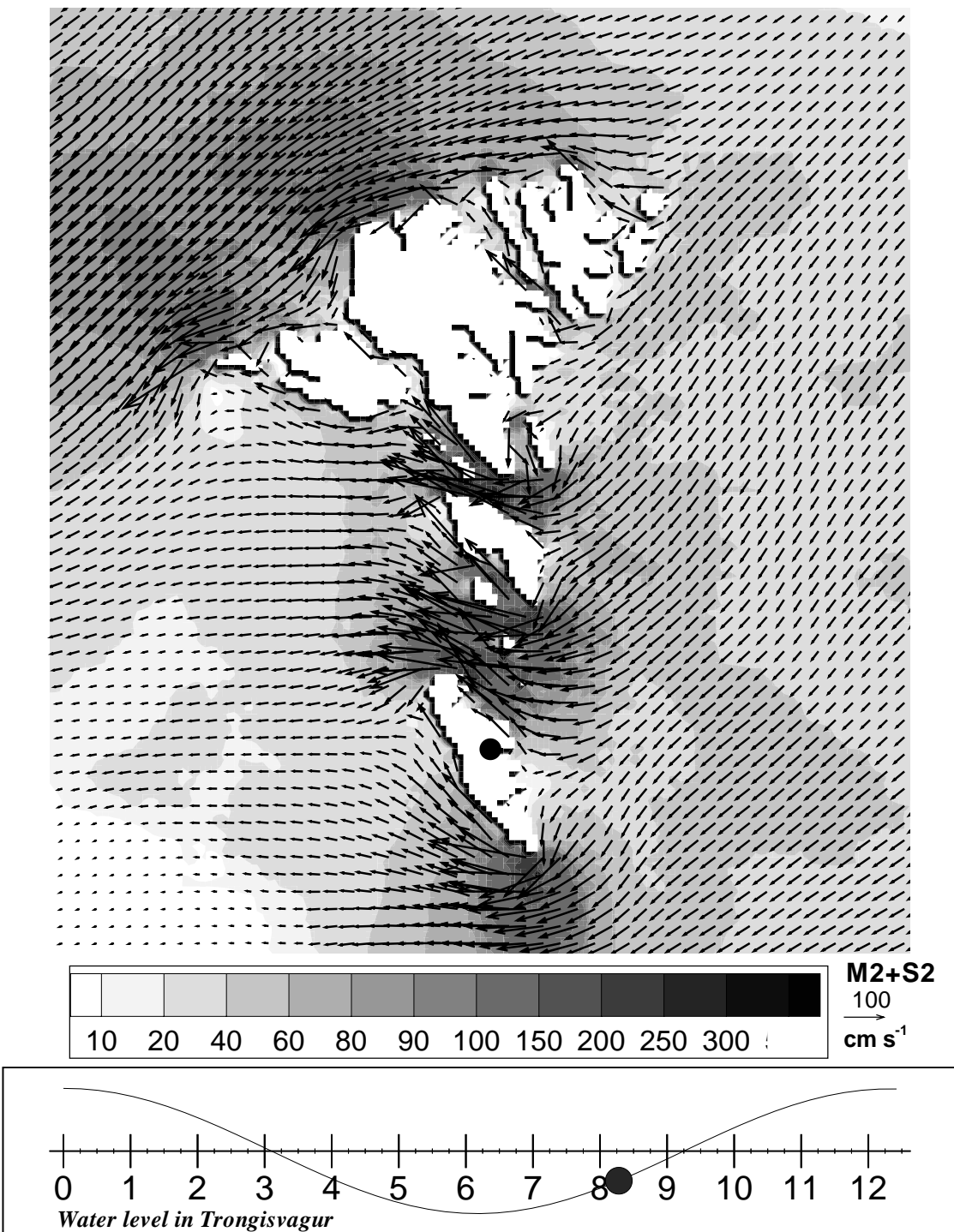


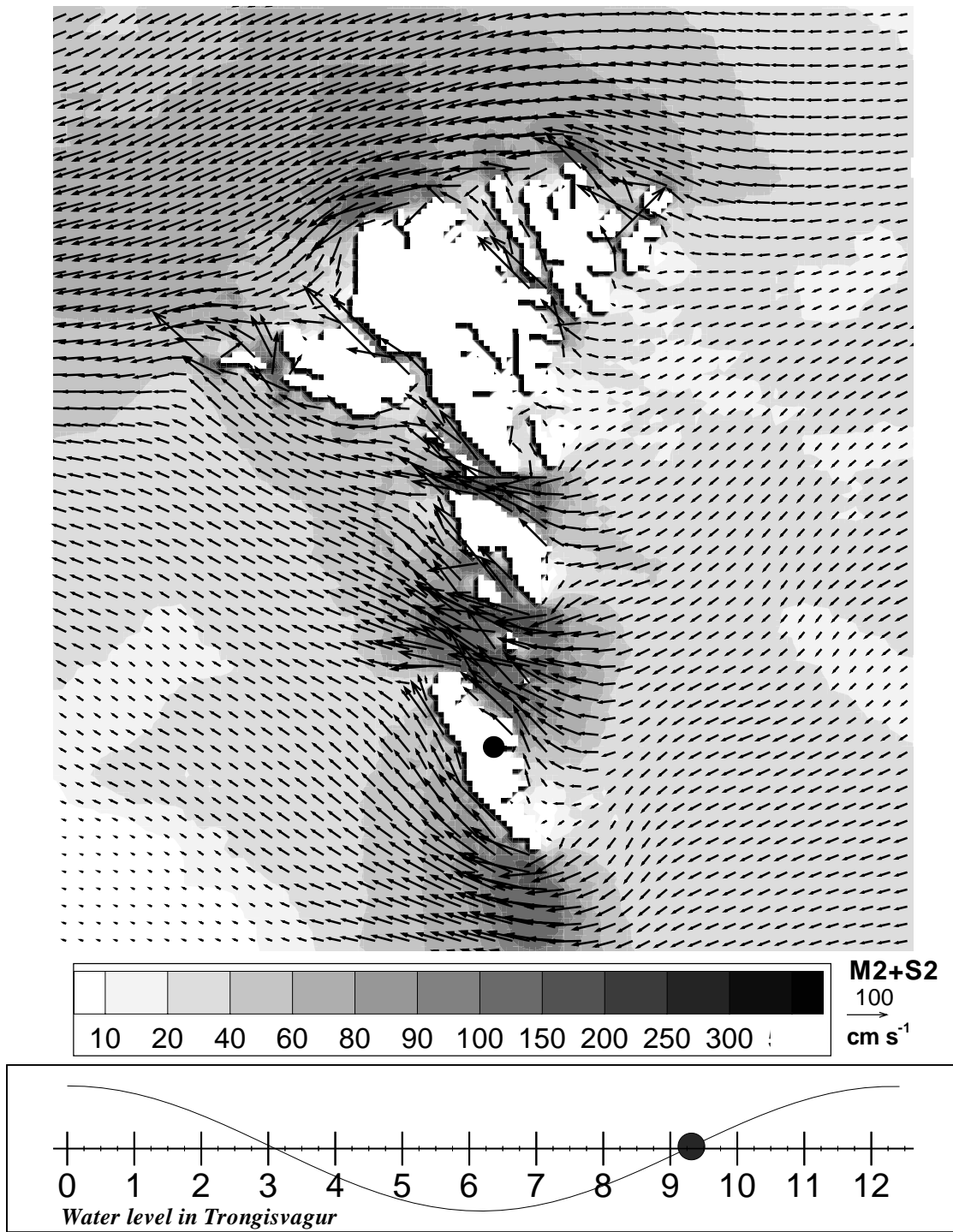


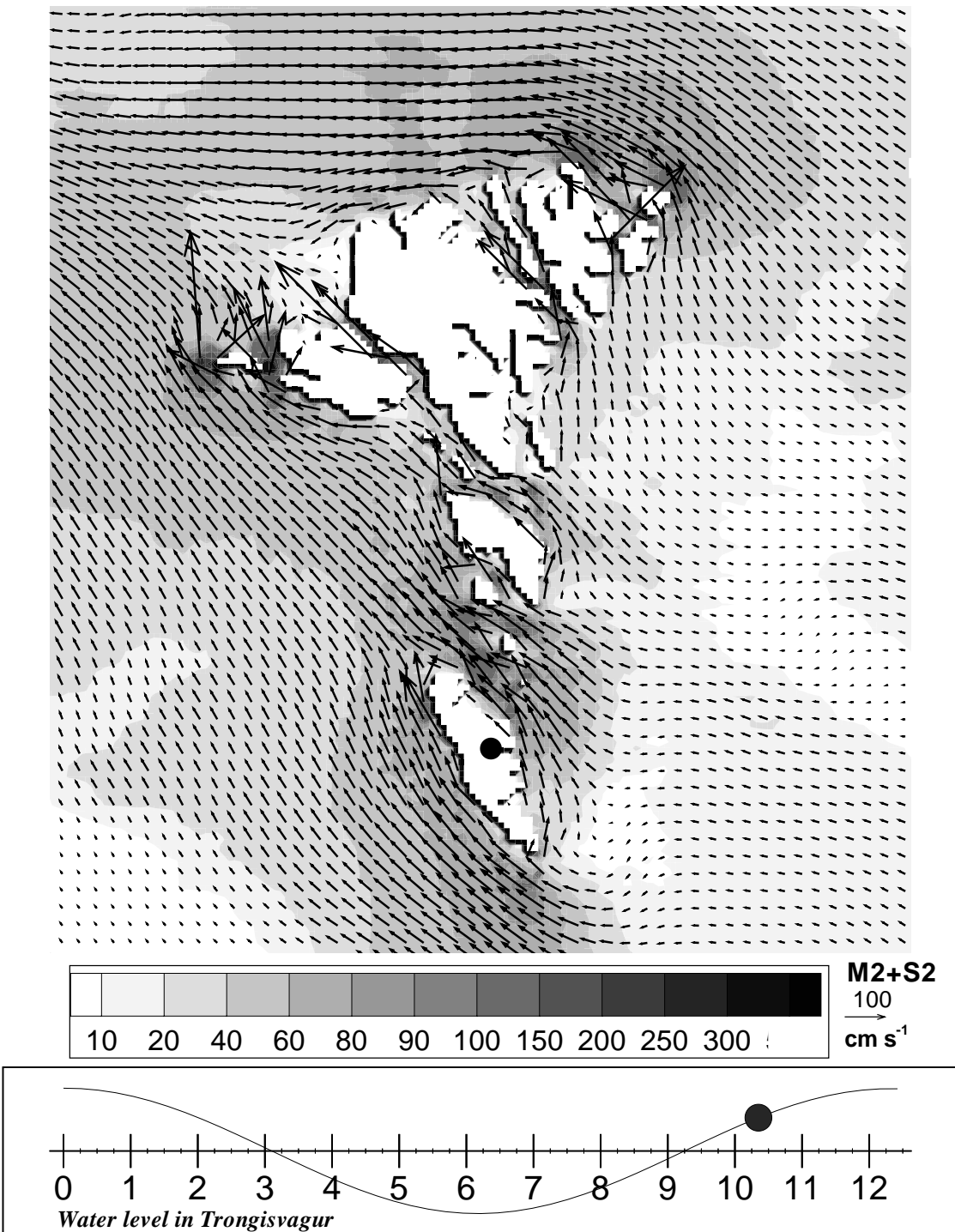


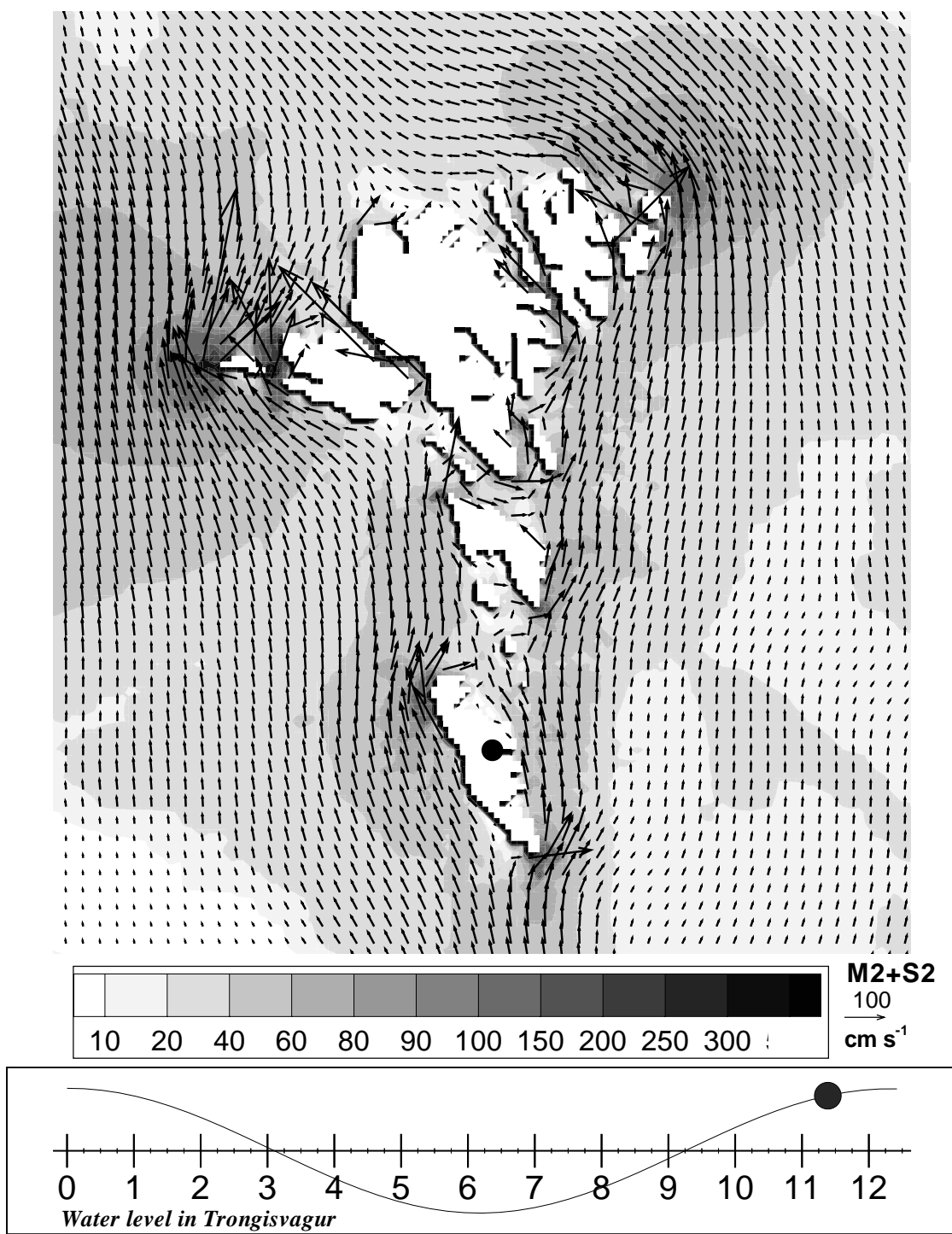


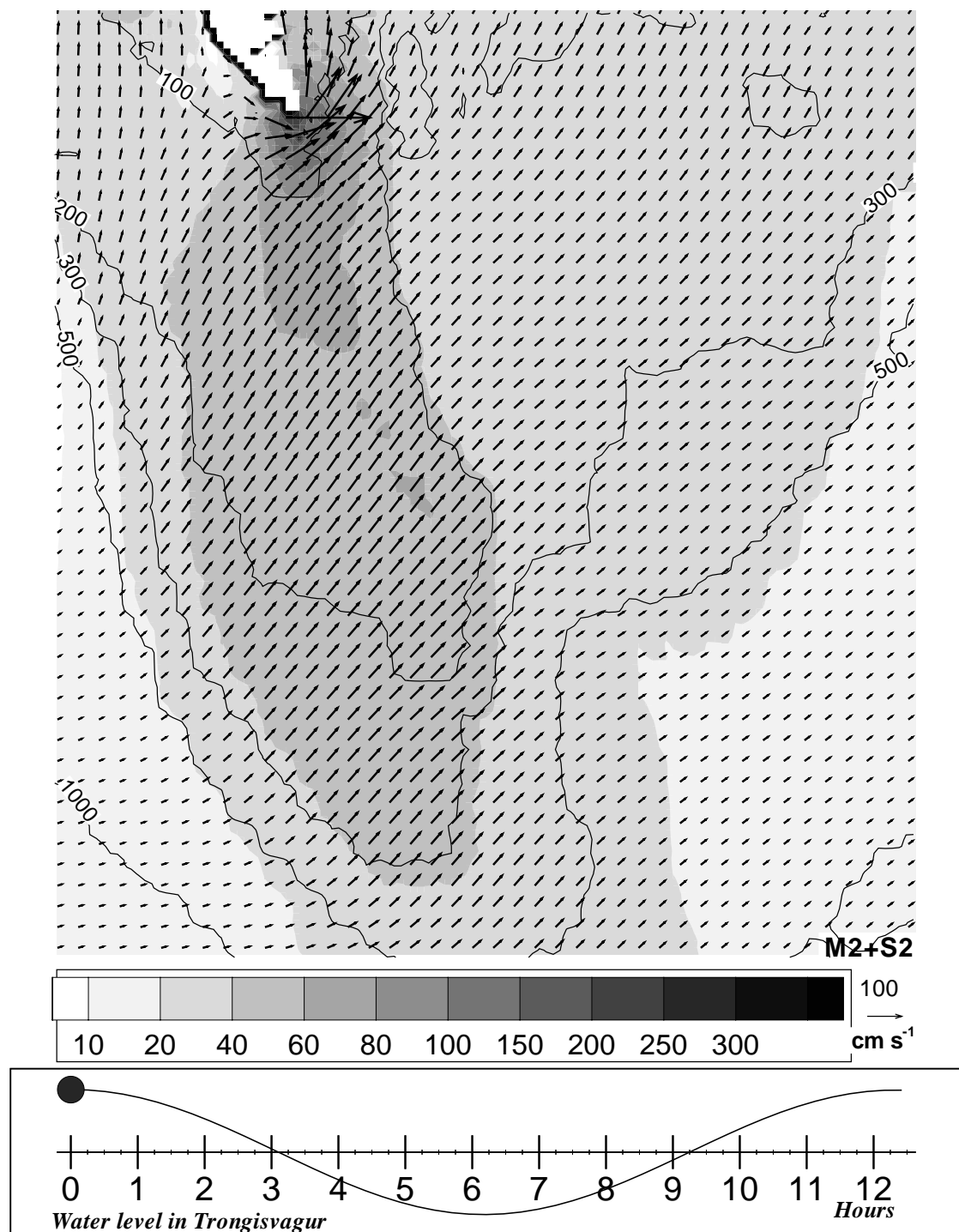


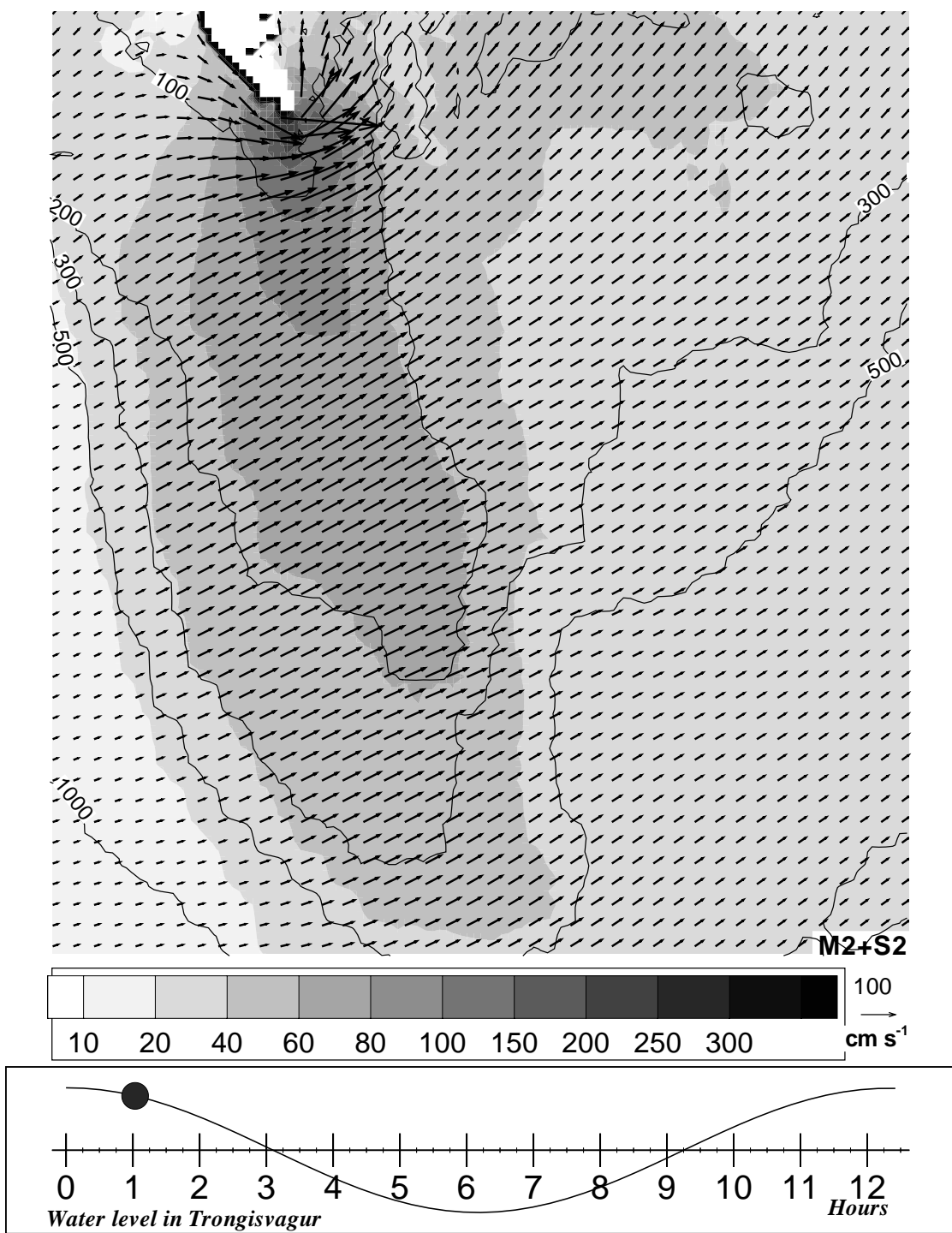


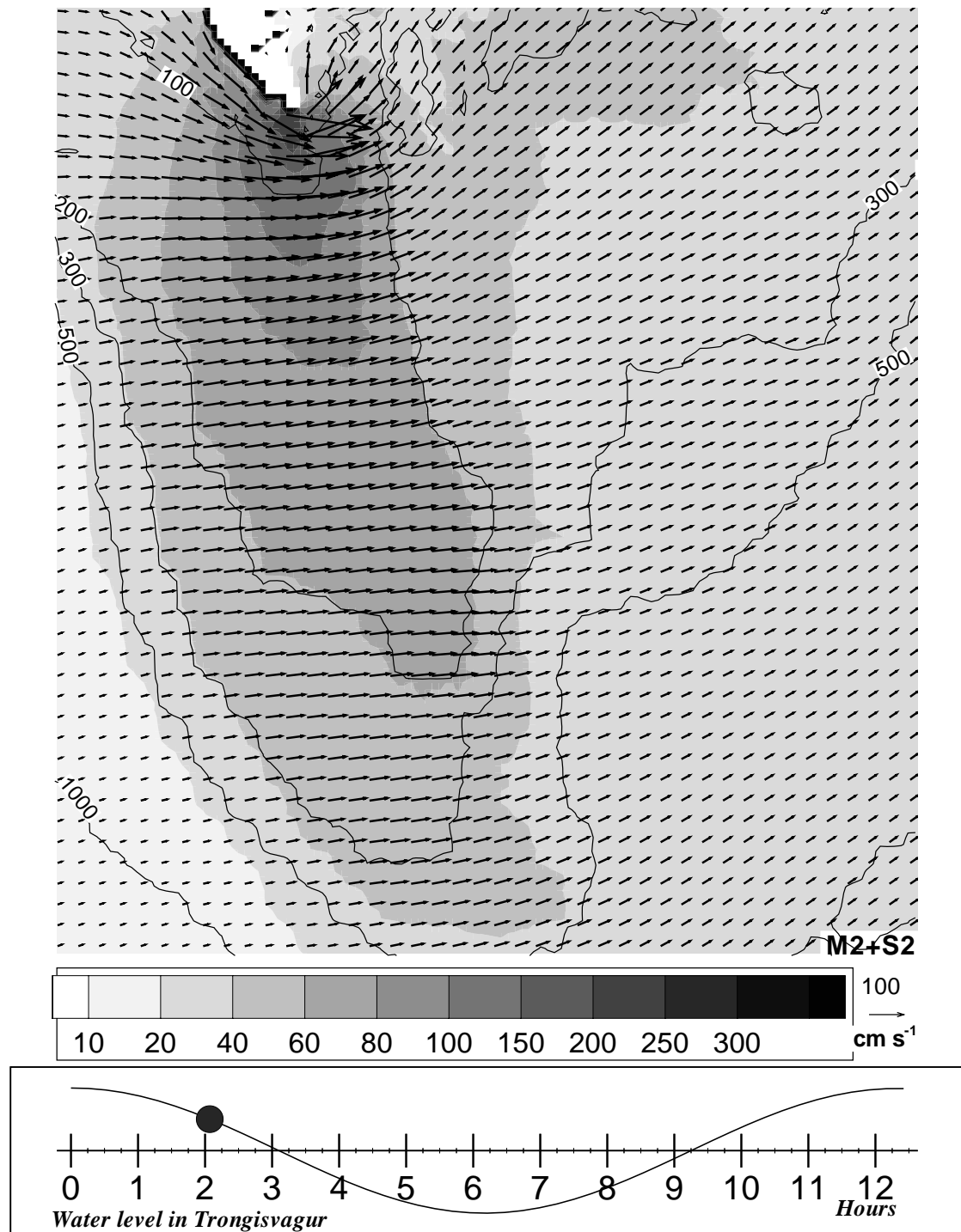


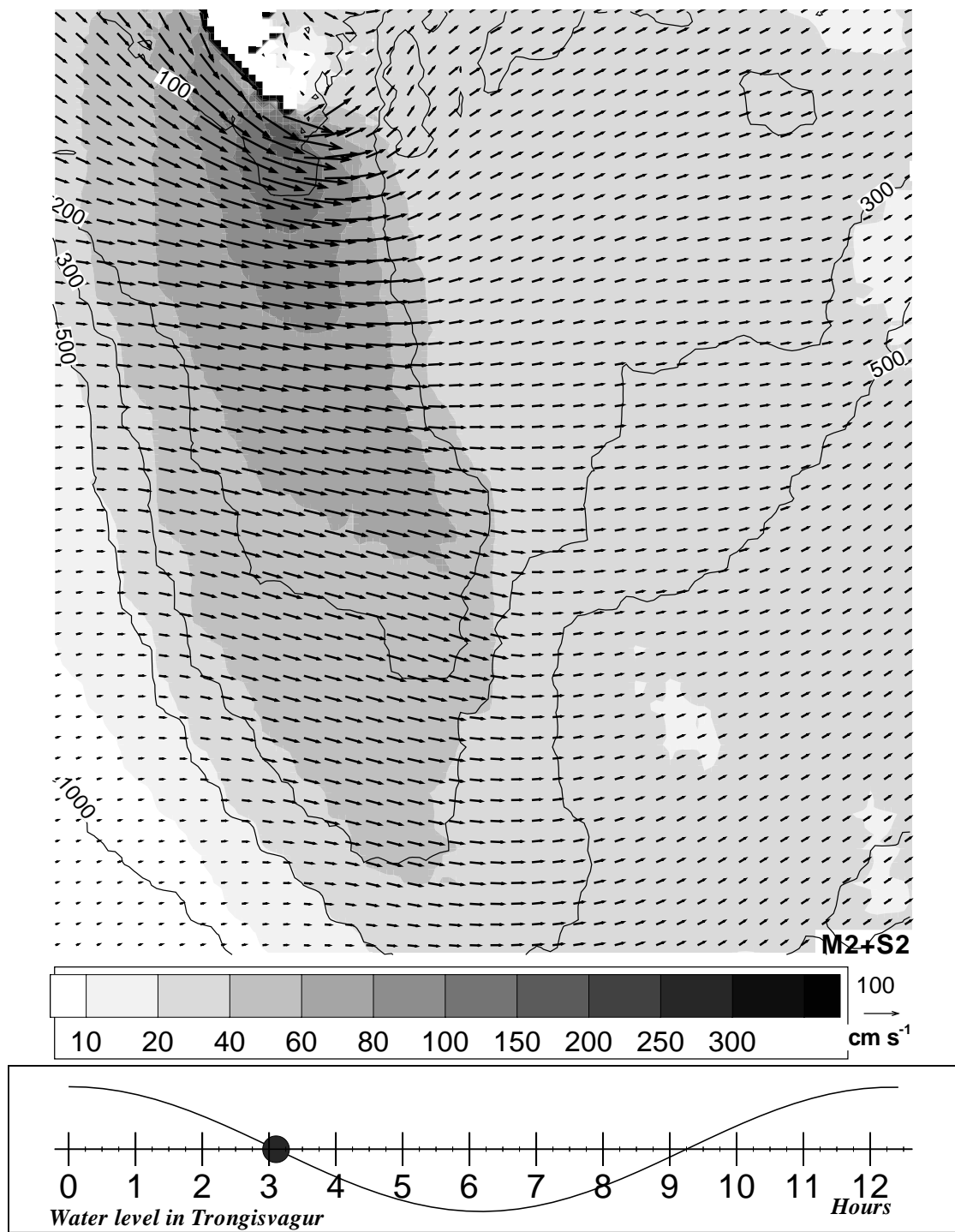


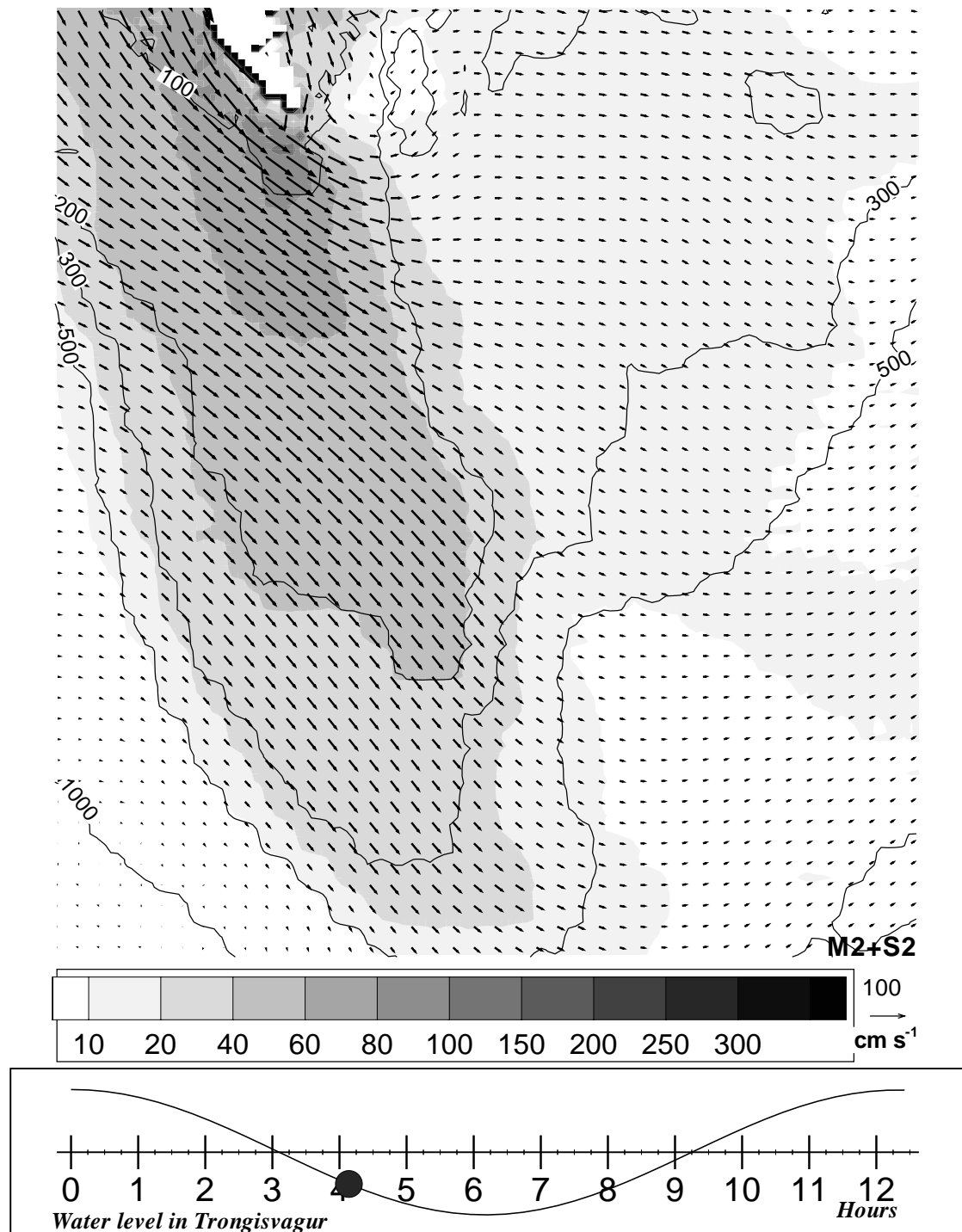


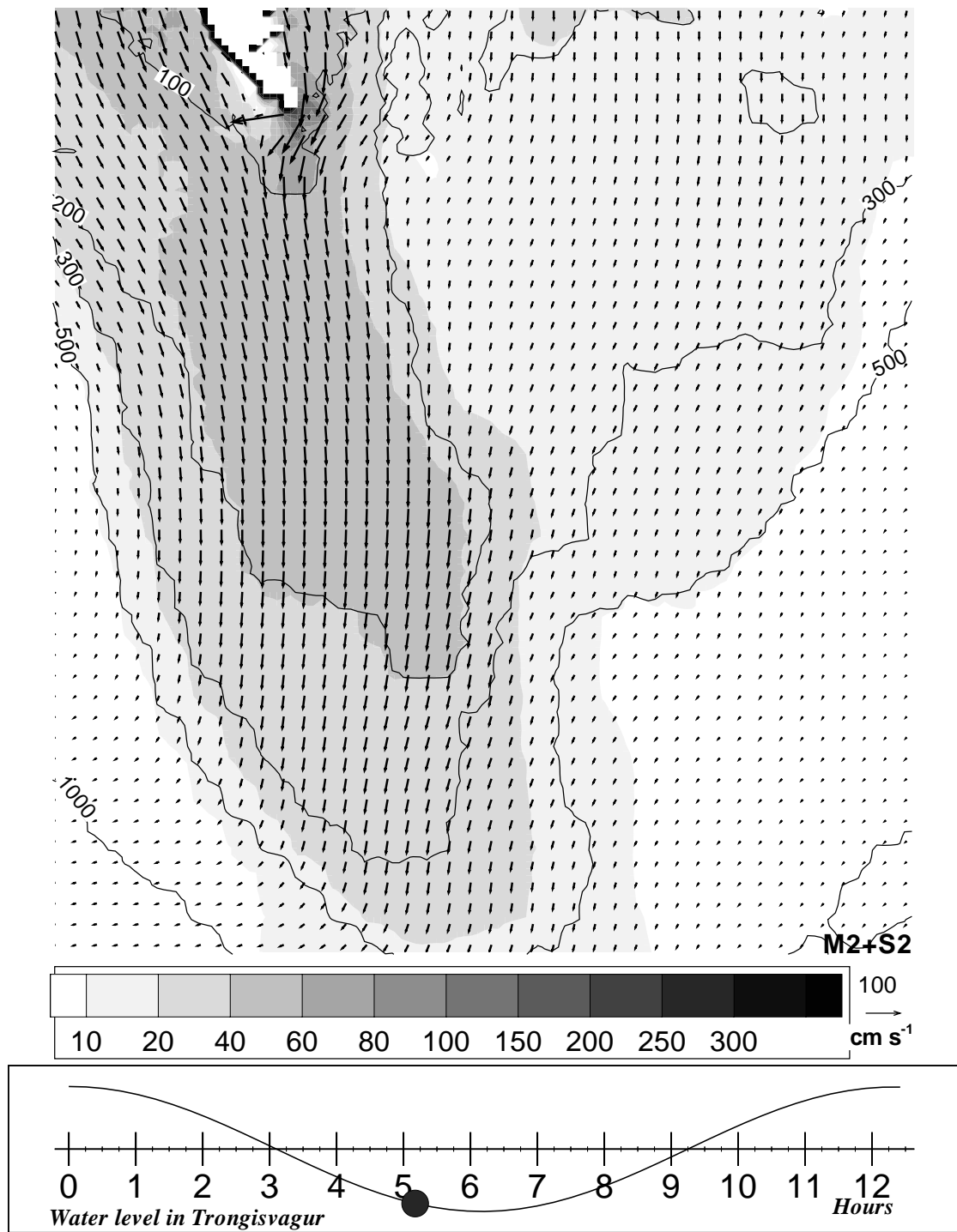
Munkagrunnimum on the southern Faroe Shelf

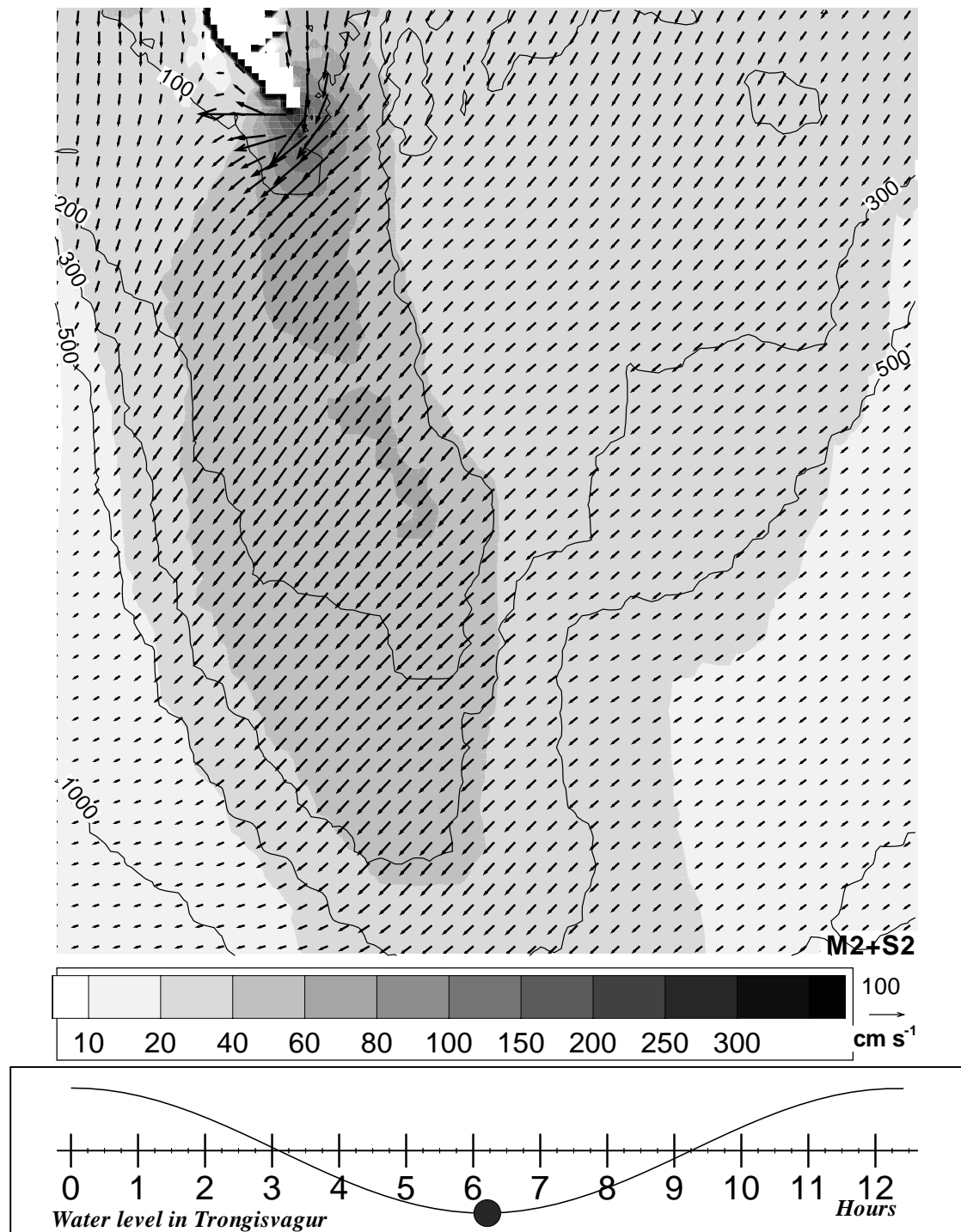


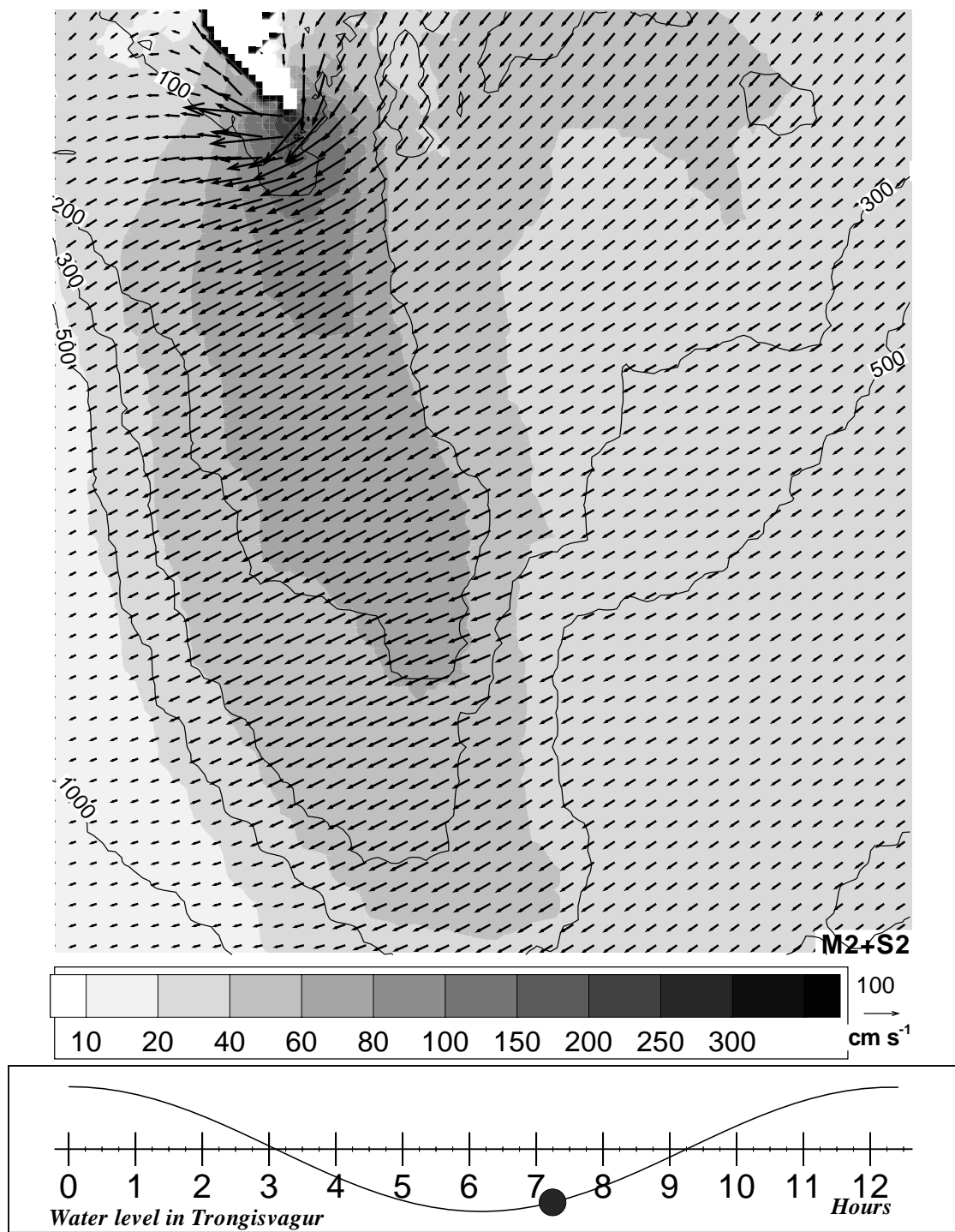


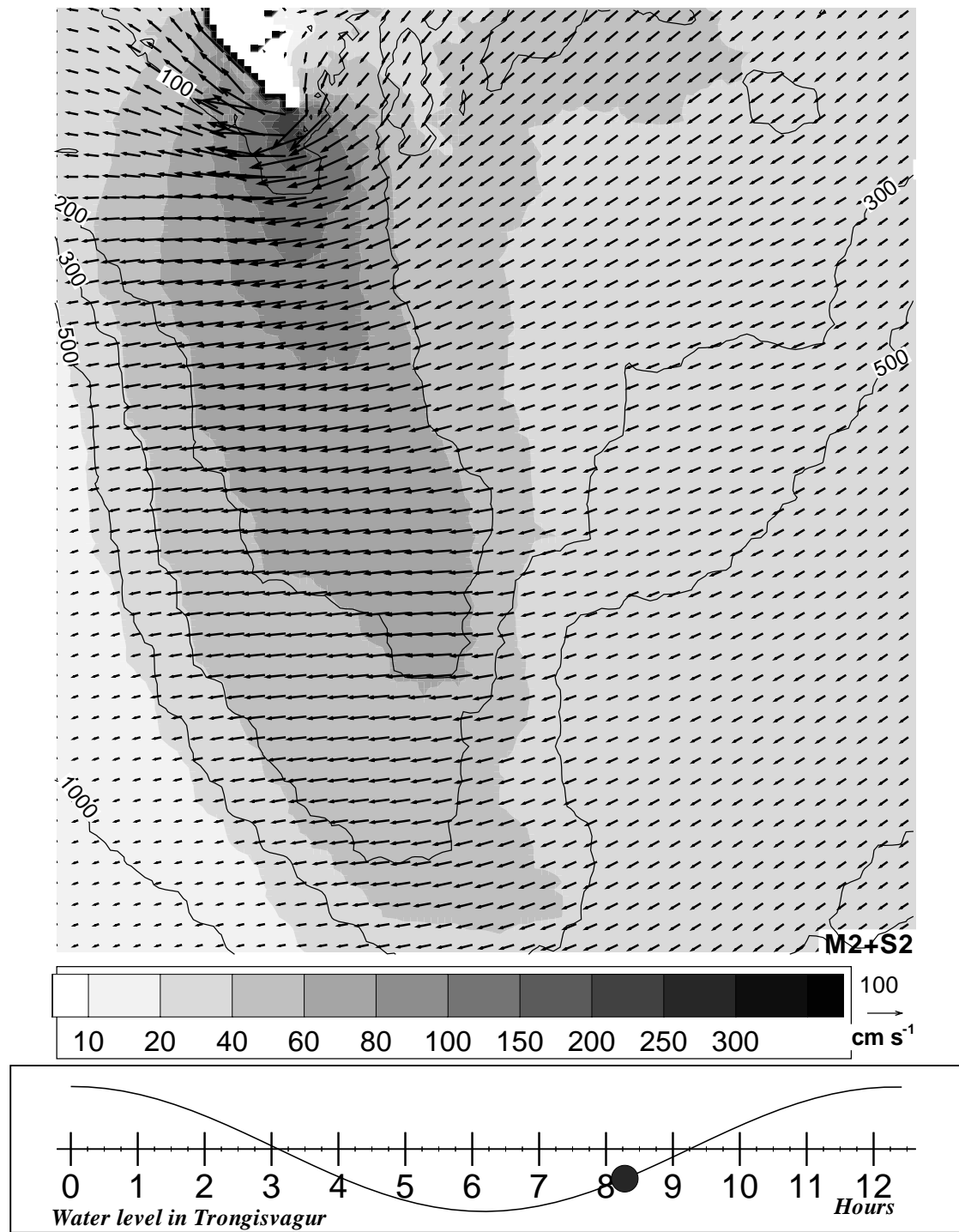


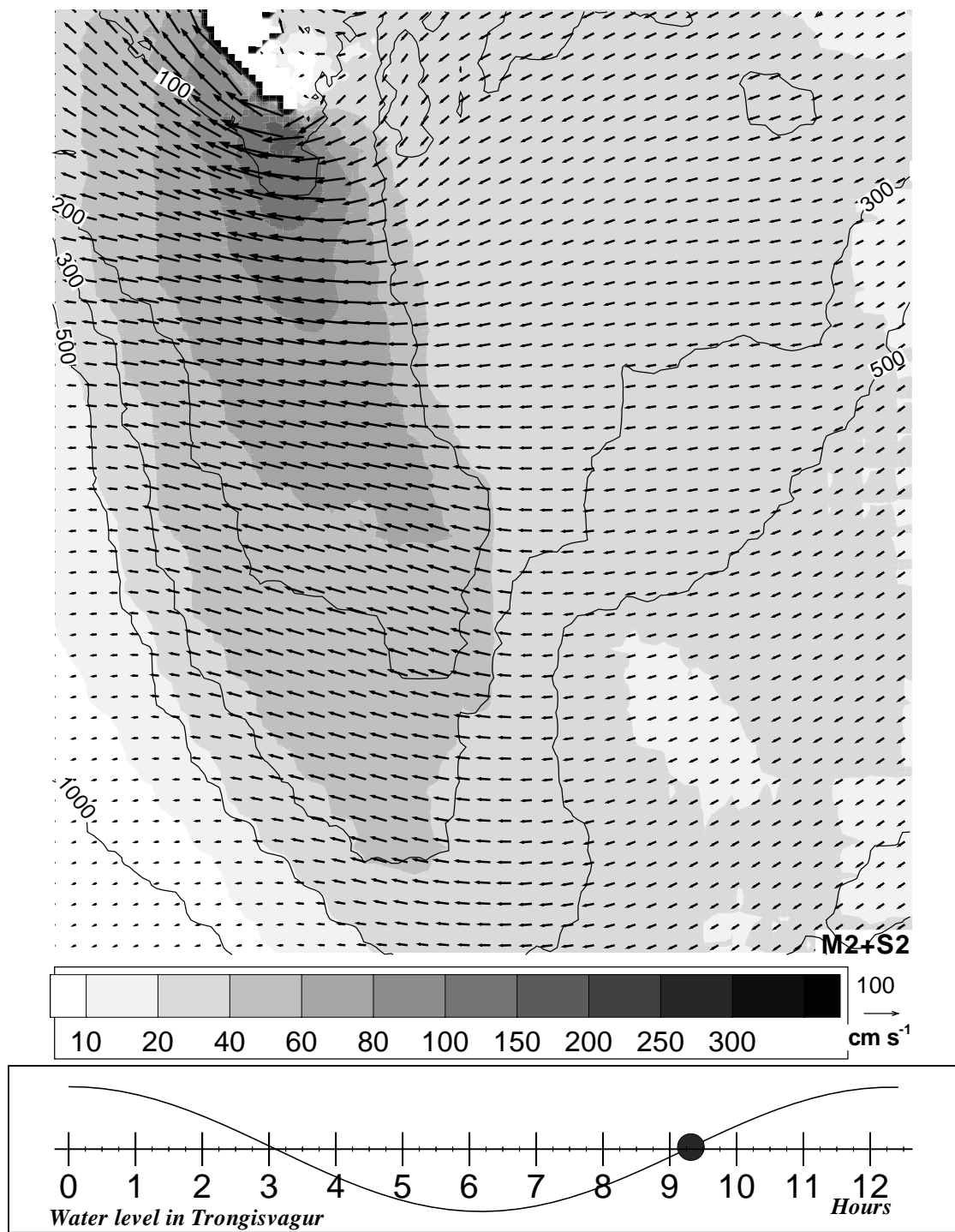


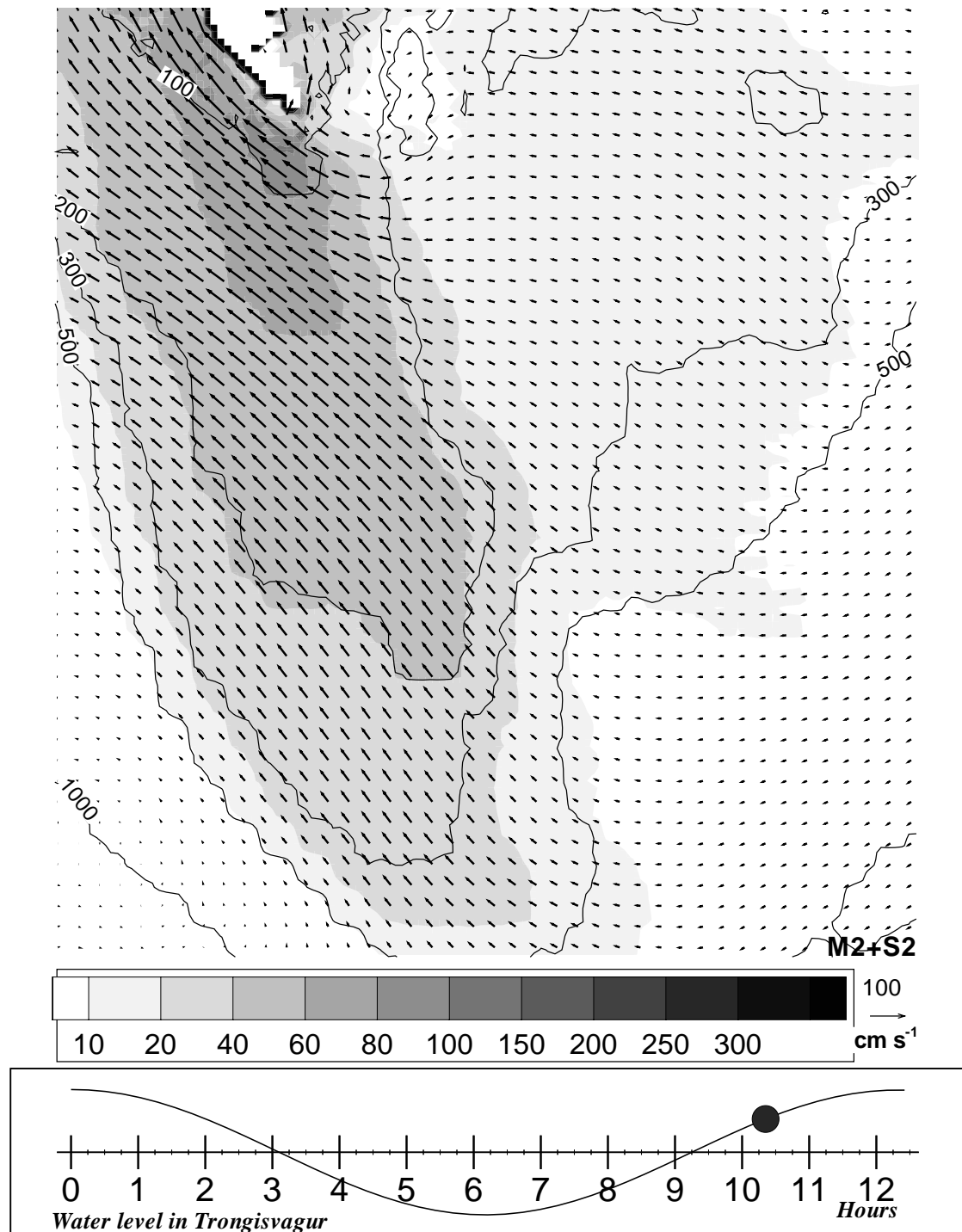


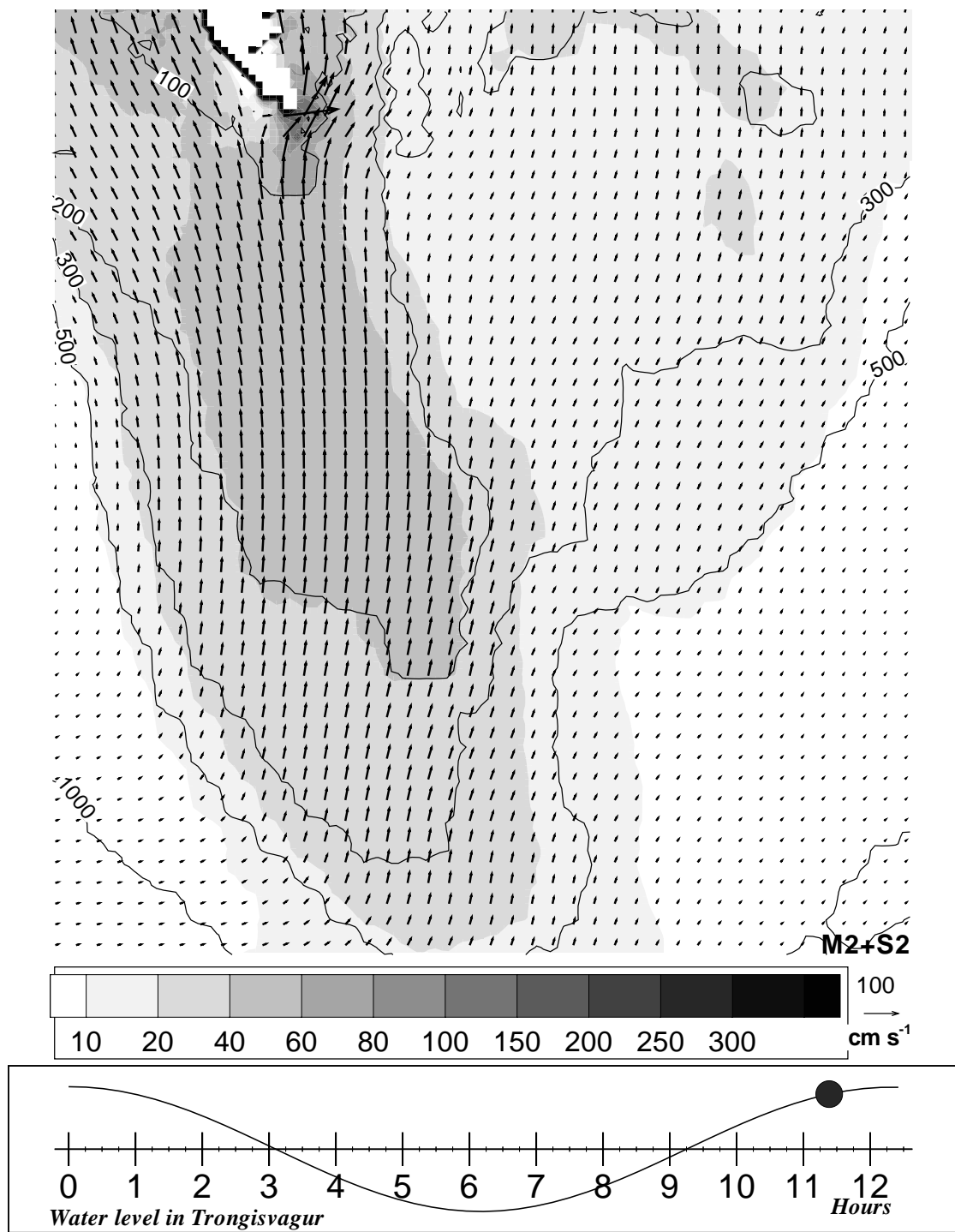












5 Database

A file is produced containing amplitude and Greenwich phase lag of the tidal elevation for each of the eight constituents, and a file containing length of major semi axis, length of minor semi axis, inclination relative to east, and net Greenwich phase lag, i.e. the tidal current ellipses parameter for each of the eight constituents. The name of the files are listed in Table 13.

The format of the files are:

```
VARIABLES="h_pha_M2"
ZONE I=555,J=455,F=BLOCK
0.16328E+03 0.16328E+03 0.16333E+03 0.16338E+03 0.16343E+03 0.16348E+03
0.16353E+03 0.16358E+03 0.16362E+03 0.16367E+03 0.16372E+03 0.16377E+03
0.16382E+03 0.16387E+03 0.16393E+03 0.16398E+03 0.16403E+03 0.16408E+03
0.16413E+03 0.16418E+03 0.16424E+03 0.16429E+03 0.16434E+03 0.16439E+03
0.16444E+03 0.16449E+03 0.16455E+03 0.16460E+03 0.16465E+03 0.16470E+03
0.16475E+03 0.16480E+03 0.16486E+03 0.16492E+03 0.16499E+03 0.16505E+03
0.16512E+03 0.16518E+03 0.16525E+03 0.16532E+03 0.16538E+03 0.16545E+03
.
.
.
```

where the header is as required by the Tecplot graphical software from Amtec Engineering, Inc. The header provide variable name and size of file. Land points are given the value 1E+36. The data are written using following Fortran code:

```
WRITE(10,'(6e12.4)')((array(j,k),j=1,jj),k=1,kk)
```

where *array* has the dimension of (ii,jj)=(555,455).

These files are available in compressed (gzip) format in directory Data on the CD-disc.

Table 13: File names and content in the data base. xx is constituent symbol.

File name	Content
h_amp_xx.res	Amplitude (cm) for the xx-tide
h_pha_xx.res	Greenwich phas lag ($^{\circ}$) for the xx-tide
E_maj_xx.res	Length (mm/sec) of major semi axis for the xx-tide
E_min_xx.res	Length (mm/sec) of major semi axis for the xx-tide
E_dir_xx.res	Inclination ($^{\circ}$) of the major axis relative to east
E_pha_xx.res	Phase of the net current motion ($^{\circ}$)

All the files mentioned above are also truncated into a Fortran direct access file. The program *pictdat3* provided as part of the tidal prediction system (next section) extracts tidal harmonics at user specified positions. The direct access file is located in directory */Predict/Data* on the CD-ROM and details how to read this file is provided on the disc in file */Predict/readme.txt*.

6 Interactive tidal presentation

This effort is to provide an interactive and graphical front-end to present results from tidal model. The long time goal is to develop the system to also be able to make tidal model results easily available to a broad user community through the Internet or other commonly available means.

This programming is done in Java, which has several benefits:

- Java is platform independent, providing access to users with common computer equipment.
- Java programs can be used and distributed in several ways; remotely over the Internet, locally as applications using the Java Runtime Environment, or distributed on f. ex. CDROM and run locally through a WWW browser.

The Java portion of this project has initially focused on intuitive visual displays (animation's) and a basic level of interactiveness.

6.1 The CD-ROM

The CD-ROM is organized into four main directories:

Data:, which contains the database generated by the presented project as described in previous section (Section 5).

Predict: contains a Fortran direct access file of the model database and executable files to read tidal harmonics from this file, and to perform predictions of the tidal height and tidal current at a user specified position and time period based on the data in the database. Details are provided in a *readme.txt* file in this directory.

Install: contains software to read the content on the CD-ROM. If they are not available on the used computer, they may be installed from the disc.

Present: contains a presentation of the results from the present project. The presentation is started by activating the file **StartHere**. The **First Page** of the system offer following options:

Tidal Charts	Tidal Current Ellipse Axis
Extreme Tidal Current	Residual Tidal Currents
Current Maps	Tidal Prediction
Documentation	Disclaimer

For each choice a short description of the further options are provided, and in the four first options a direct link is to a model bathymetry map (Figure 1).

Tidal Charts

Color versions of the tidal charts in Section 4.1.

Tidal Current Ellipse Axis

Color versions of the tidal current ellipse axis maps in Section 4.2.1, and blow up maps for the Faroese Shelf area..

Extreme Tidal Currents

Color versions of the maximum current contour maps in Section 4.2.2. Here maps are provided for all eight constituents.

Residual Tidal Currents

Color versions of the residual current maps in Section 4.2.3. In addition to the maps presented in this report regional maps of the M_2 residual current are included.

Current Maps

Contains color versions of the current maps in Section 4.2.4 for every roughly 0.25 hour through a semidiurnal tidal cycle. Also presented are current vector maps, where the color contours shows the tidal elevation. Two options for presentation of the maps are provided:

- 1 The maps are animated (as a movie) through a Java script.
- 2 The maps are included into a Quicktime Viewer, which provides options to look at single maps, step forward/backward map by map, and to run animations. Based on the experience by testing the system on various machines it is however recommended to use option 1 for smooth animations.

The time is provided graphically as in the plots in Section 4.2.4. Using the maps in combination with tidal time tables like Farvandsvæsenet [1998] provides current maps to any time.

Tidal Prediction

A system suitable to extract data at wanted location from the database aranged into a Fortran 'direct access' file, and to made a tidal prediction based on these data are available as executeable files on directory /Predict on the CD-ROM. The system

must however be copied into the used computer, before it can be run. Details are given in a `readme.txt` file, which is readable from this location on the CD-ROM through a link.

Documentation

Contains a `.pdf` file of the present report, and short versions of the model equations, simulation runs, and validation towards parameters based on measured data.

Disclaimer

Contains the disclaimer of the present report.

7 Conclusion

A 0.5 nautical miles resolution model is run for the Faroe area for eight of the most important constituents in the area. Several runs are performed for some of the constituents, and based on comparison with tidal harmonics derived from measurements the results from particular runs are selected to be included in the tidal data base and presentation.

Tidal harmonics based on measurements by tidal gauges and current meters are collected from various available sources and included in the present report. The major part of the current meter data are from the recently compiled report by Hansen and Larsen [1999]. Tidal current harmonics based on current profile measurements are adopted from Sherwin et al. [1999].

The model results are validated towards measurement based data. The simulated semi diurnal tide is found to be in excellent agreement with measurements, while the simulation of the diurnal tide is slightly less successfull, although the variance between model and measurement derived parameters is comparable with the variance between different current timeseries at the same site or differences between analysis results from different sources at the same site for the elevation. Details of the model performance are provided in Section 3 and the accuracy of the presented model results is provided in Table 12.

The results are presented as

- tidal charts for each constituent,
- tidal current ellipse axis maps for each constituent,
- extreme tidal current maps,
- current maps of residual currents generated by M_2 , S_2 , O_1 , and K_1 .
- tidal current maps for the entire model domains and two sub-domains. These are estimated from the model derived M_2 and S_2 and calculated when these constituents are in phase, i.e. average spring tide.

The graphic presentation of the model results and the data base is incorporated into a interactive presentation system developed in Java, which is platform independent. The presentation system includes color versions of all figures in this report and some additional figures. Tidal current maps included in this report, but with roughly 0.25 hours interval, and similar maps for the surface elevation are included in the system to be presented as traditional maps or as animation's. In combination with traditional tidal time tables current and elevation maps to are provided to (nearly) any time.

References

- O. B. Andersen. Global ocean tides from ERS 1 and TOPEX/POSEIDON altimetry. *J. Geophys. Res.*, 100(C12):25,249–25,259, 1995.
- D. E. Cartwright, A. C. Edden, R. Spencer, and J. M. Vassie. The tides of the northeast Atlantic Ocean. *Phil. Trans. R. Soc. London*, 298:87–139, 1980a.
- D. E. Cartwright, J. M. Huthnance, R. Spencer, and J. M. Vassie. On the St. Kilda shelf tidal regime. *Deep Sea Res.*, 27:61–70, 1980b.
- D. J. Ellet. Bottom topography to the west of the Wyeville–Thomson Ridge. *Deutsche Hydr. Zeitschrift*, 41:23–33, 1988.
- Farvandsvæsenet. Tidevandstabeller, Færøerne, 1999, 1998.
- R. Flather. Result from a model of the North East Atlantic relating to the Norwegian Coastal Current. In R. Sætre and M. Mork, editors, *The Norwegian Coastal Current*, pages 427–458, Norway, 1981. Univ. of Bergen.
- R. A. Flather. A tidal model of the north-west European continental shelf. *Mém. Soc. R. Sci. Liège*, 6^e série, tome X:141–146, 1976.
- U. Fleischer, F. Holzkamm, K. Vollbrecht, and D. Voppel. Die Struktur des Island-Färö-Rückens aus geophysikalischen Messungen. *Deutsche Hydr. Zeitschrift*, 27: 97–113, 1974.
- M. G. G. Foreman. Manual for tidal heights analysis and prediction. Pacific Marine Science Report 77–10, Dep. of Fisheries and Oceans, Institute of Ocean Sciences, Patricia Bay, Sidney, B. C., Canada, 1977.
- Føroya Jarðfrøðissavn. Bathymetric Map of the Faroe Shelf, 1981. Tórshavn, Faroe Islands.
- B. Gjevik, E. Nøst, and T. Straume. Model simulations of the tides in the Barents Sea. *J. Geophys. Res.*, pages 3337–3350, 1994.
- B. Gjevik and T. Straume. Model simulations of the M_2 and the K_1 tide in the Nordic Seas and the Arctic Ocean. *Tellus*, 41A:73–96, 1989.
- P. D. Glorioso and R. A. Flather. A barotropic model of the currents off SE South America. *J. Geophys. Res.*, 100(C7):13427–13440, 1995.
- P. D. Glorioso and R. A. Flather. The Patagonian Shelf tides. *Prog. Oceanogr.*, 40: 263–283, 1997.
- G. Godin. *The analysis of tides*. University of Toronto, 1972.

- B. Hansen. Sea level variations and currents on the Faroe Plateau and their relation to the hydrography. Technical Report 39, Inst. of Phys. Oceanogr., University of Copenhagen, Denmark, 1978.
- B. Hansen. Residual flow and temperature on the Faroe Plateau during the first half of 1978 in relation to th circulation. *Publ., C:18*, Int. Counc. for the Expl. of the Sea, Copenhagen, 1979.
- B. Hansen. Residual and tidal currents on the Faroe Plateau. *Int. Counc. for the Expl. of the Sea, Copenhagen*, C:12:19 pp, 1992. Hydrogr. Committee.
- B. Hansen, D. Ellet, and D. Meldrum. Evidence for an anticyclonic circulation on Faroe Bank. *Publ., C:15*, Int. Counc. for the Expl. of the Sea, Copenhagen, 1986.
- B. Hansen, E. Gaard, and J. Reinert. Physical effects on recruitment of Faroe Plateau cod. *ICES mar Sci. Symp.*, 198:520–528, 1994.
- B. Hansen, S. Heinesen, and K. Simonsen. Current measurements in Vestmannasund, Faroe Islands. Technical report, Fiskirannsóknarstovan, Nóatún, FR-100 Tórshavn, Faroe Islands, 1991a. 27pp.
- B. Hansen and K. M. Larsen. Traditional current meter observations in Faroese offshore waters 1977–1994. Data report, Fiskirannsóknarstovan, 1999.
- B. Hansen, D. Meldrum, and D. Ellet. Satellite-tracked drogue paths over Faroe Bank and the Faroe- Iceland Ridge. *Publ., C:25*, Int. Counc. for the Expl. of the Sea, Copenhagen, 1991b.
- F. Heinesen. Tidal current around the Faroe Islands. Set with 12 current maps, Klaksvík, Faroe Islands, 1985.
- J. M. Huthnance. Extensive slope currents and the ocean–shelf boundary. *Prog. Oceanogr.*, 29:161–196, 1992.
- Z. Kowalik. Modelling of topographically amplified diurnal tides in the Nordic Seas. *J. Phys. Oceanogr.*, 24:1717–1731, 1994.
- Z. Kowalik and A. Y. Proshutinsky. Topographic enhancement of tidal motion in the western Barents Sea. *J. Geophys. Res.*, 100(C2):2613–2637, 1996.
- Z. Kowalik and A. Y. Proshutinsky. Down loaded from their web-page, 1998.
- E. A. Martinsen, B. Gjevik, and L. Røed. A numerical model for long barotropic waves and storm surges along the western coast of Norway. *J. Phys. Oceanogr.*, 9:1126–1138, 1979.

- F. Mesinger and A. Arakawa. Numerical methods used in atmospheric models. Technical Report 17, 1, WMP–ICSU Joint Organizing Committe, 1976. GARP Publ. Ser.
- W. H. Munk and D. E. Cartwright. - . *Phil. Trans. R. Soc. London*, 259(A):533–581, 1969.
- D. Prandle. The influence of bed friction and velocity eddy viscosity on tidal propagation. *Cont. Shelf Res.*, 17(11):1367–1374, 1997.
- J. Rasmussen. *Øldir og upphav*. Emil Thomsen, Tórshavn, Faroe Islands, 1981.
- D. G. Roberts, P. M. Hunter, and A. S. Laughton. Bathymetry of the northeast Atlantic: continental margin around the British Isles. *Deep Sea Res.*, 26:29–43, 1979.
- E. W. Schwiderski. On charting global tides. *Rev. of Geophys. and Space Phys.*, 18 (1):242–268, 1980.
- T. J. Sherwin, W. R. Turrell, D. R. G. Jeans, and S. Dye. Eddies and a mesoscale deflection of the slope current in the Faroe–Shetland Channel. *Deep Sea Res.*, 46: 415–438, 1999.
- A. Sielecki. An energy-conserving difference scheme for storm surge equation. *Mon. Weather Rev.*, 96:150–156, 1968.
- K. Simonsen. Tidevand i Vestmannasund. Thesis for the bach. of sci. degree, Náttúrvísindadeildin, Fróðskaparsetur Føroya, Faroe Islands, 1989.
- K. Simonsen. The tides on the Faroe Shelf and an attempt to simulate the M_2 -tide in the area. Master’s thesis, Geophysical Institute, University of Bergen, Allégaten 70, N-5007 Bergen, Norway, 1992.
- B. Sinha and R. D. Pingree. The principal lunar semidiurnal tide and its harmonics: baseline solutions for M_2 and M_4 constituents on the North–West European Continental Shelf. *Cont. Shelf Res.*, 17(11):1321–1365, 1997.
- H. Westerberg. Benthic temperature in the Faroe area. Technical report, University of Gothenburg, Dep. of Oceanography, Sweden, 1990.